DISSERTATION

METHANE EMISSION REDUCTION FROM LARGE-BORE NATURAL GAS TWO-STROKE ENGINES

Submitted by

Titilope Ibukun Banji

Department of Mechanical Engineering

In partial fulfilment of the requirements

For the Degree of Doctor of Philosophy

Colorado State University

Fort Collins, Colorado

Fall 2025

Doctoral Committee:

Advisor: Daniel Olsen

Bret C. Windom
Dan Wise
Joe von Fischer

OBJ

ABSTRACT

METHANE EMISSION REDUCTION FROM LARGE-BORE TWO-STROKE NATURAL GAS ENGINES

Methane emissions from over 7000 large-bore natural gas engines used for gas compression in the United States result from combustion inefficiency and the escape of unburned methane through the crevices. Methane is a strong greenhouse gas with a warming potential 28 times that of carbon dioxide. The Inflation Reduction Act passed by the Biden administration in 2022 imposes a methane 'waste' fee that accumulates yearly to invest in clean energy and climate action starting in 2024. This study aims to reduce methane emissions from large-bore natural gas engines by utilizing fuel injection techniques, thereby advancing sustainable energy development.

Natural gas primarily contains methane, and not all the methane from the engine fuel (natural gas) undergoes complete combustion in the engine cylinder. The inefficient combustion in large-bore engine cylinders has been associated with poor mixing within the cylinder at ignition. There have been efforts to enhance in-cylinder mixing in engines, and improved combustion variability and performance have validated the viability of improved in-cylinder mixing as a retrofit technology for these engines. Work aimed at enhancing mixing in the cylinders of large-bore engines has been conducted using experimental and numerical methods. Previous studies and experiments have established the potential for high-pressure fuel injection to improve in-cylinder mixing. This study addresses three key questions: how much pressure is sufficient to improve combustion efficiency through high-pressure fuel injection, how effective late-cycle high-pressure fuel injection is in

reducing methane emissions, and what role the ring pack crevice volume plays in methane emissions from large-bore natural gas two-stroke engines.

The engine modeled using CONVERGE Studio for CFD and tested for experimental studies was the large-bore 4-cylinder GMV 4TF engine. For the improved mixing and injection pressure sensitivity study, the model was simulated for four major sets of configured cases: baseline establishment, ideal mixing case development, injection pressure variation, and low-pressure, high-momentum cases. The results of this work demonstrate that improved mixing can potentially reduce methane emissions by half, and high-pressure fuel injection also enhances in-cylinder mixing in the main combustion chambers of large-bore engines. The optimal timing for the injection at different injection pressures was determined, and the limitations in each case were identified. It was concluded that fuel injection at 700 psi at -115 degrees BTDC gave the best mixing case. The level of mixing in low-pressure fuel injection systems was also found to be improved by having high-momentum fuel injection using increased flow areas at injection.

The late-cycle high-pressure fuel injection and crevice volume study explored fuel injection pressure and timing optimization, crankcase methane emissions quantification and mitigation, ring-pack methane quantification, and the impact of the piston-cylinder crevice volume on methane emissions. While varying injection pressures and injection timing on the engine, the performance and methane emission characteristics were measured during experimental tests. Also, a model of the engine was created for computational fluid dynamics (CFD) simulations using CONVERGE Studio. Experimental results showed that methane emissions are minimized with late-cycle fuel injection at 500 psi and 100 degrees BTDC. Computational results showed that the ring pack contributes up to 34% of methane emissions in the large bore engine model. A last

computational study also confirmed the flow of methane from the ring pack to the MCC and eventually out through the exhaust.

This study showed that fuel injection conditions and the ring-pack crevice volume affect the mixing levels in the main combustion chamber of large-bore engines and directly impact the amount of methane emissions released through the exhaust.

ACKNOWLEDGMENTS

I want to acknowledge the immense contribution of my advisor, Dr. Daniel Olsen, to the direction, depth, and completion of this work. His guidance, encouragement, and technical insight have been invaluable throughout my research and academic journey.

I am also grateful to my committee members, Dr. Bret Windom, Dr. Dan Wise, and Dr. Joe von-Fisher, for their support, constructive feedback, and the time they dedicated to reviewing my work. Their perspectives enriched the quality and scope of this dissertation.

Special thanks to the faculty and staff of the Mechanical Engineering Department for fostering a rigorous yet supportive academic environment that has contributed greatly to my growth as a researcher.

This work was funded in part by the Compressor and Pump Station Technical Committee of the Pipeline Research Council International (PRCI) under contract project code CPS17-08, contract code PR179-22207, and contract code PR179-21205. Their support provided critical resources that enabled the advancement of this research.

I am thankful for the use of the Powerhouse Energy Campus facilities and for the dedication of the administrative and technical staff, Hilary, Kirk, Mark, Colin, and Andrew Z, as well as research associate Nelson Xie, whose hands-on support, technical expertise, and readiness to help ensured successful experiments, simulations and smooth operations.

To my colleagues and peers, Greg, Miguel, Tolu, Felipe, Rachel, Arturo, and the entire Industrial Engines research team, thank you for the stimulating conversations, thoughtful questions, and collaborative spirit. You made the days in the lab both productive and enjoyable.

I also want to appreciate my friends, Michael Adekanbi, Toluwalope John, and Ezekiel Alaba, for their prayers, encouragement, and constant check-ins throughout this journey. Your friendship was a source of strength and joy, especially during challenging seasons.

Above all, I give thanks to God, whose grace sustained me through every stage of this journey.

I am deeply grateful to my husband, Elijah, for his constant love, strength, and encouragement; to my dad and mum for their sacrifices, prayers, and belief in my dreams; and to my siblings for their unwavering support.

This dissertation would not have been possible without the collective support of each of you. Thank you.

DEDICATION

To God, my husband, Elijah Odunayo Osuntade, and my parents, Mayowa Zacharia Banji and Comfort Olutomi Banji.

TABLE OF CONTENTS

LIST OF FIGURES

LIST OF TABLES

1. Introduction

1.1 Background – Natural Gas Transport and Compression using Integral Gas Compressor Engines

Natural gas is used for various applications, but primarily for electric power generation and industrial applications [1]. Natural gas produced and processed in the United States is used both within and outside the country. To transport natural gas across and within states in the US, gas compression is crucial. Over 1700 compression stations spread across the nation house integral natural gas compressors along the pipelines [2]. These compressors are mostly powered by slow-speed (about 300 rpm), large-bore (14”-22”) reciprocating engines, as shown in Figure 1-1. Many of these engines have been operating for over 50 years [3]. Due to their heavy construction, slow speed, and low power density, they are very reliable and potentially could operate for another 50 years. Ensuing emissions regulations are the primary impediment to their continued use on the pipelines. Low-cost retrofit technologies must be developed for these engines to reduce emissions and meet future emissions limits. The Inflation Reduction Act passed by the Biden administration in 2022 imposes a methane ‘waste’ fee on facilities with leaks and vents, which progresses and accumulates yearly starting in 2024 to invest in clean energy and climate action. This study aims to improve the efficiency of the natural gas system and avoid the adverse impact of regulations on the natural gas industry [4] and the potential effect of methane emissions on the environment by employing multiple in-cylinder methane reduction techniques for large-bore two-stroke natural gas engines.

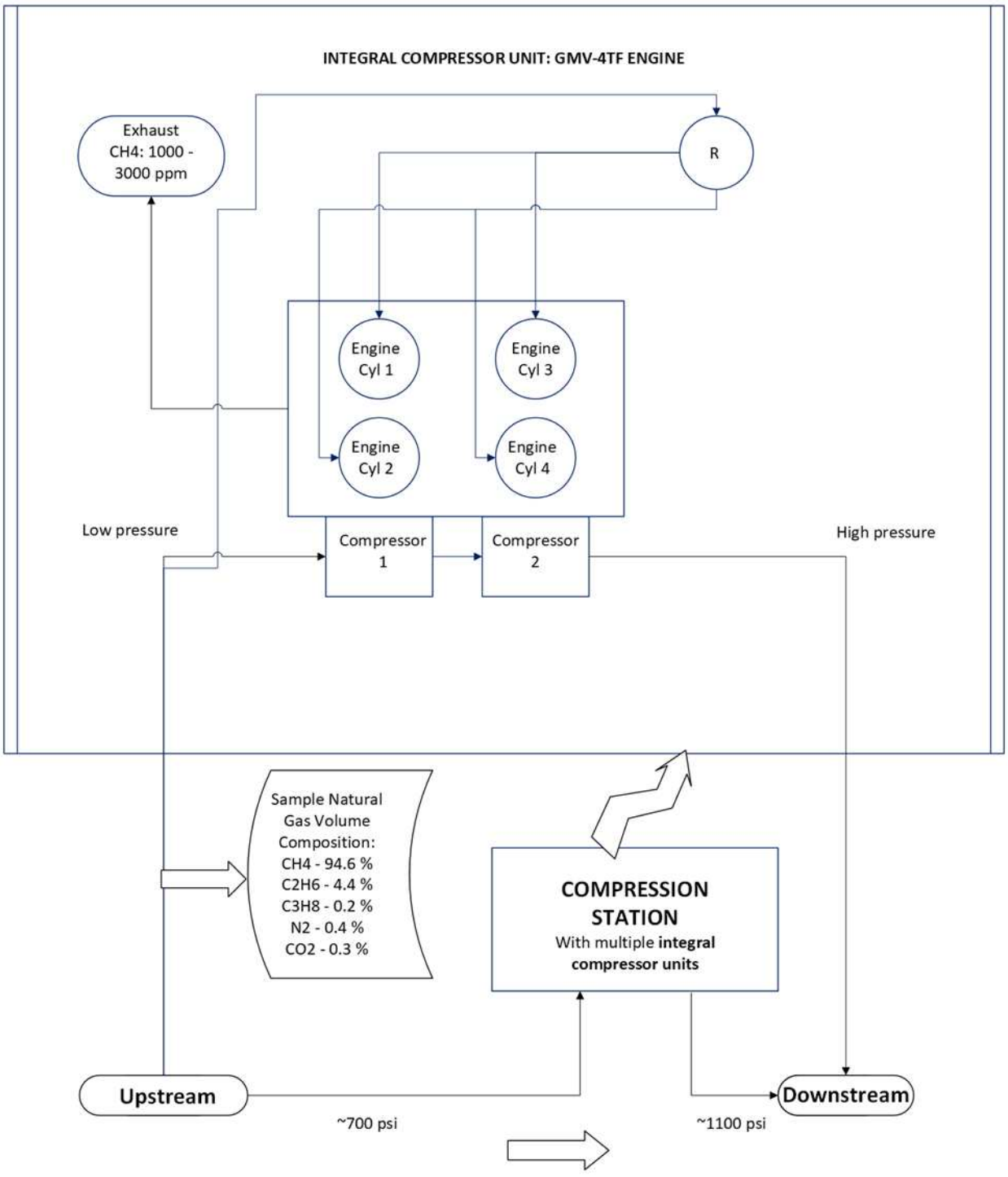

Figure 1-1 Schematic Representation of an Integral Compressor Engine in a Natural Gas Compression Station with Pressure Differences and Methane Concentrations.

Methane has approximately 28 times the warming potential of carbon dioxide [5]. Methane emissions from large-bore natural gas engines stem from the escape of unburned methane through pathways such as the exhaust and crankcase vent. Each of the 7000 natural gas compressor engines along natural gas pipelines distributed across the United States at compressor stations emits methane [6]. At least 150 countries have endorsed the Global Methane Pledge to reduce the amount of global methane emissions recorded in 2020 by 30% by 2030 to attain less than 1.5 °C temperature rise by 2050 [7]. This calls for more attention to the sources of methane emissions and studies on reducing their occurrence. Large-bore natural gas engines are either two-stroke or four-stroke, but have similar fuel measurement and regulation systems. Natural gas production and processing sites [8] which make use of large-bore natural gas compression engines give off methane emissions. For example, the compressors, unlit flares, and tanks in 508 upstream oil and gas sites in British Columbia were found to release up to 80% of the methane emissions, with compressors (which include natural gas engines) contributing most - 54% - of those methane emissions due to methane slip through the exhaust of the engines and other paths [9] like the crankcase.

1.2 Purpose of the Study

Combustion inefficiency in the main chamber of large-bore natural gas engines is the major source of methane emissions. Figure 1-2 shows the processes involved in methane emission formation in the GMV-4TF engine, leading to poor combustion efficiency [10]. Fuel is injected into the engine when the main combustion chamber contains air and residual combustion gas, containing low residual methane. Rich and lean air-fuel pockets (relative to the average air-fuel ratio) develop in the main combustion chamber due to imperfect mixing. During the compression process, some of the air-fuel mixture is forced into the ring pack. Combustion takes place, and more mixture flows

into the ring pack as pressure rises due to combustion. Bulk and wall quenching occurs in the main combustion chamber, and unburned methane escapes combustion. Some of the methane stored in the ring pack returns to the main combustion chamber. This methane is partly oxidized if the cylinder gas temperature is high enough, but survives when cylinder gas temperature is low and reactions are “frozen”. By the time the exhaust ports are open, the methane left in the main combustion chamber and the ring pack gets emitted during scavenging. Some reasons for poor combustion efficiency include wall quenching, bulk flame quenching, fuel short-circuiting when fuel reaches the exhaust ports when they are still open, an air-fuel mixture trapped in the piston top land crevice, and methane stored in the piston ring pack [11], [12], [13]. Flame quenching occurs in lean-burn natural gas engines when the bulk charge is extinguished away from the combustion chamber surfaces at quench zones, as the air-fuel mixture is very close to the lean combustion limit and the flame front becomes over-stretched [14], [15]. The walls of an engine's combustion chamber draw heat and reactive radicals from the flame, disrupting the combustion process. Wall quenching, or extinction, happens when the flame meets the cooler walls. Quenching can also happen near crevice openings, narrow spaces like the gap between the piston crown and cylinder wall. When the flame is quenched, a small amount of unburned fuel-air mixture remains in front of it. Whether this leftover mixture contributes to hydrocarbon emissions depends on how much of it is later oxidized [10].

When there is an overlap in intake and exhaust, some unburned fuel escapes as methane emissions. Lean-burn engines have combustion at lower temperatures than rich-burn engines, leading to incomplete oxidation of the fuel compounds, with methane being an average of 90% of the fuel. Poor air-fuel mixture in the main combustion chamber due to pockets of rich or lean mixtures results in uneven combustion. To improve in-cylinder mixing, high-pressure fuel injection has

been explored as a solution [16].

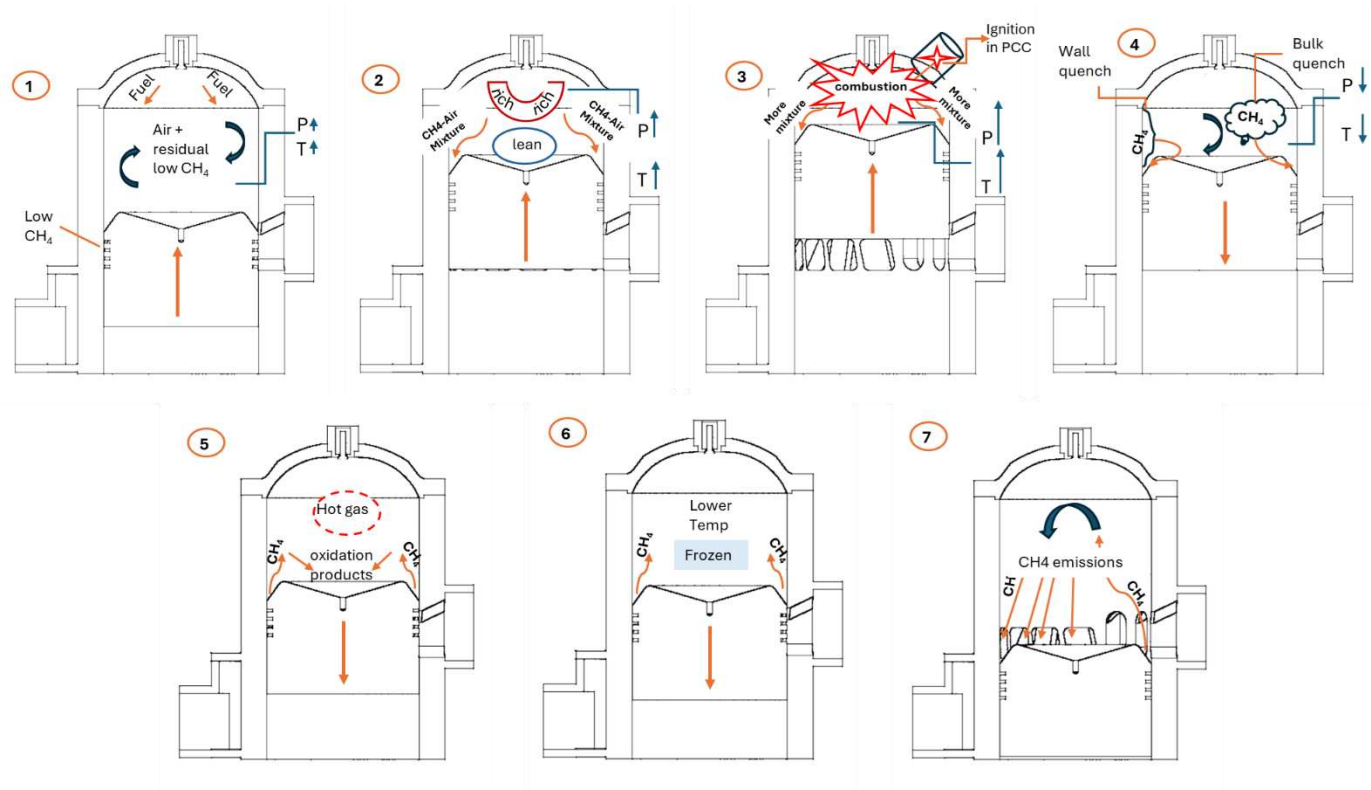

Figure 1-2 Methane Emission Formation in a Large Bore Two-Stroke Natural Gas Fueled Lean-Burn Engine with Direct Injection.

High-pressure fuel injection (HPFI) is a fuel injection strategy that has been proven to reduce methane emissions in large-bore engines. Figure 1-3 shows the brake-specific methane emissions versus NO_x emissions in the GMV-4TF during a previous study on high-pressure fuel injection [17]. The results from two of the three valves considered in the study are evaluated here. These two valves were the MGAV with a fuel pressure of 28 psi and the Pipeline Pressure Gas Admission Valve (PLGAV), injecting fuel at 500 psi. From the results of this comparison, it is seen that the use of the high-pressure valve reduced methane emissions for all the tested points at different boost pressures. The data presented in a cross-plot format (Figure 1-3) illustrates that HPFI can reduce

CH_4 emissions at the same NO_x level.

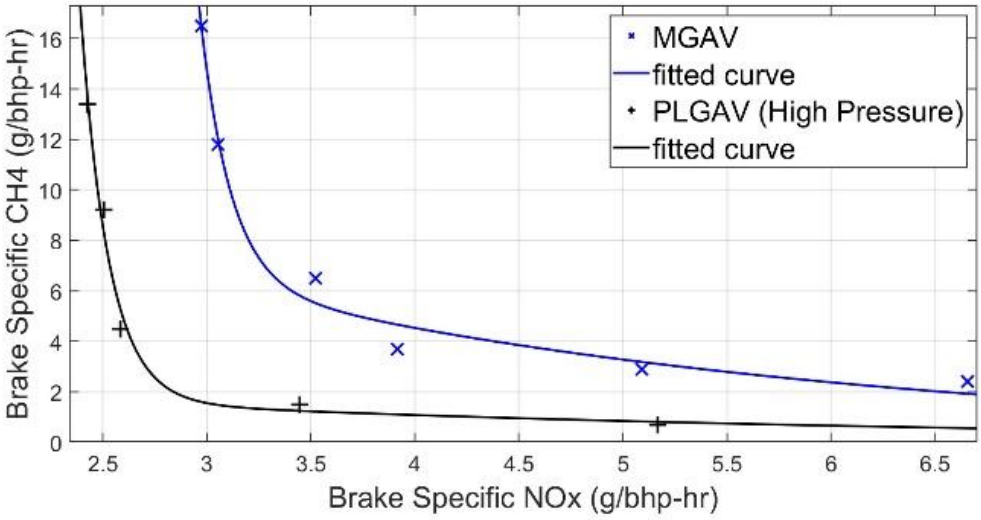

Figure 1-3 Brake-specific CH4 vs NOx emissions in HPFI Study [17]

In-cylinder mixing is critical to combustion efficiency in engines [18]. Fuel injection at high pressure results in increased momentum and turbulent kinetic energy (TKE) which improves mixing in the engine cylinder. In a computational study [19] using low-pressure (4 bar/58 psi) and high-pressure (34 bar/493 psi) fuel jets in Fluent and Star CD, the maximum TKE of the high-pressure jet was 22 m^2/s^2 while that of the low-pressure jet was 12.5 m^2/s^2. The results show reduced methane emissions due to improved combustion efficiency. [20] injected fuel at 5, 20, and 40 MPa (725, 2900, and 5802 psi) in a gasoline direct injection single-cylinder engine and showed reduced particulate matter and hydrocarbon emissions with fuel injection at high pressures. Increasing fuel injection pressures have resulted in improved hydrocarbon (HC) emissions [17] and can be further improved by optimizing fuel injection timing.

The use of fuel injection strategies that involve injection timing optimization has yielded positive results in different engines in terms of emissions. In a study on a single-cylinder four-stroke SI

engine fueled with gasoline and n-butanol, the HC emissions were seen to reduce when fuel was injected at 64 degrees crank angle (CA) before the inlet valves opened [21]. Other researchers have also evaluated the effect of single and double injection as part of fuel injection strategies. It was discovered in a study that the use of double injection in a gasoline direct injection (GDI) engine yielded a 31.81% decrease in HC emissions [22] when compared to single injection. In this present study, the impact of late-cycle high-pressure fuel injection (injection after exhaust ports close) on methane emissions is explored. The idea is that late fuel injection will lead to less unburned fuel and more air compressed into the ring pack. Crevice volumes in an engine include crevices in the piston ring pack, valve seat, spark plug, and cylinder gasket head, but the piston ring pack is typically most significant and contributes to hydrocarbon emissions, both methane and non-methane HC emissions [23]. Reducing the amount of methane emissions that are released as blowby through the ring pack will impact the total emissions released from large-bore two-stroke natural gas-fueled engines.

The engine used to investigate the fuel injection parameters in this work operates on a two-stroke cycle. Nominally, fuel injection in this engine occurs towards the end of the scavenging stroke and the beginning of the compression stroke. Poor mixing is one of the causes of residual unburned methane in the main cylinder of the engine, which escapes through the exhaust after a complete cycle due to incomplete combustion. Unburned methane that is protected from combustion in crevices, especially the ring pack, contributes to these emissions as well. Methane protected in the ring pack can flow into the combustion chamber during expansion or pass through the ring pack and exit the engine through the crankcase vent. Combustion chamber crevice volume mechanisms are known contributors to hydrocarbon emissions, including methane [23]. Increasing injection pressure is a means to improve in-cylinder mixing, and this facilitates better combustion, thereby

reducing the amount of unburned methane after combustion.

1.3 Research Focus

The research in this dissertation focuses on three major areas outlined in the following chapters (Chapters 2, 3, and 4). Each chapter was designed to address various factors related to reducing methane emissions in large-bore lean-burn two-stroke natural gas engines. One experimental study and three computational studies were involved in this research.

Chapter 2 details the use of CFD to explore different ways in which the mixing in the cylinder of the GMV-4TF engine can be improved. It examines the setup of a baseline case, which was validated using previous experimental data, and uses CONVERGE for CFD to run simulations on it to obtain results on mixing levels and methane emissions. An ideal mixing case is also examined in the chapter to determine the advantage of improved mixing on methane emissions. Then, injection pressures and timings are varied, and the results based on methane emissions and other performance characteristics are evaluated. Lastly, the injector flow area for 150 psi fuel injection is increased after iterations of measurements. The results are examined in the context of existing literature.

In Chapter 3, late-cycle high-pressure fuel injection is studied using experiments and computational studies. The experimental setup for the first part of the study is described in this chapter, with all parameters related to the setup during the test days. The computational setup is also described, and all the settings used in creating the cases are outlined. Separate results from the experimental study and CFD are presented for various injection pressures and injection timings. The experimental and computational results are then compared. From the computational study as well, additional insights are obtained regarding the contribution of the ring pack crevice

volume to methane emissions. These results are compared with previous studies in literature.

The focus of Chapter 4 is on the modeling of the top land crevice volume and surrounding factors, including allocation and grid optimization. The top land crevice is allocated to the main combustion chamber and the ring pack as two different approaches, and the base grid size is varied for optimization. The in-cylinder mixing, methane emissions, flow in and out of the ring pack, and methane oxidation results are examined to determine if the results would be grid independent and to visualize the action of the ring pack.

1.4 Research Questions

This study will answer questions related to reducing methane emissions from large bore engines, such as:

1. Can methane emissions be reduced through fuel injection pressure and timing optimization?
2. Does the crankcase vent gas make a significant contribution to overall engine methane emissions?
3. How significant is the crevice volume methane emission to overall engine methane emissions?

1.5 Research Objectives

The objectives of this work include:

1. To improve combustion efficiency through better mixing,
2. To optimize fuel injection pressures,

3. To limit the escape of methane emissions through the crankcase,
4. To reduce the amount of methane trapped in the ring pack by optimizing fuel injection pressure and timing.
5. To understand the impact of the piston-cylinder crevice volume on methane emissions.

The techniques explored involve fuel injection strategies, including high-pressure fuel injection pressure and timing optimization, and crankcase methane emissions quantification and mitigation. Both numerical simulations and experimental investigations were carried out on the Cooper Bessemer GMV-4TF engine. The findings from this work will help large-bore engine manufacturers improve engine performance and reduce methane emissions. This research will also help improve existing large-bore natural gas engines that are in use in the field by the retrofit technologies developed as a result.

2. Improved In-Cylinder Mixing – Injection Pressure Sensitivity

2.1 Overview

The inefficient combustion in large-bore engine cylinders has been associated with poor mixing within the cylinder at ignition. Previous efforts to enhance in-cylinder mixing in engines and improved combustion variability and performance have validated the viability of improved in-cylinder mixing as a retrofit technology for these engines [17]. Work aimed at enhancing mixing in the cylinder of large-bore engines has been performed using experimental and numerical means. The commercial CFD software CONVERGE is utilized for numerical simulations. CONVERGE for CFD is an appropriate tool critical for understanding the complex fluid dynamics of the air-fuel mixture that is ignited in the cylinder of large-bore natural gas engines and improving its operation.

From previous studies and experiments, including those conducted at Colorado State University (CSU), the potential for high-pressure fuel injection to improve in-cylinder mixing has been established [16]. This chapter focuses on using CONVERGE to examine the sensitivity of fuel injection pressure to mix in large-bore engines. The adaptive mesh refinement CONVERGE provides leveraged in many other commercial software used for CFD simulations and improves the accuracy of this study on in-cylinder mixing in large bore engines. The scope of this study spans establishing a baseline case, investigating the case of uniform heterogeneity to determine a minimum methane emissions point, and varying injection pressure cases, including flow area considerations for lower pressures.

2.2 Approach

The Cooper-Bessemer GMV-4TF natural gas engine was modeled using SolidWorks for CAD and imported into CONVERGE for performing CFD simulations. It is a slow-speed (300 rpm) 2-stroke cycle engine with a 14 in. bore and 14.75 in. stroke. Four model configurations were used,

(1) the baseline case,

(2) the ideal uniform mixing case,

(3) various injection pressure cases using the Siemens HPFI valve at a range of injection timing values, and

(4) adjusted valve flow area to increase momentum at low injection pressure.

The results from these configurations served as the deliverables. Each case was configured for high-pressure fuel injection and parameters such as injection pressure and injection timing were varied to investigate optimal mixing points while monitoring key parameters such as fuel slip, pollutant emissions, and cylinder pressures. The engine with its four cylinders (two currently visible) is shown in Figure 2-1. The external view of the physical fuel valve that was modeled during the simulations is shown in Figure 2-2. The HPFI valve is mounted on the cylinder head, replacing the original valves previously used with lower pressure limits. The fuel valve was configured for high-pressure fuel injection, but the cylinder (GMVH-11-1B 01300) and cylinder head used (GMVH 11-6A) were the original equipment manufacturer (OEM) configurations.

Figure 2-1 The GMVH Engine at the Engines and Energy Conversion Laboratory at CSU

Figure 2-2 High-Pressure Fuel Injection Set-up on GMVH Cylinder Head

To achieve the goals of this study, which involves an in-cylinder investigation, CFD was employed rather than experimental investigations. Using CFD also allowed for attaining engine conditions that would otherwise be difficult to reach during experimental testing, such as the uniform mixing scenario [3]. The repeatability and ease of control when it comes to the use of computational

models in CFD for this study also presented an advantage. To this end, CONVERGE CFD Studio version 3.0 was used throughout the study. The software features such as the SAGE detailed chemistry solver, adaptive mesh refinement (AMR), and fixed embedding (FE) were applied to each case.

2.2.1 Nominal High-Pressure Fuel Injection CFD Baseline

High-pressure fuel-injection has been explored in previous studies and benefits have been established. However, creating a baseline case for the GMV-4TF engine was crucial for this project, for effective comparison with subsequent improved mixing cases. One cylinder was modeled representing each of the four cylinders of the GMV-4TF engine. Specifically, cylinder #2 was utilized. Data used for validation came from cylinder #2 such as piston motion and combustion pressure data from previous experimental studies conducted on the engine for hydrogen blending tests [24]. Measurements were obtained from the GMV-4TF engine located at the Powerhouse Energy Campus.

The baseline case was split into two sections, the combustion cycle model, and the scavenging cycle model, to reduce computation time. Figure 2-3 shows the scavenging cycle model which has all the features of the combustion process, as well as geometry related to the scavenging process such as the intake and exhaust ports, pre-chamber nozzle, PCC fuel inlet, and main chamber fuel-injection valve. The components are listed as the boundaries and classified under regions as shown in Figure 2-4. The combustion cycle model geometry contains only parts related to the combustion chamber, which are the cylinder head, pre-combustion chamber (PCC), spark plug, piston, and cylinder liner as seen in Figure 2-5 and Figure 2-6. The two baseline case models had a constant NOx value of 0.5 g/bhp-hr, with the OEM PCC included in the computer aided drawing (CAD) model. In these models, fuel was injected at a nominal value for high-pressure fuel injection, 500

psi, and a nominal injection timing of 115 degrees BTDC. The combustion model was validated with the latest existing experimental combustion data and matched in terms of the location of peak pressures (LoPP). Figure 2-7 shows the top view of the intake bores, which are in pairs, and the identical exhaust ports. Figure 2-8 shows a cross-section of the scavenging cycle geometric model when the piston is at the top dead center (TDC) and at the bottom dead center (BDC). The main parameters of the model are shown in Table 2-1.

Table 2-1 CFD Baseline Geometric Model Parameters

Parameters	**Dimensions**
Bore – in (mm)	14.00 (355.6)
Stroke – in (mm)	14.75 (374.7)
Connecting rod length – in (mm)	35.1 (892)
Crank speed (rpm)	299.8
PCC volume (in^3)	3.46
PCC nozzle diameter – in (m)	0.32 (0.008)
Number of intake ports	8
Intake bores height – in (m)	2.83 (0.072)
Intake bores set 1 width – in (m)	2.80 (0.071)
Intake bores set 2 width – in (m)	2.60 (0.066)

Intake bores set 3 width – in (m)	2.48 (0.063)
Intake bores set 4 width – in (m)	2.20 (0.056)
Number of exhaust ports	5
Exhaust ports height – in (m)	4.29 (0.109)
Exhaust ports width – in (m)	2.20 (0.056)

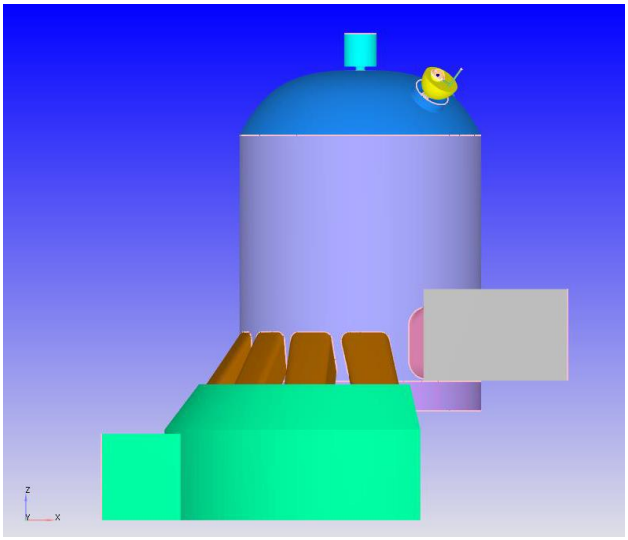

Figure 2-3 Scavenging Cycle Geometric Model. This cycle spans from -254 to 0 degrees ATDC and accounts for the scavenging process

ID	Color	Name	Region Name
0		Not Assigned	Region Undefined
1	WAL-F	piston	cylinder
2	WAL-D	piston skirt	Dependent
3	WAL-F	crevice bottom	cylinder
4	WAL-F	liner	cylinder
5	WAL-F	cylinder head	cylinder
6	INF-F	air inlet	intake
7	WAL-F	intake manifold	intake
8	WAL-F	intake ports	intake
9	OUT-F	exhaust outflow	exhaust
10	WAL-F	exhust manifold	exhaust
11	WAL-F	exhaust ports	exhaust
12	INF-F	injector gas inlet	injector
13	WAL-F	injector gas pipeline	injector
14	WAL-F	injector valve seat	injector
15	WAL-F	injector valve top	injector
16	WAL-F	injector valve bottom	cylinder
17	INF-F	prechamber gas inlet	pcc gasline
18	WAL-F	prechamber gas pipeline	pcc gasline
19	WAL-F	prechamber	pre-chamber
20	WAL-F	prechamber cover	cylinder
21	WAL-F	spark plug electrodes	pre-chamber
22	WAL-F	spark plug electrode gap	pre-chamber
23	WAL-F	prechamber nozzle	pre-chamber
24	WAL-F	spark plug cover	pre-chamber
61	WAL-F	shroud	cylinder
62	WAL-F	valve wall	cylinder

Figure 2-4 Boundaries and Regions in the Scavenging Cycle Model

The combustion model was tuned to match experimental data using the engine CFD model configuration shown in Table 2-2. The combustion pressure was tuned by varying the ignition timing. A stable grid size of 8mm in the Cartesian x, y, and z axes was determined for tuning, and a final grid size of 4mm and 8mm was used in the combustion and scavenging models respectively. The Courant-Friedrichs-Lewy (CFL) limits were determined to imitate the engine operation. A variable time-step selection was applied, with the initial, minimum, and maximum time steps being 5e-07, 5e-07, and 2e-05 respectively. The solver was set to use successive over-relaxation (SOR) methods to evaluate momentum, pressure, density, energy, species, turbulent kinetic energy (TKE), dissipation rate, elliptic relaxation function, velocity scale ratio, radiation, and wall

distribution equations. For wall distribution equations, SOR was used as a precursor for the built-in CONVERGE BICGSTAB solver. Berkeley's GRI 3.0 chemical mechanism was also applied to the two models. For the scavenging cycle case setup, there were 4 elements (C, H, O, and N) and 8 major species – O2, N2, CO, CO2, CH4, C2H6, C3H8, and H2O. However, for the combustion cycle, there were 5 elements, 573 species, and 375 reactions in the mechanism. A constant baseline value of NOx emissions was fixed at 0.5g/hp-hr.

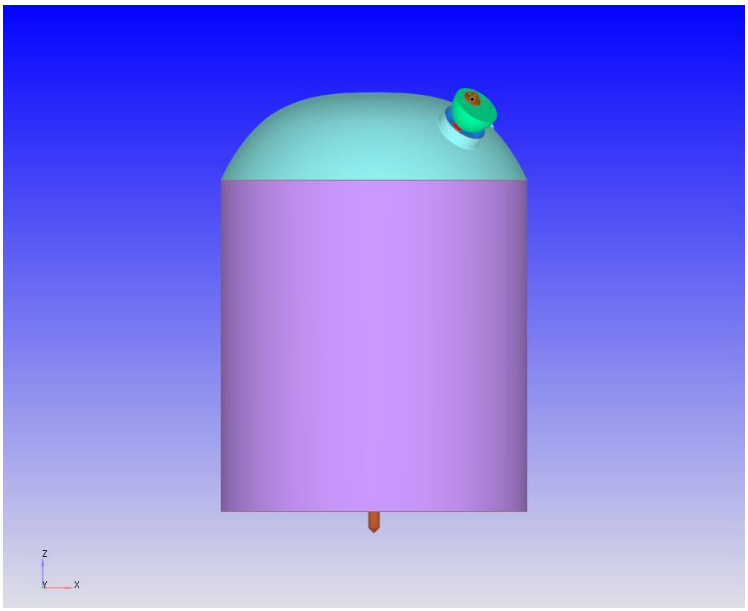

Figure 2-5 Cross-section of the Combustion Cycle Geometric Model. This cycle is like the scavenging cycle geometric model, but with only regions involved in combustion. Cycle spans from -10 to 110 degrees ATDC

ID	Color	Name	Region Name
0		Not Assigned	Region Undefined
1	WAL-F	piston	cylinder
4	WAL-F	liner	cylinder
5	WAL-F	cylinder head	cylinder
16	WAL-F	injector valve bottom	cylinder
20	WAL-F	prechamber cover	cylinder
21	WAL-F	prechamber nozzle	prechamber
22	WAL-F	prechamber	prechamber
23	WAL-F	rcg spark plug	prechamber
24	WAL-F	rcg spark plug electrodes	prechamber

Figure 2-6 Boundaries and Regions in the Combustion Cycle Model

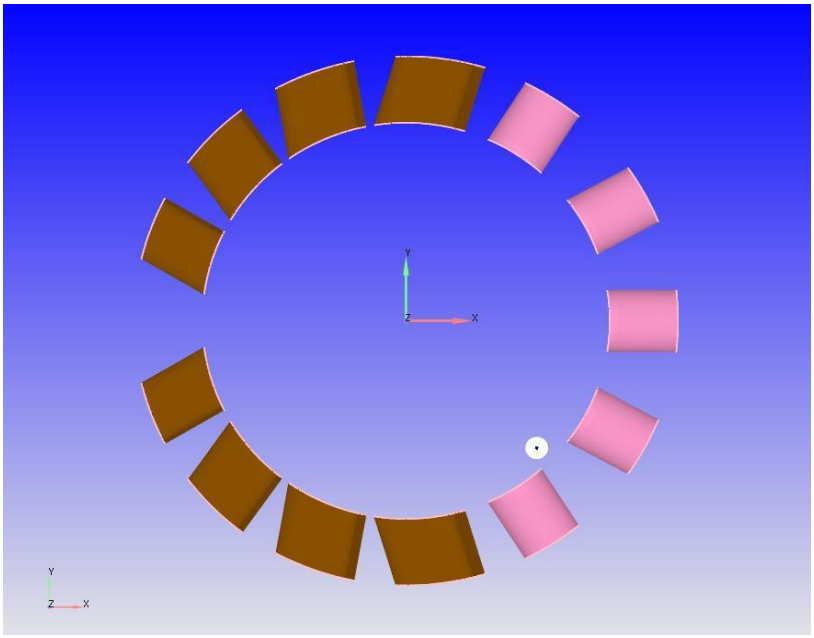

Figure 2-7 Top View of the Intake Bores and Exhaust Ports. The intake bores are in pairs and the exhaust ports are identical

(a.)

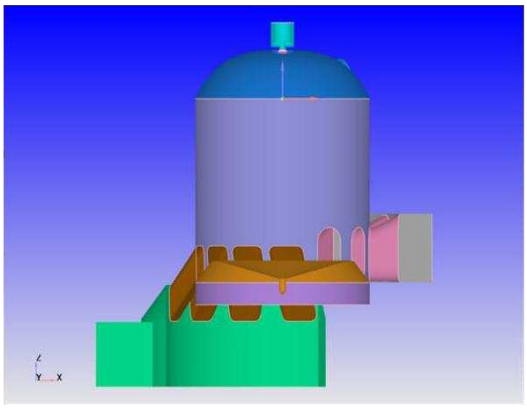

(b.)

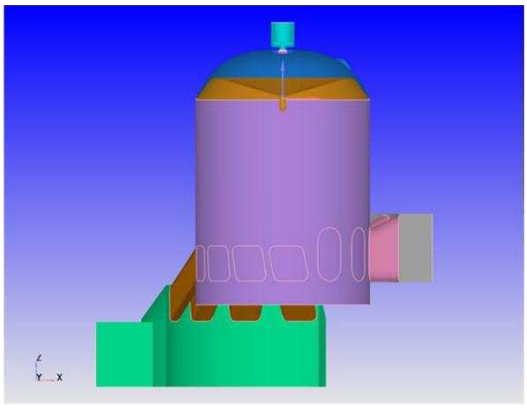

Figure 2-8 Cross-Section of Geometric Model. (a.) at BDC and (b.) at TDC

Table 2-2 Model Configuration

Parameter	**Configuration**
Fuel Injection Mode	High-pressure fuel injection
Prechamber design	OEM PCC
Chemical Mechanism	Berkeley
Baseline Injection Pressure (psi)	500
Baseline Injection Timing (deg ATDC)	-115 to -95
Ignition Timing (deg ATDC)	-1.5
Turbulent Prandtl number	0.9
Turbulent Schmidt number	0.78

Scavenging model start time (deg ATDC)	-254
Scavenging model end time (deg ATDC)	0
Combustion model start time (deg ATDC)	-10
Combustion model end time (deg ATDC)	110
Initial time step	5E-07
Minimum time step	5E-07
Maximum time step	2E-05
Main combustion chamber turbulent kinetic energy (m^2/s^2)	1.0
Main combustion chamber turbulent dissipation (m^2/s^2)	120
Maximum convection CFL limit	1
Maximum diffusion CFL limit	20
Maximum Mach CFL limit	500
Droplet motion time-step control multiple	1.5
Droplet evaporation time-step control multiple	9999
Chemical time-step control multiple	0.5
Collision grid time-step multiple	1

Moving boundary time-step multiple	0.5

2.2.2 Ideal Uniform In-Cylinder Mixing at Spark

The next case after the baseline was established focused on forcing the measure of heterogeneity ($\emptyset_{SD}$) in the cylinder to be at a value of zero, implying an ideal uniform mixture. This parameter measures the standard deviation of the equivalence ratio throughout the spatial points in the cylinder and reports the degree of heterogeneity within the engine main chamber, and is defined in Equation 1.

Equation 1: Equivalence Ratio Standard Deviation

$$\emptyset_{SD} = \frac{\sqrt{\sum_i^n (\emptyset_{ave} - \emptyset_i)^2}}{n-1} \qquad \text{Equation 1}$$

Where:

$\emptyset_{SD}$ = Equivalence ratio standard deviation

i = Individual spatial point

n = Total number of spatial points

$\emptyset_{ave}$ =Average equivalence ratio

$\emptyset_i$ = Equivalence ratio at each spatial point in the engine cylinder (main combustion chamber).

The standard deviation values range from zero (0) to one (1) in the cylinder, with values that tend

toward one (1) indicating poor mixing and those tending to zero (0) indicating improved mixing. A value of zero, therefore, indicates perfect mixing. This is completely ideal and cannot be attained by the engine under normal operating conditions. However, it gives a reference point of the lower limit of what is attainable concerning methane emissions via improved mixing. The case was set up using the same conditions as the baseline – the same mass flow rate and other injection conditions, with the only change being the ideal measure of heterogeneity. It was tuned to have the same location of peak pressure, peak pressure, and work per cycle as the baseline. The fuel injection pressure in this model remained at 500 psi, and the injection timing was 115 degrees BTDC. The results from this uniform mixing set-up provided a basis for comparison for subsequent cases but were first compared with the baseline.

2.2.3 Injection Pressure Variation

Injection fuel pressure variation was conducted to investigate high-pressure fuel injection as a strategy to improve in-cylinder mixing. The fuel injection pressures for the five (5) CFD cases used for the injection pressure variation were 150 psi, 300 psi, 600 psi, 700 psi, and 800 psi. These are in addition to the 500-psi baseline. Each of these cases was run using different injection timing modes.

2.2.3.1 Constant Injection Timing

The first variation of injection pressures was carried out using the same injection timing, 115 degrees BTDC, which is the nominal injection timing for the baseline 500-psi fuel injection simulation. This was the first run, and the results were recorded. However, the injection timing was not optimal for some of the injection pressures, and that led to the next set of cases.

2.2.3.2 Optimal Injection Timing Investigation

To get the optimal injection timing for each injection pressure, cases were set up using the matrix shown in Table 2-3. Each injection pressure was examined at various injection timings to identify the best mixing case, but attention was also paid to cases where fuel slip occurred, and such cases were discarded.

Table 2-3 Optimal Injection Timing Investigation Simulation Matrix

Injection Pressure (psi)	**Injection Timing (degrees)**						
150	-145	-135	-125	-115			
300	-145	-135	-125	-115			
500			-125	-115	-105		
600			-125	-115	-110	-105	-100
700			-125	-115	-110	-105	-100
800			-120	-115	-110	-105	-100

After the investigation was completed, the cases with the optimal fuel injection timings for each injection pressure were compared. This gave an insight into the trend of mixing within the cylinder as injection pressure increased.

2.2.4 High Momentum Cases for Lower Pressures

The injection duration for the cases examined so far varied inversely with the pressure. This direct

relationship between the fuel injection pressure and the injection duration led to very long injection durations for the 150-psi and 300-psi cases. The 150-psi fuel injection lasted for 66.67 crank angle degrees (37 milliseconds) while the 300-psi fuel injection lasted for 33.33 crank angle degrees (18.5 milliseconds). The nominal fuel injection in these simulations at 500 psi lasted for an injection duration of 20 crank angle degrees (11.1 milliseconds). Considering that the fuel injection time for the lower pressures, particularly that of 150 psi, is much longer than the nominal fuel injection, the flow area of the fuel injection valves for the lower pressures was increased, to maintain a constant fuel injection duration and compare accordingly. For the increased flow area, the new geometry implied an increased momentum for the low-pressure case, but a constant mass of fuel injected per cycle. The changes listed in Table 2-4 below were developed by applying scale factors to the shroud diameter, poppet diameter, and the valve-lift for the fuel valve in the engine model. This resulted in new calculated flow areas detailed in Table 2-5.

Table 2-4 Dimension Comparison for Nominal Fuel Valve Design and Low Pressure Increased Flow Area Cases

Parameter	**Nominal Dimension** ***in (mm)***	**New Dimension** ***in (mm)***
Shroud diameter	0.756 (19.2)	0.861 (21.9)
Poppet diameter	0.709 (18.0)	0.709 (18.0)
Maximum valve lift	0.025 (0.64)	0.086 (2.18)

Table 2-5 Increased Flow Areas for Low-Pressure Injection

Parameters	**Nominal Flow Area** *in^2 (mm^2)*	**New Flow Area** *in^2 (mm^2)*
Seat-flow area	0.029 (18.9)	0.097 (62.9)
Shroud-poppet annulus	0.054 (35.1)	0.187 (121)
Port annulus	0.098 (63.0)	0.146 (94.3)

2.3 Results from CFD Simulations

2.3.1 Baseline Case

The baseline case was set up in CONVERGE Studio v3.0 using a previously developed geometric model with validated parameters from the GMV-4TF. The geometric model used is shown in Figure 2-9 and the dimensions are as described in the preceding section of this chapter. Some key parameters for tuning the baseline are shown in Table 2-6. These parameters are interrelated, and one cannot be changed without impacting the other parameters. As a result, all the parameters cannot be simultaneously matched to experimental data. For this study, the location of peak pressure (LoPP) and mass of fuel delivered values are matched to previous experimental data within ±5% [24]. The baseline combustion pressure trace is shown in Figure 2-10 combined with experimental data, focused on the location of peak pressure. The LoPP for the mean experimental cycle LoPP was at 18.2 degrees ATDC, while that of the baseline simulation was 18.4 degrees ATDC. The maximum cylinder pressures of the baseline simulation and experimental data average

were 511.3 and 548.9 psi, respectively.

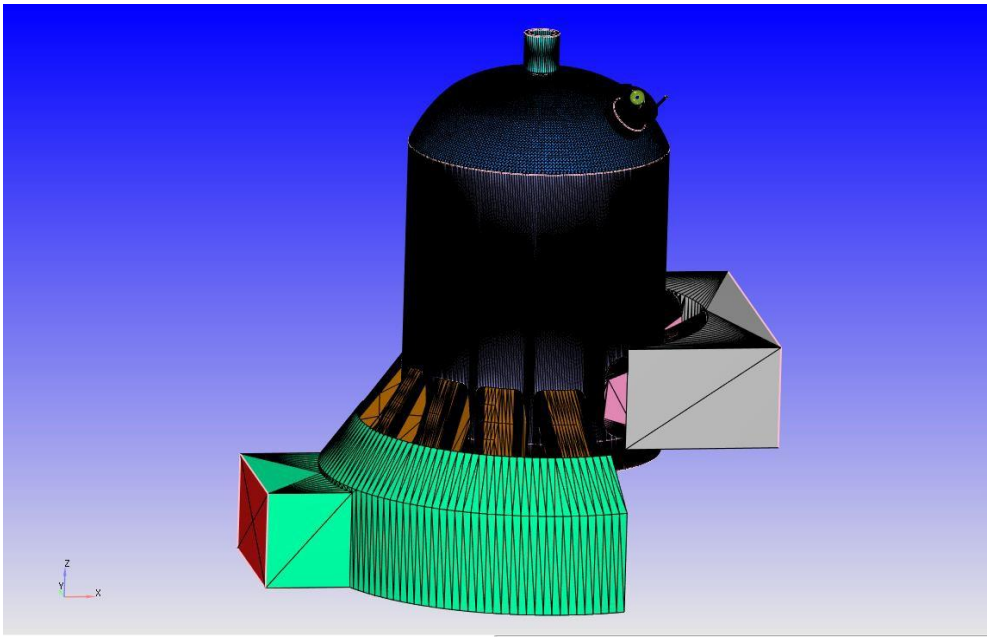

Figure 2-9 CFD Geometric Model (showing surface edges) of the Engine Cylinder, Head and Fuel Valve.

Table 2-6 Parameters Used in Tuning CFD Baseline - Fuel Injection at 500 psi and -115 degrees

Parameters	**Baseline**	**Experiment**
Location of peak pressure (degrees)	18.4	18.3
Peak pressure (psi)	511.3	548.9

Mass flow rate of fuel (kg/s)	0.0214	0.0208
NOx (g/bhp-hr)	0.5	0.3
CH_4 (g/bhp-hr)	10.4	6.1
Ignition timing (degrees)	-1.5	-3.5
Brake power (bhp)	353.8	439.9

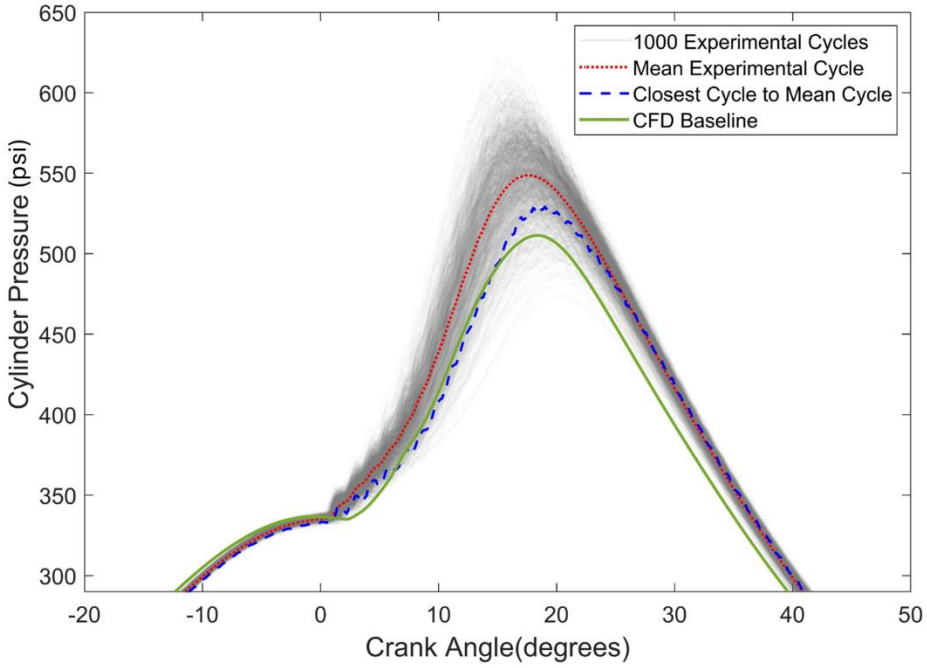

Figure 2-10 Cylinder Pressure Trace for Baseline

2.3.2 Ideal Uniform Mixing Results

The ideal mixing case is shown in Figure 2-11 shows a perfect mixing at spark (-1.5 degrees

ATDC). The model used here was the combustion cycle model to visualize events in the engine cylinder during the combustion process. The cylinder pressure trace was tuned to match the baseline in terms of location of peak pressure and peak pressure. Compared to the baseline case, this setup shows better mixing, lower values of heterogeneity represented by the equivalence ratio standard deviation from spark to the end of the cycle. The most important point at which to compare fuel-air mixing heterogeneity is at the spark. As combustion ensues, this parameter is less meaningful.

The effect of uniform mixing at the ignition point on residual methane in the cylinder is shown in Figure 2-12. The amount of unburned methane left in the cylinder at the end of the cycle is reduced by more than half (from 2.29×10^{-5} kg to 1.06×10^{-5} kg) when the combustion occurs from a point of perfect mixing. This result gives a lower limit of methane emissions for improved mixing in the cylinder and shows potential for the next set of simulations by validating the reduction in methane emissions with improved mixing.

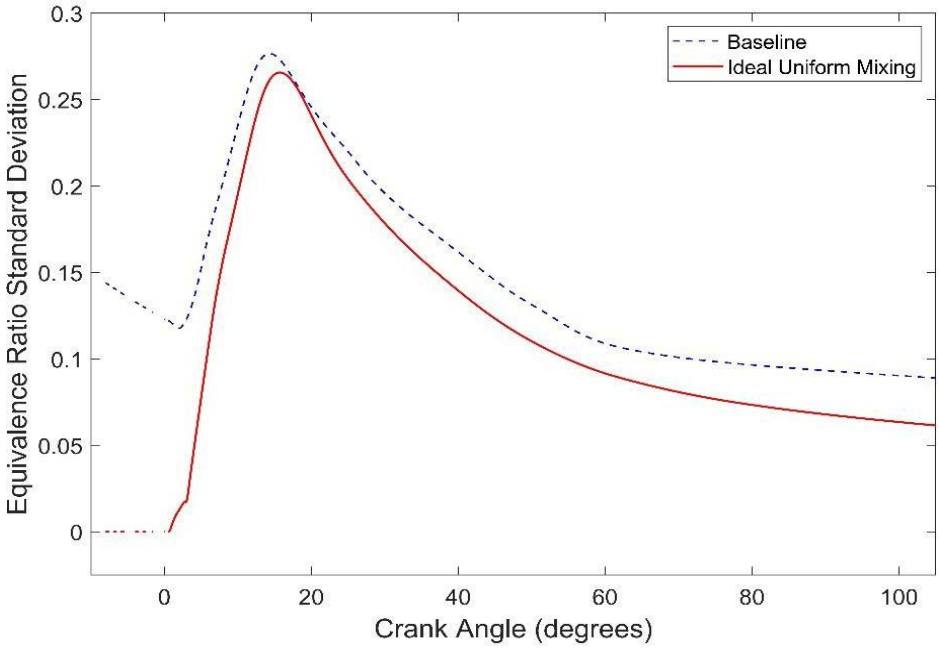

Figure 2-11 Ideal Uniform Mixing Case. CFD case with equivalence ratio standard deviation of 0 (indicating perfect mixing) at the point of ignition (-1.5 degrees ATDC) in the combustion cycle.

(a.)

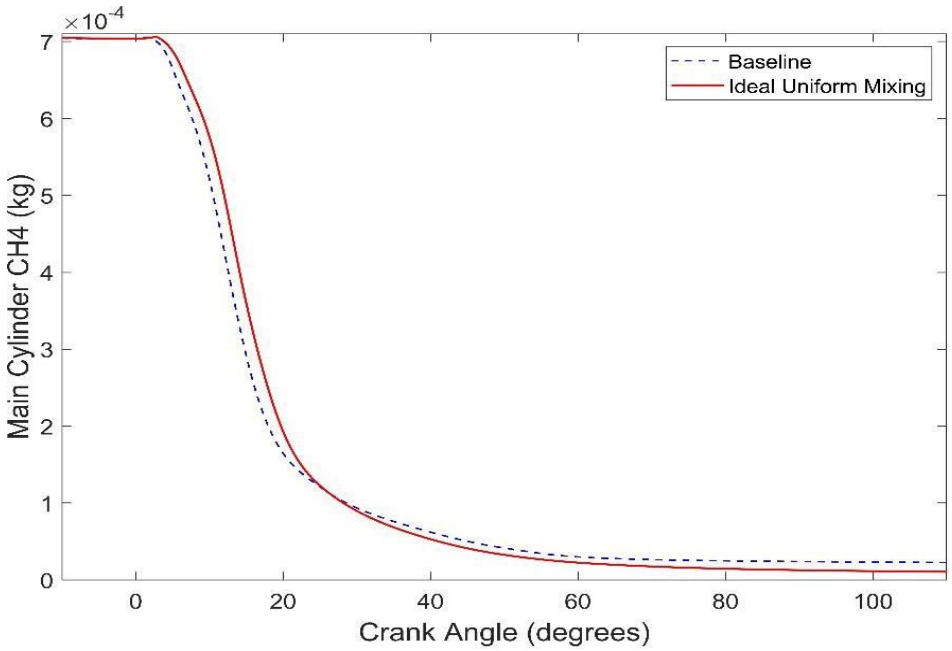

(b.)

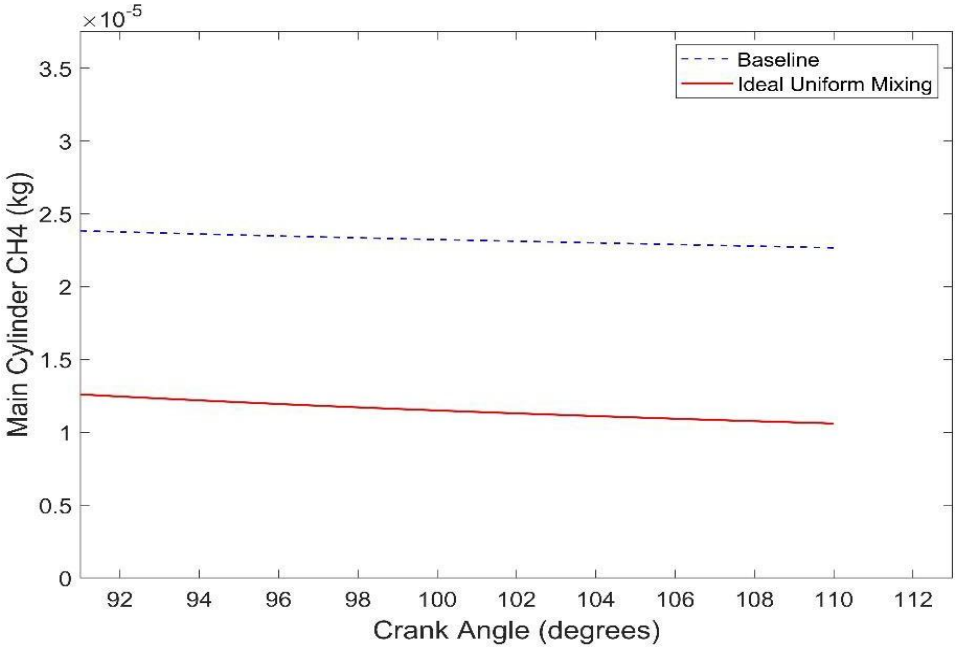

Figure 2-12 Methane in Main Cylinder – Combustion Cycle. (a.) -250 to 110 degrees ATDC

and (b.) 92 to 110 degrees ATDC.

2.3.3 Injection Pressure Variation

The fuel injection pressures used for this set of simulations varied from low to high pressures. The first runs of fuel injection simulations were conducted at -115 degrees ATDC and there was a clear trend of improvement in in-cylinder mixing. However, this injection timing that was used was clearly the optimum injection timing for fuel injected at 500 psi, and suboptimal for the other injection pressures. An optimal injection timing investigation was then carried out on the other pressures, 150, 300, 500, 600, 700, and 800 psi. The results of the optimal injection timing variations are shown in Figure 2-13.

In Figure 2-13, the points with the best mixing can be identified for each injection pressure. However, for the 150 psi and 300 psi cases, there were cases with significant fuel slip out the exhaust ports. Figure 14 shows the fuel slip for 150 psi injection at -145 degrees ATDC. Figure 15 shows the baseline case (500 psi fuel injection at 115 degrees BTDC) with less than significant fuel slip. The 150-psi fuel injection cases had 1.6% fuel slip when the injection timing was at -145 degrees ATDC. At 300 psi there was a 10.3% fuel slip when natural gas was injected at -145 and 0.6% fuel slip for injection at -135 degrees ATDC.

Figures 2-16 to 2-21 show binning plots for the optimal mixing points at each injection pressure. The mean equivalence ratio is represented by the tallest bins and the variation of the equivalence ratio across the mass of the air-fuel mixture in the engine cylinder is illustrated by how close other bins are to the level of the tallest bin. It is clear from the images that fuel injection at 700 psi gave the best mixing at ignition (-1.5 degrees ATDC), as the bins are closer than that of other injection

pressures. Similarly, Figure 2-22 shows the summary of the optimal mixing points for each of the injection pressures. The general trend of the optimal points is a downward trend in the direction of improved mixing with increasing pressures. The first spike from that of 150 psi to that of 300 psi is because of the limits of injected fuel slip. There is a significant improvement in mixing at 700 and 800 psi compared to the nominal injection pressure of 500 psi. However, the last slight increase in standard deviation at 800 psi requires more investigation in further studies.

2.3.4 Low Pressures and High Flow Area Injection

The injection of fuel at 150 psi and 300 psi (low pressures) was simulated using the same geometry as the higher pressures of 500 psi, 600 psi, 700 psi, and 800 psi. However, the constant flow area used for these cases made the injection duration for the low pressures relatively very long. To maintain the same injection duration while keeping mass flow constant by increasing the momentum, the flow area for low-pressure fuel injection was increased by applying scale factors to the shroud diameter, poppet diameter, and lift of the fuel valve, shown in Figure 23. The mass of fuel delivered is shown in Figure 24, for the baseline case (500 psi injected at 115 degrees BTDC), 150 psi injection with the same geometry, and 150 psi injection with an improved geometry – high momentum case. Figure 24 shows that the high-momentum case was matched very closely with the baseline in terms of injection duration and the mass of fuel delivered to the main cylinder of the engine model.

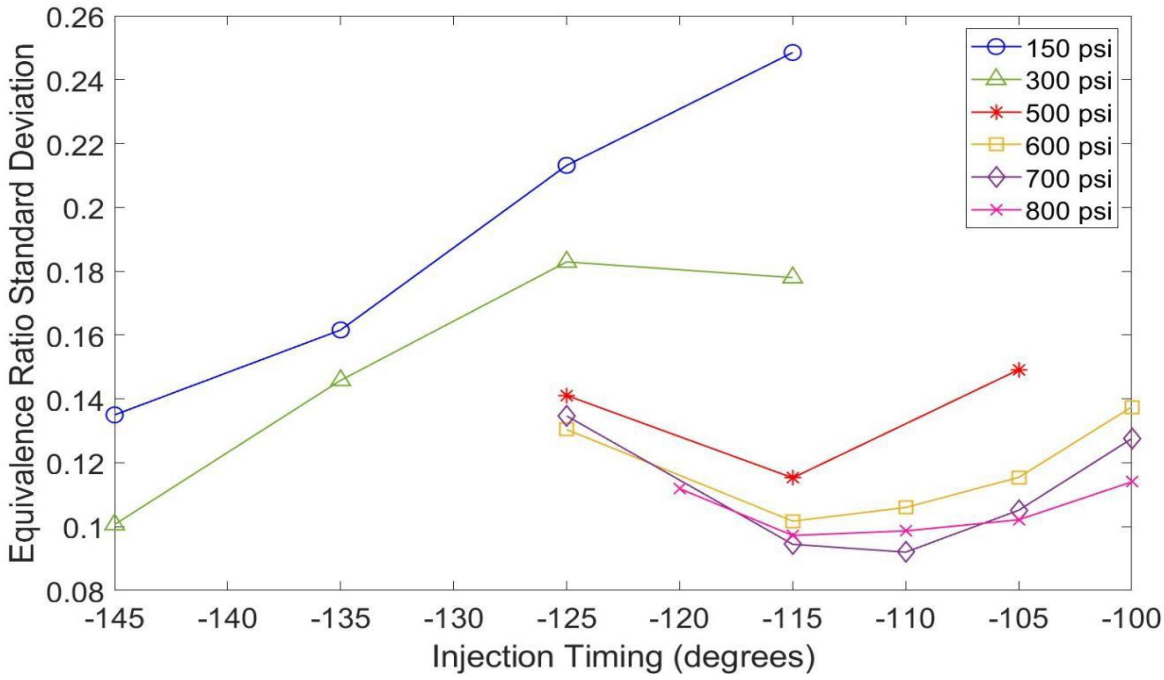

Figure 2-13 Optimal Injection Timing Investigation

(a.)

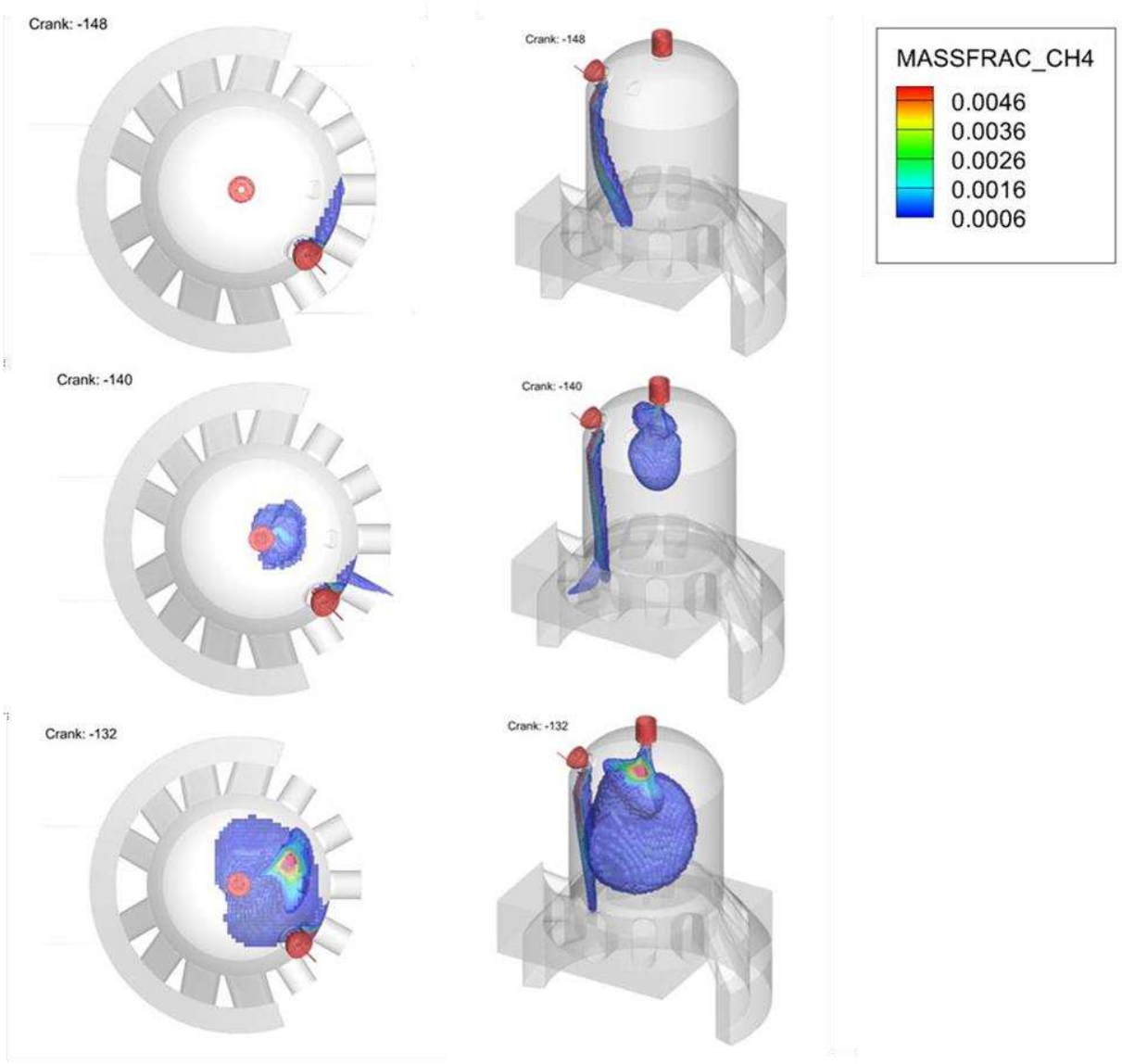
Crank: -148
Crank: -148
MASSFRAC_CH4
0.0046
0.0036
0.0026
0.0016
0.0006
Crank: -140
Crank: -140
Crank: -132
Crank: -132

(b.)

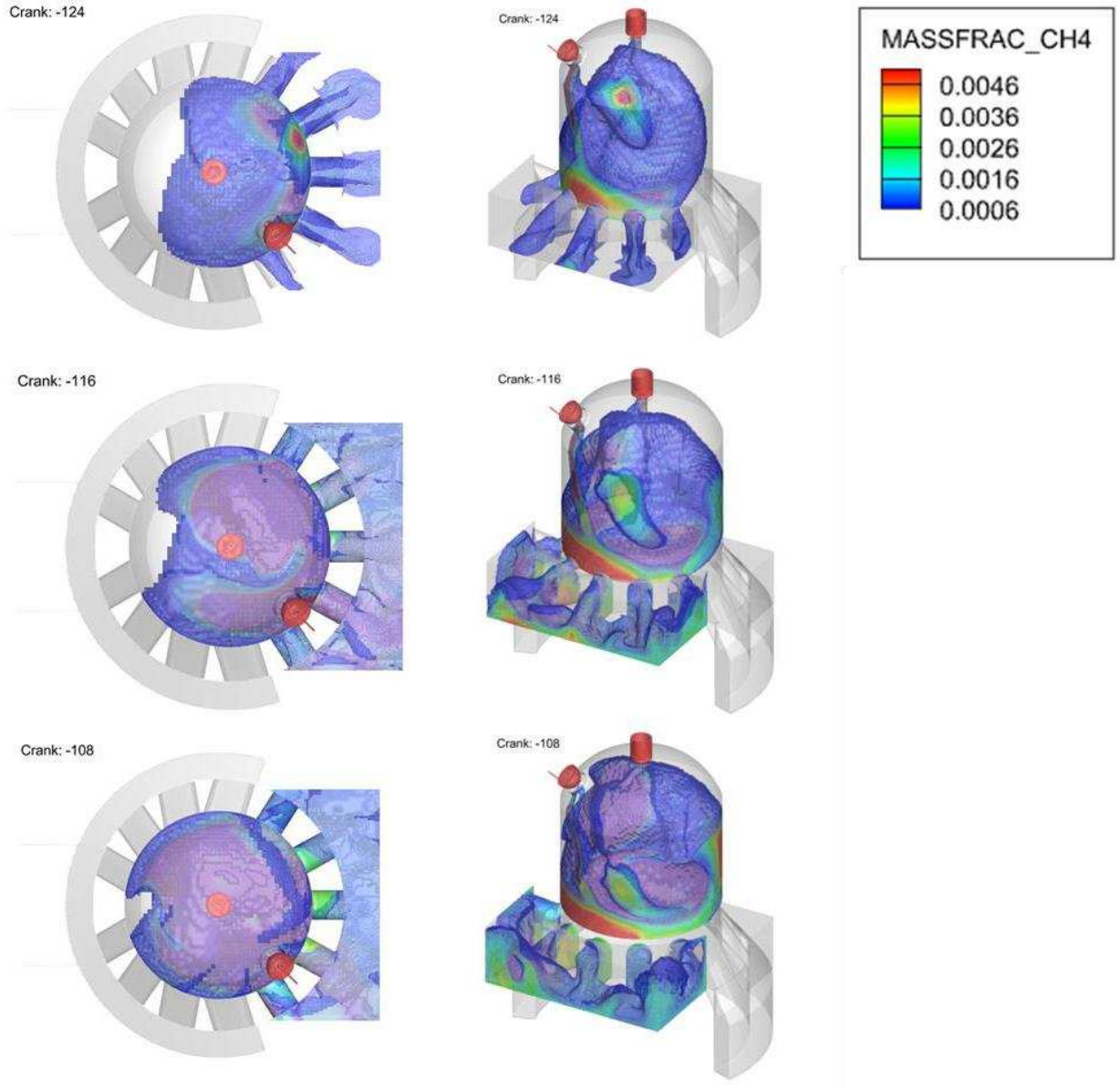

Figure 2-14 Fuel slip. 15(a) and (b) show 1.6% slip of fuel injected at 150 psi and -145 degrees ATDC (early in the cycle)

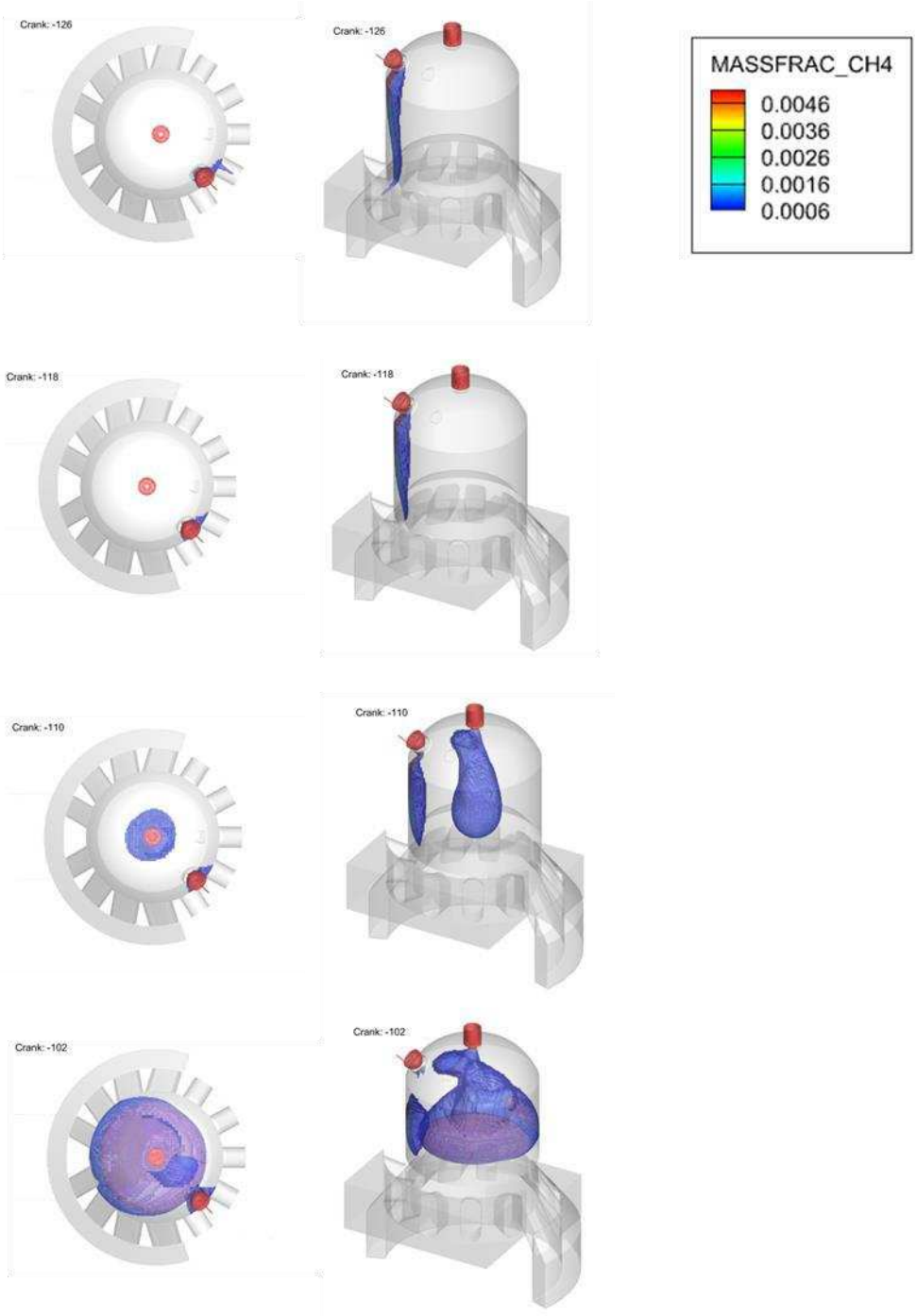

Figure 2-15 Baseline Case with No Slip from Injected Fuel at 500 psi and -115 degrees ATDC

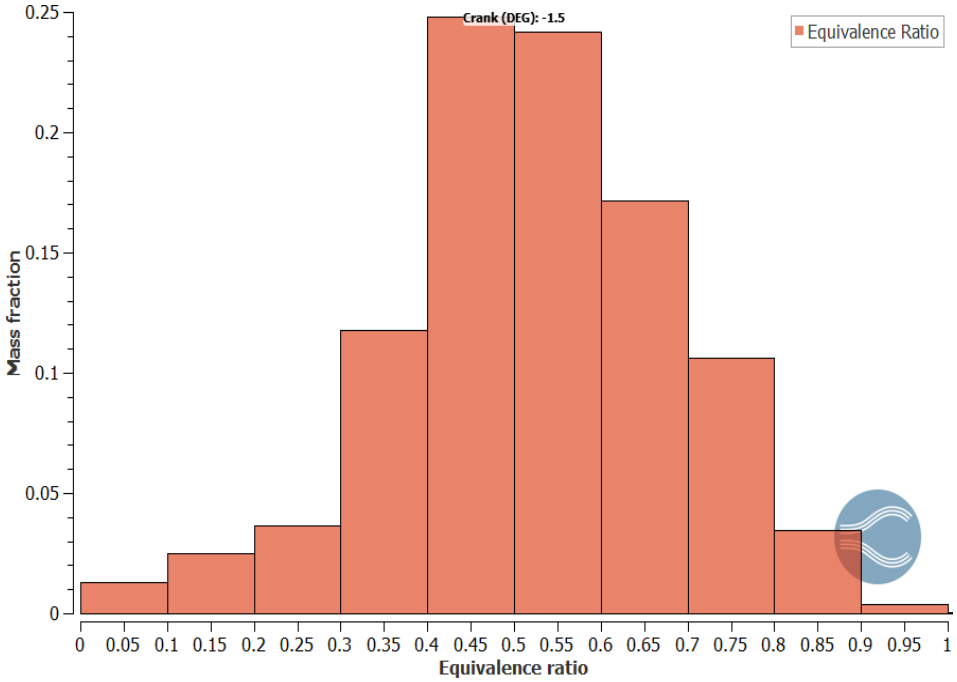

Figure 2-16 150 psi - Optimal Mixing

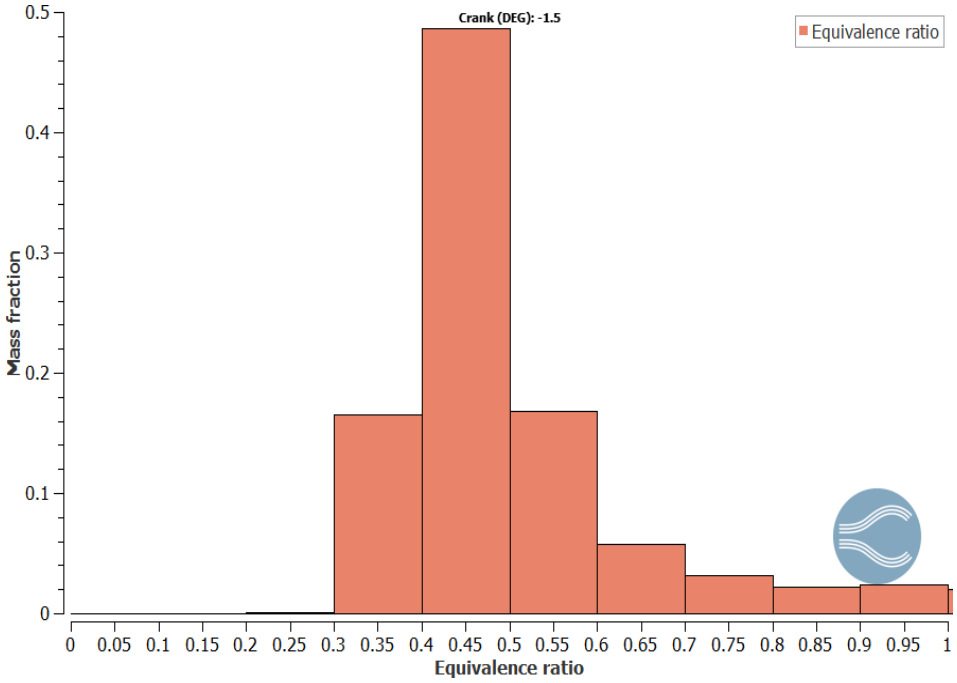

Figure 2-17 300 psi - Optimal Mixing

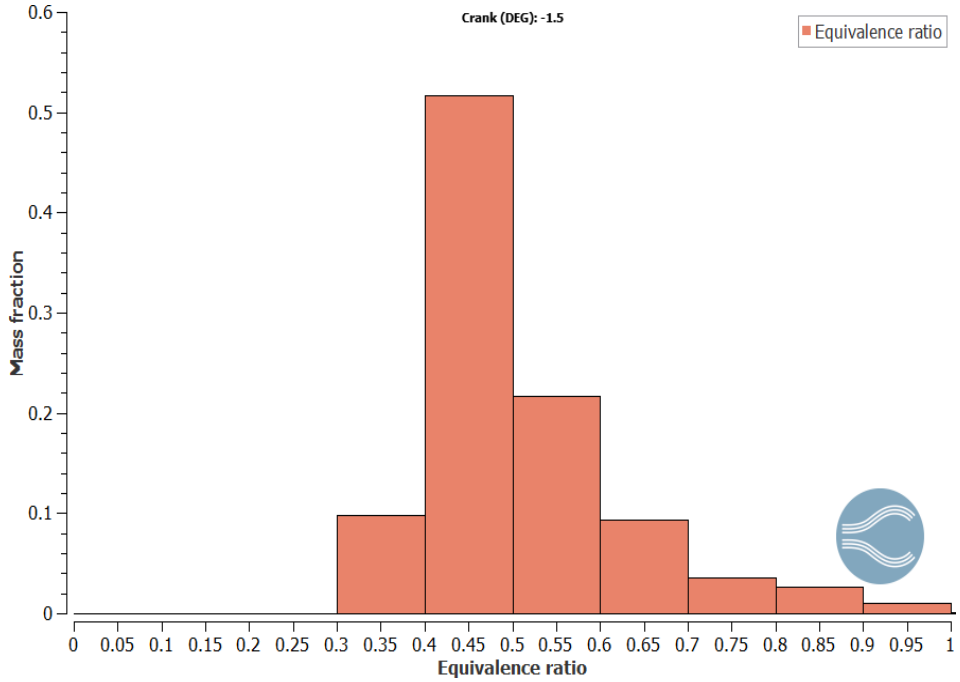

Figure 2-18 500 psi - Optimal Mixing

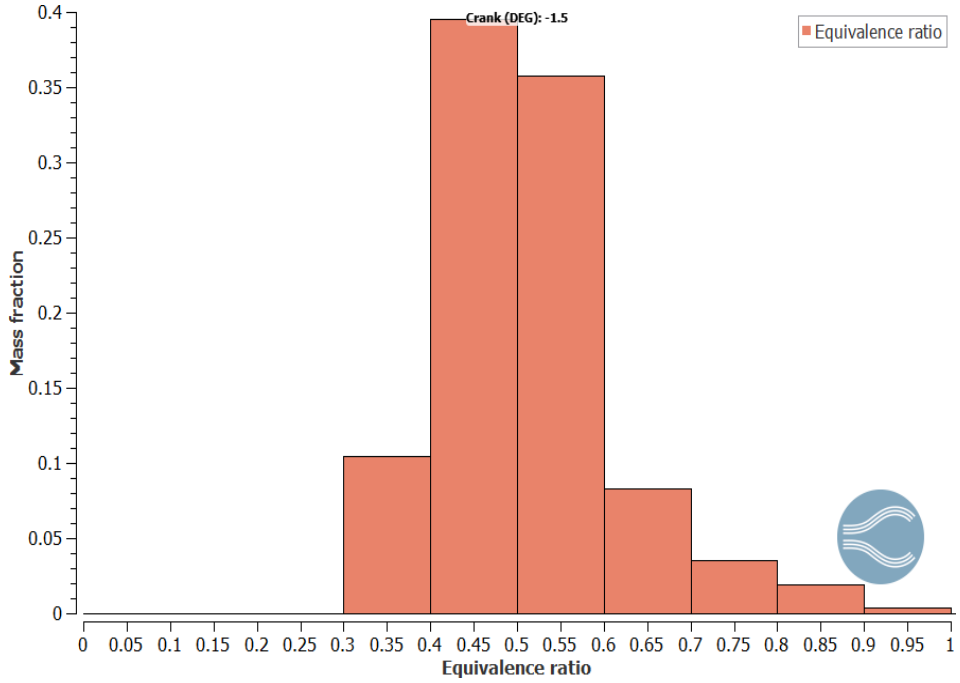

Figure 2-19 600 psi - Optimal Mixing

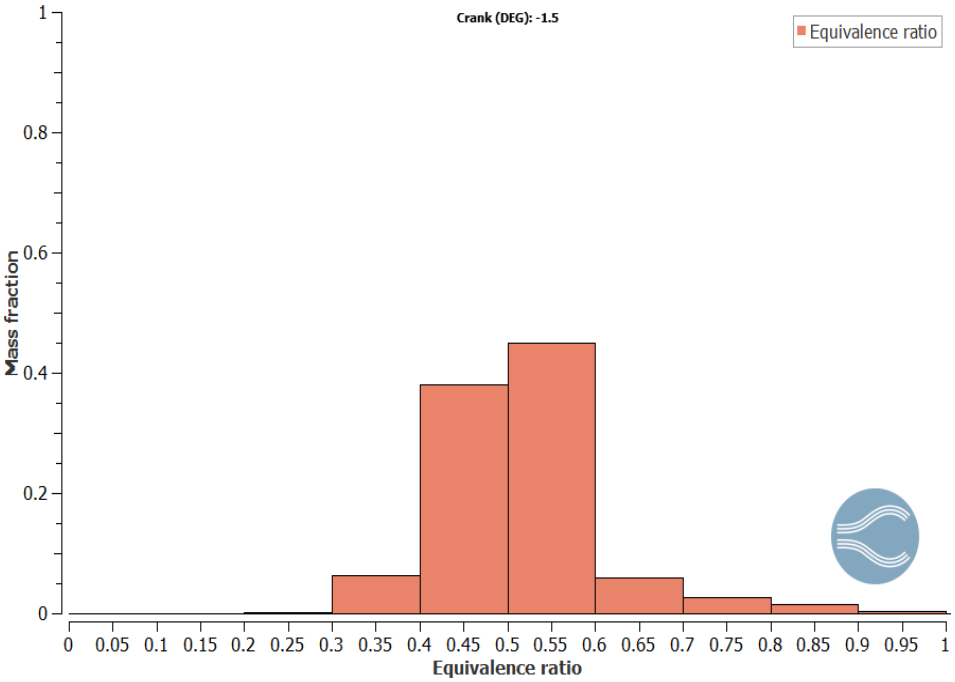

Figure 2-20 700 psi - Optimal Mixing

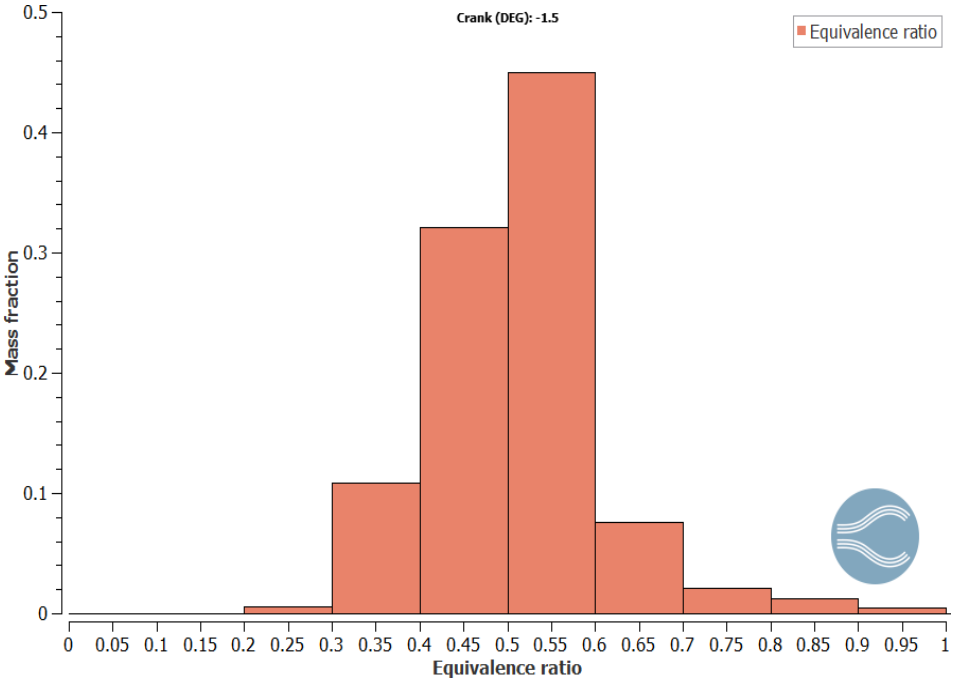

Figure 2-21 800 psi - Optimal Mixing

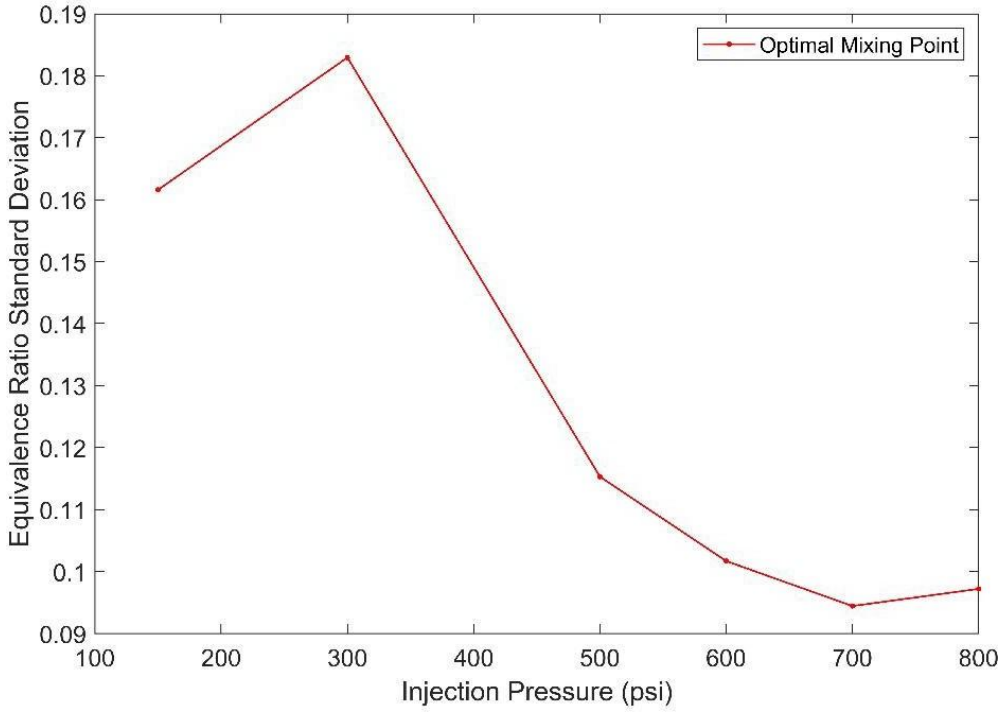

Figure 2-22 Optimal Mixing Points

The result in Figure 24 allows for a fair comparison of the two injection pressures. The results in Figure 25 show that the case with an increased flow area has a 39% improvement in mixing at the start of ignition (1.5 degrees BTDC) when compared to the low-pressure (150 psi) case at the same injection timing (115 degrees BTDC) using the initial geometry. The increased flow area case has a standard deviation of equivalence ratio at spark that is closer to baseline 500 psi case. This is due to the higher momentum that the low-pressure injection (150 psi) had with the new geometry – increased valve flow area - compared to that of the initial geometry, that impacts the mixing in the cylinder.

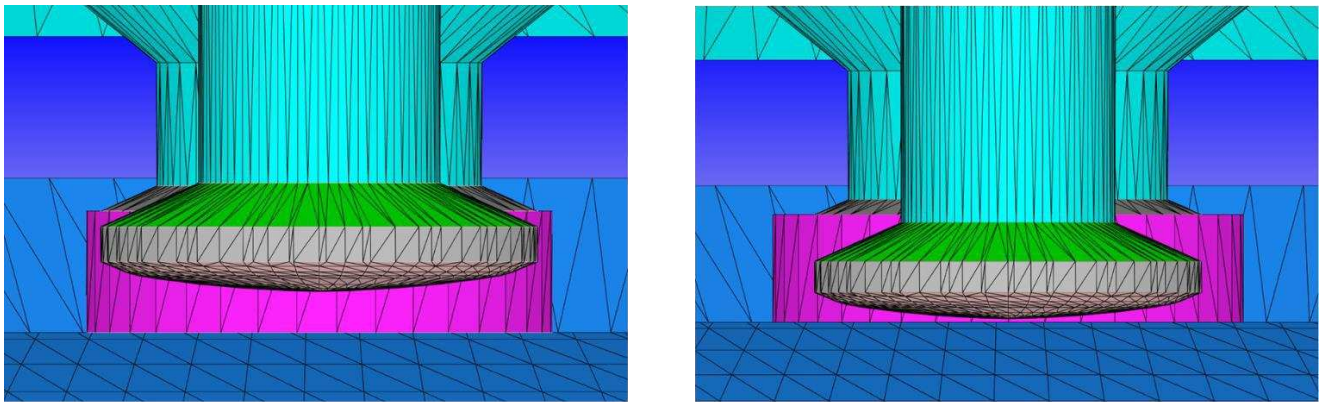

a. Initial geometry

b. Increased flow area

Figure 2-23 Increased Flow Area for Low-Pressure High-Momentum Case – (increased seat flow area, shroud poppet annulus and stem-port annulus)

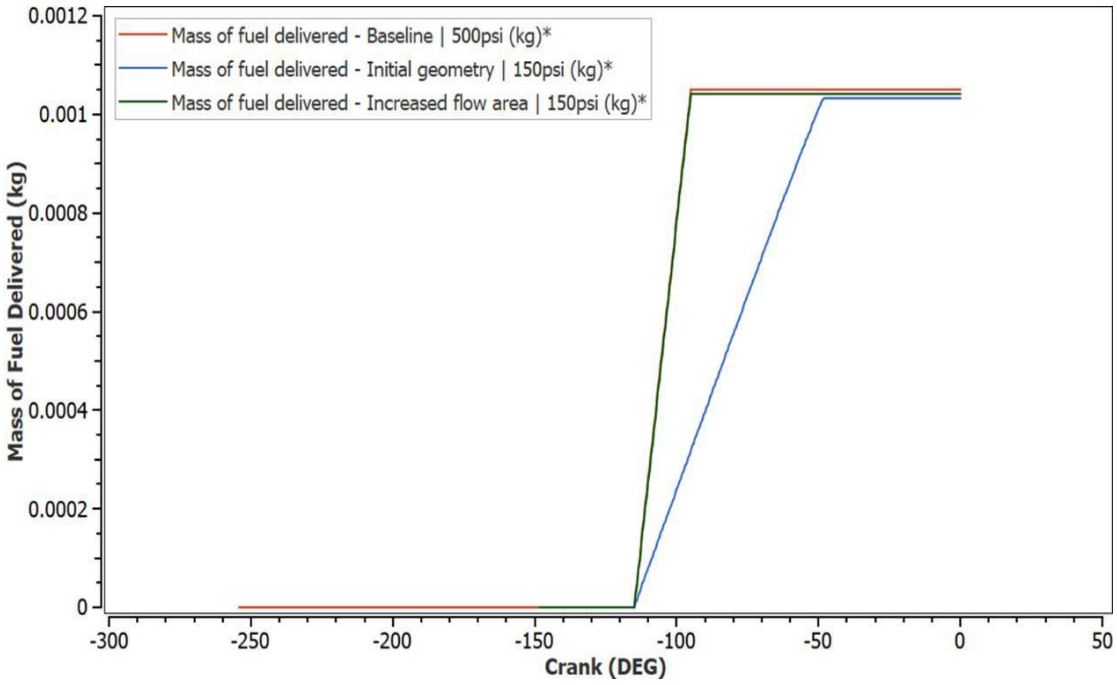

Figure 2-24 Low-pressure, High-momentum Case: Mass of Fuel Delivered

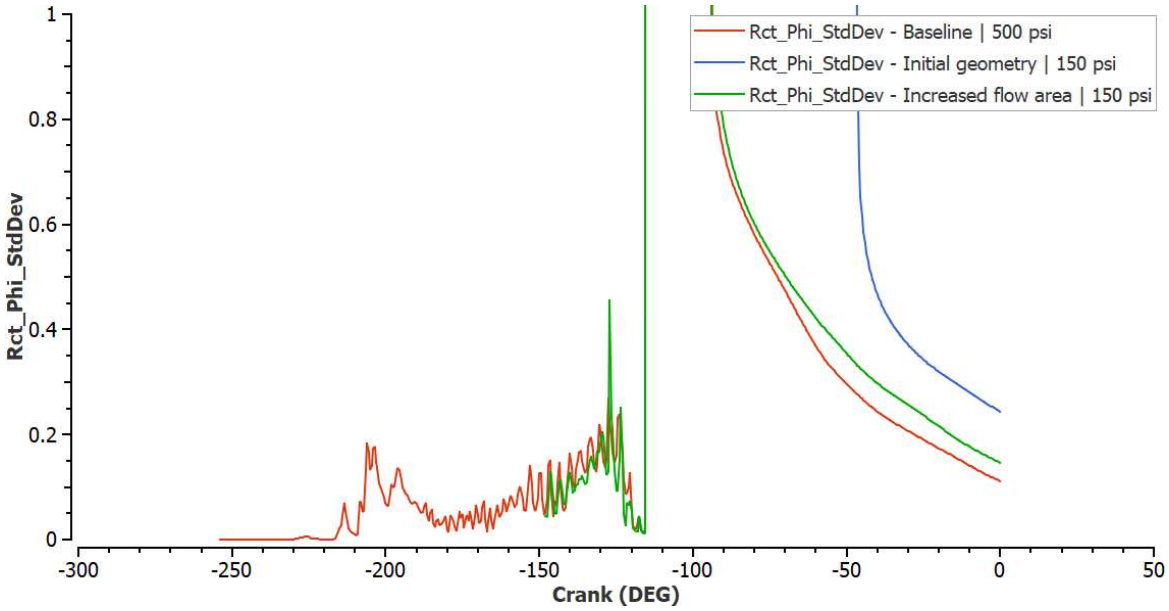

Figure 2-25 Low-pressure, High-momentum Case: In-Cylinder Mixing

2.4 Discussion

The study in this chapter on improved in-cylinder mixing showed that mixing is sensitive to changes in injection pressure, momentum, and timing. The results from the study were gathered based on the baseline CFD case results, which served as a reference for all other cases. The lowest attainable amount of methane emissions based on the ideal, or perfect, mixing case was identified to be about half of the baseline methane emissions due to the improved combustion efficiency that reduces the amount of unburned methane that can escape into the exhaust during scavenging.

Beyond the ideal case, varying the injection pressures indicated improved in-cylinder mixing with increasing injection pressures, but at an optimal injection timing. For the high-pressure cases, the mixing improves initially as the injection timing becomes late in the engine cycle up to a point where it starts to worsen. The non-monotonic trend of mixing levels with changes to injection timing can be attributed to various factors beyond fuel injector design or the engine load and speed. For early injection, fuel is

introduced at a time when the scavenging flow dominates, and tumble/swirl and turbulence are not yet fully developed [10]. This results in ineffective mixing due to stratified fuel in the residual scavenging flow, as it is suggested in a related study that early injection results in combustion with weaker stratification [25]. As compression begins after port closure, the residual large-scale turbulence is concentrated in the cylinder. At optimal injection timings, fuel loss through the exhaust ports due to scavenging is avoided, and turbulence levels have increased, resulting in better mixing. Injection beyond the optimal points, later in the cycle, results in a reduction in available time for the fuel to mix before ignition, leading to poor mixing, poor combustion stability, and elevated emissions [26].

Increasing the injection pressure of fuel in large bore engines improves the mixing of air and fuel in the main combustion chamber up to 700 psi, where it slightly declines. The more obvious trend of improved mixing is due to the high momentum associated with the air-fuel mixture when fuel is injected at higher pressures [27]. Further investigation needs to be conducted on the flow field in high-pressure fuel injection to understand the reason for the final decline in mixing at 800 psi (increase in heterogeneity).

Increasing the flow area in the fuel injection valve design and geometry for low injection pressures, such as 150 psi, improves the mixing in the engine cylinder at that same pressure, almost the same mixing as the 500-psi baseline case. The increased flow area matches the injection duration and mass of fuel delivered and allows for increased momentum when fuel is admitted into the cylinder. The improved mixing for the injection with increased flow area can be attributed to higher momentum, similar to locally premixed combustion observed in another study with a larger injector nozzle diameter [28].

This study identified two approaches to improve mixing: increased injection pressure or increased flow area. Both increase the momentum of the fuel jet and improve mixing. There are opportunities to reduce the cost of enhanced mixing and to reduce methane emissions by achieving similar mixing to the 500-psi high-pressure fuel-injection (HPFI) baseline.

3. Late Cycle High-Pressure Fuel-Injection

3.1 Overview

A significant percentage of methane emissions in large bore two-stroke engines stem from partial oxidation products when the fuel, natural gas, is burned, constituting combustion inefficiency in the engine [29]. The methane emissions from these engines result from various mechanisms such as bulk quenching, short-circuiting, and incomplete combustion in the crevice volume. Much of the emissions from short-circuiting have been addressed by the introduction of direct injectors in spark ignition two-stroke engines, but the processes in the main cylinder and crevice volumes of these engines are still being studied and have not been understood in detail. Late-cycle high-pressure fuel injection would result in more air and less fuel being forced into the crevice volumes during compression.

To address combustion inefficiency, more studies have considered the in-cylinder combustion action and how to improve it. Studies have shown how high-pressure fuel injection increases the momentum of the fuel jet injected, leading to improved mixing and improved combustion. Kim et al. [19] conducted a computational study on high-pressure fuel injection using Fluent and Star-CD using low-pressure (4 bar) and high-pressure (34 bar) fuel jets. They observed that the maximum turbulent kinetic energy (TKE) of the high-pressure jet was 22 m^2/s^2 compared to that of the low-pressure jet at 12.5 m^2/s^2 implying better mixing and promising more complete combustion. A previous experimental study by Hoffman et al. [20] using fuel injected at 5, 20, and 40 MPa in a gasoline direct injection single-cylinder engine had shown reduced particulate matter and hydrocarbon emissions with fuel injection at high pressures. The optimization of injection pressures has given promise for improved mixing, but some other parameters for fuel injection can be optimized, such as injection timing. To this end, the present study approaches methane emission reduction in large-bore natural gas engines by exploring late-cycle high-pressure fuel-injection as shown in Figure 3-1.

Fuel injection has a major impact on the emissions characteristics of any engine with direct fuel injection. For large-bore engines subject to significant methane emissions, high-pressure fuel injection can reduce the amount of hydrocarbon emissions, but it can be further improved by injection timing optimization. Optimizing the fuel injection timing can reduce the amount of methane trapped in crevices such as the ring pack, which can flow into the combustion chamber during expansion or exit through the crankcase vent as blowby through the ring pack. Combustion crevice volume mechanisms are known to contribute to hydrocarbon emissions, both methane and non-methane hydrocarbon emissions [30], [31], [32]. The contribution of the ring pack to hydrocarbon (HC) emissions was estimated by Salazar and Ghandhi [33] using experimentally measured blowby data and a simplified geometric model of the ring pack for a small utility model. In that study, it was concluded that at high loads, most HC emissions observed in the engine came from the ring pack crevices, but the simplified model could not fully explain the observed ring pack emissions. Real-time HC emissions were also observed. Using modern computational studies to investigate the crevice volumes will provide insight into the contribution of the ring pack to methane and general hydrocarbon emissions.

This study investigates the impact of two major fuel injection parameters – injection pressure and injection timing – on methane emissions using experimental and computational studies. The objectives of this study include improving combustion efficiency through better mixing, reducing the amount of methane trapped in the ring pack, and limiting the escape of methane emissions through the crankcase.

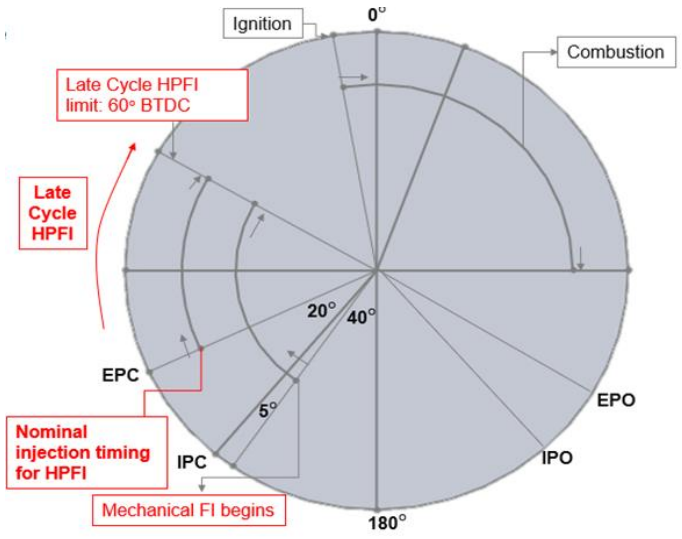

Figure 3-1 Late-Cycle High-Pressure Fuel Injection in a Two-Stroke Cycle

3.2 Approach

3.2.1 Experimental Study

The test engine utilized in this study is the Cooper-Bessemer GMV-4TF, a typical large-bore engine widely used for natural gas compression in the United States [17]. Both experimental tests and computational fluid dynamics (CFD) analyses were conducted using the GMV-4TF engine. This engine is a 4-cylinder, lean-burn, direct-injected, two-stroke, slow-speed engine operating at 300 rpm, with a 14-inch (35.6 cm) bore and a 14.75-inch (37.5 cm) stroke, rated at 440 bhp (330 kW). The engine is depicted in Figure 3-2. For this study, high-pressure fuel-injection and precombustion chamber ignition were employed, enabling the ultra-lean operation to achieve low NOx emissions (~0.5 g/bhp-hr).

Figure 3-2 GMV-4TF engine housed at the Powerhouse Energy Campus, Colorado State University

For the experimental tests and analyses, the engine was equipped with a water-brake dynamometer and piezoelectric combustion pressure sensors. These sensors played a critical role in collecting high-speed combustion data, which was analyzed in real-time to determine peak pressures (PP), indicated mean effective pressure (IMEP), location of peak pressures (LoPP), and their respective coefficients of variation (COVs) in each of the four cylinders. Additionally, an automated turbocharger simulator was employed to regulate the boost and exhaust pressures. Figure 3-3 provides an overview of the experimental test setup. To assess the species composition and quantities in the engine exhaust, a Fourier Transform Infrared (FTIR) spectrometer and a 5-gas analyzer were used. Sensors were also installed in the crankcase vent to measure the mass flow rate, pressure, and temperature. The FTIR and 5-gas analyzers were further utilized to evaluate the gas composition in the crankcase vent.

The engine was operated at its rated speed and load, with the NOx level maintained at 0.4 ± 0.1 g/bhp-hr using a NOx sensor-based feedback control system [34]. An outlier (0.705 g/bhp-hr NOx) occurred with

fuel injected at 500 psi injection pressure and -140 degrees start of admission (SOA). Combustion balancing was achieved with a cylinder-to-cylinder average peak pressure tolerance of ± 5% and a cylinder-to-cylinder location of peak pressure tolerance of ± 1 degree. The engine configuration for this study included high-pressure fuel injection valves and the original equipment manufacturer (OEM) pre-combustion chambers (PCCs). Combustion and performance results from Cylinder #2 were specifically monitored and evaluated for CFD validation. The test plan involved variations in injection pressure and injection timing. A Woodward fuel injection controller regulated engine speed at each injection pressure by adjusting injection duration at a fixed start of fuel admission (SOA), with the injection duration varying by changing the end of fuel admission (EOA). Table 3-1 presents the engine test matrix. Fuel injection pressures ranged from 150 psi to 650 psi (the maximum attainable pressure for the engine's natural gas supply system). The start of fuel admission was evaluated for early, nominal, and late fuel injection at various pressures.

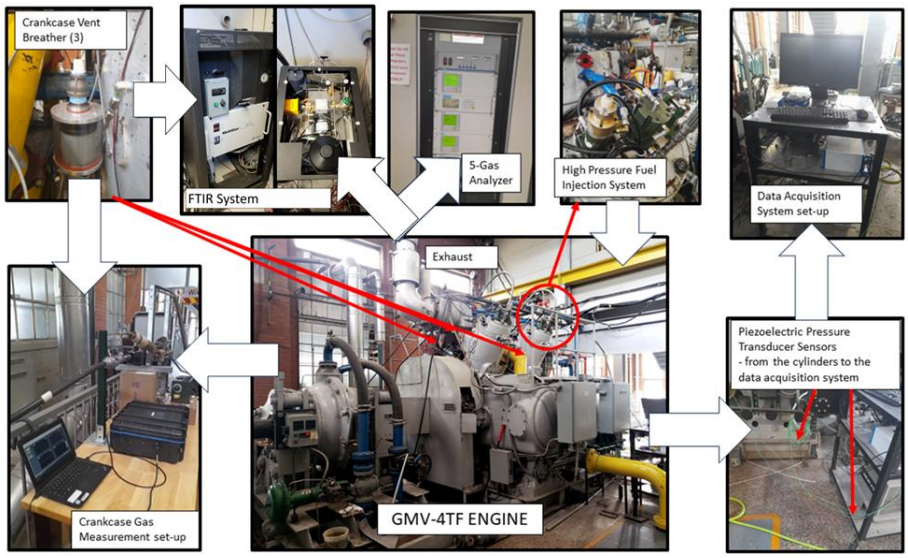

Figure 3-3 Engine Experimental Set-Up for Late-Cycle High-Pressure Fuel Injection Study

Table 3-1 Engine Experimental Test Matrix for Late-Cycle High-Pressure Fuel Injection Study

Day	Fuel Injection Pressure (psi)	Start of Admission (degrees)	Objective
1	500 (PCC flow Sweep)	-120	Minimizing COV of peak pressures
1	500	-140 to -60	Investigating fuel injection timing effects
2	650 (maximum)	-120 to -60	"
2	300	-135 to -75	"
3	150	-145 to -95	"

The crankcase vent gas was measured using a measurement probe, engine breathers connected with a rubber hose, and relevant fittings set up while the engine was running as carried out in [35]. A heated line was linked to the engine FTIR and a 5-gas analyzer was used in the experimental test to determine the composition of the crankcase vent gas compounds. The flow rate, pressure, temperature, and percentage of oxygen in the crankcase were measured continuously using LabView. For use with LabView, the parameters were collected using a JTEC VF563B flowmeter, gauge pressure sensor, a K-type thermocouple, oxygen sensor, CCV8000 Canister – for collecting oil particles upstream of the flowmeter – to avoid contamination of the flowmeter – and the National Instruments Data Acquisition (NI-DAQ) hardware.

3.2.2 Computational Fluid Dynamics (CFD) Study

Here, the CFD model was simulated under various conditions to provide insights into the behavior within the engine's combustion chamber. A key contribution of the CFD simulations was the "crevice volume"

model, which provided valuable results regarding the action of the ring pack and its impact on methane emissions in both the exhaust and crankcase of the GMV-4TF engine.

3.2.2.1 Baseline

For the baseline CFD case, the geometric model developed in CONVERGE Studio is depicted in Figure 3-4, with the geometric boundaries shown in Figure 3-5. The front view illustrates the cylinder, head, intake, and exhaust ports, pre-combustion chamber (PCC), exhaust manifold, intake manifold, and fuel injection valve. Figure 3-6 presents the intake and exhaust ports and Figure 3-7 shows the cross-section of the geometric model when the piston is at the top dead center (TDC) and bottom dead center (BDC). The model was set up to include the crevice volume, detailing the ring pack, which consists of four compression rings. Figure 3-8 displays the crevice model given by Converge, which was integrated into the engine CFD model.

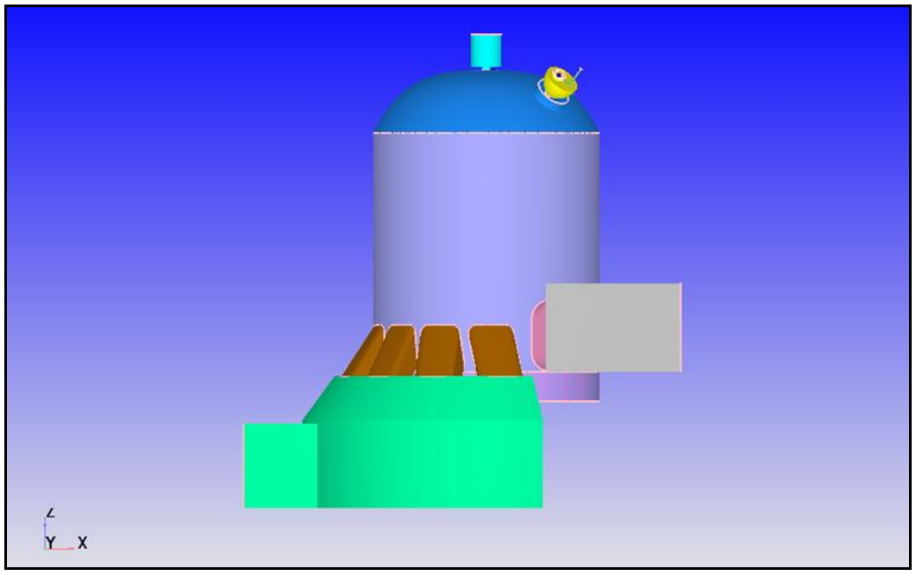

Figure 3-4 Front View of CFD Geometric Model for the GMV-4TF Engine in Converge Studio v 3.0

ID	Color	Name	Region Name
0		Not Assigned	Region Undefined
1	WAL-F	piston	cylinder
2	WAL-D	piston skirt	Dependent
3	WAL-F	crevice bottom	cylinder
4	WAL-F	liner	cylinder
5	WAL-F	cylinder head	cylinder
6	INF-F	air inlet	intake
7	WAL-F	intake manifold	intake
8	WAL-F	intake ports	intake
9	OUT-F	exhaust outflow	exhaust
10	WAL-F	exhust manifold	exhaust
11	WAL-F	exhaust ports	exhaust
12	INF-F	injector gas inlet	injector
13	WAL-F	injector gas pipeline	injector
14	WAL-F	injector valve seat	injector
15	WAL-F	injector valve top	injector
16	WAL-F	injector valve bottom	cylinder
17	INF-F	prechamber gas inlet	pcc gasline
18	WAL-F	prechamber gas pipeline	pcc gasline
19	WAL-F	prechamber	pre-chamber
20	WAL-F	prechamber cover	cylinder
21	WAL-F	spark plug electrodes	pre-chamber
22	WAL-F	spark plug electrode gap	pre-chamber
23	WAL-F	prechamber nozzle	pre-chamber
24	WAL-F	spark plug cover	pre-chamber
61	WAL-F	shroud	cylinder
62	WAL-F	valve wall	cylinder

Figure 3-5 Boundaries in the Geometric Model of the CFD model for the GMV-4TF Engine in Converge Studio v 3.0

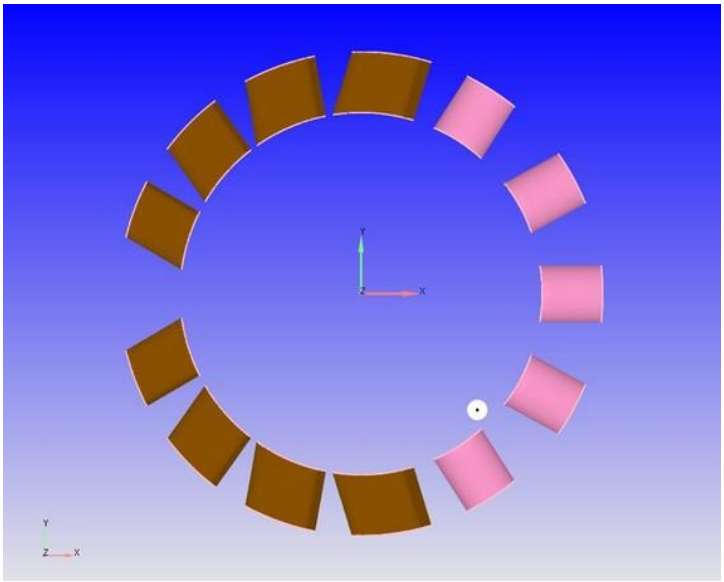

Figure 3-6 Intake Ports (In Pairs) and Exhaust Ports (Identical) in the CFD Geometric Model in

Converge Studio v 3.0

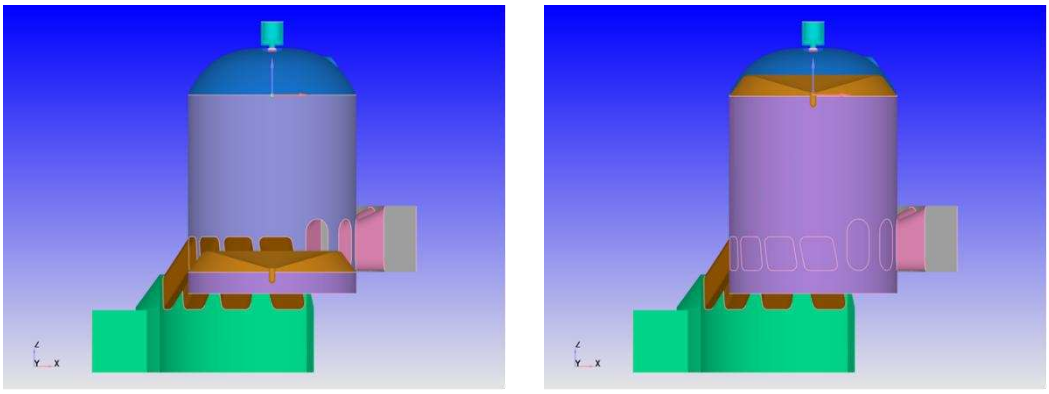

(a) **(b)**

Figure 3-7 Cross Section of the CFD Geometric Model of the GMV-4TF Engine in Converge Studio v 3.0. (a) at bottom dead center (BDC) (b) at top dead center (TDC)

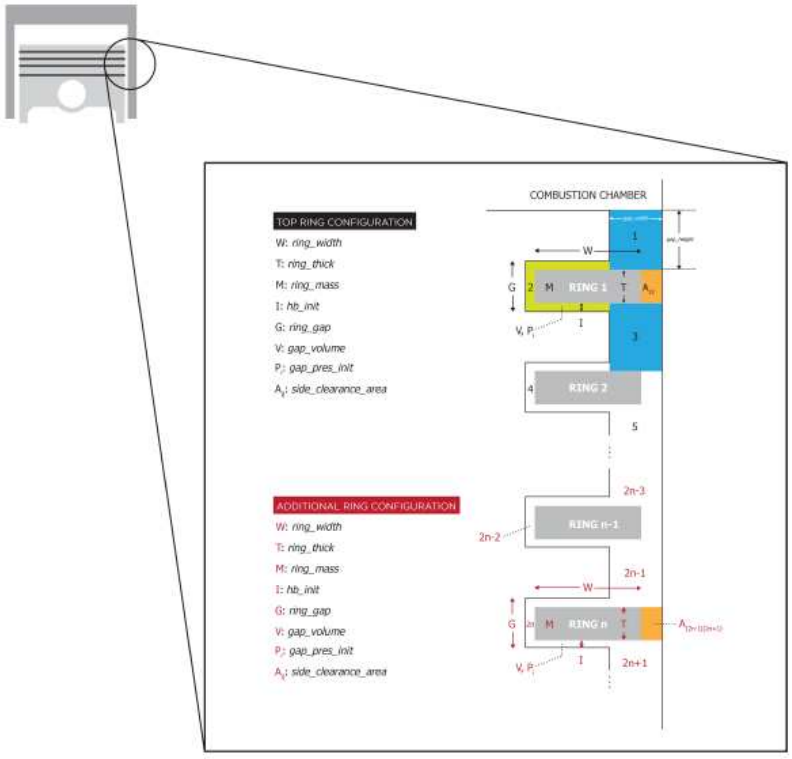

Figure 3-8 Rings and Flow Passages in the Ring Pack Crevice Volume from Converge Studio v 3.1 Manual [36]

According to [37], discharge coefficients (C_D) for crevice gas motion typically have a value of approximately 0.86. Other studies suggest estimating the discharge coefficient using the expression in Equation 2 [38], [39].

Equation 2: Discharge Coefficient

$$C_D = 0.85 - 0.25\left({}^{P_D}/_{P_U}\right)^2 \qquad \text{Equation 2}$$

Where:

C_D = Discharge coefficient

P_D = Downstream pressure

P_U = Upstream pressure

In this study, the discharge coefficient was tuned to 0.25 based on pressure trace and blowby results from experimental data. The rings in the ring pack create a crevice volume in the spaces between each ring and the cylinder wall, between each ring and the piston, and between the piston and the cylinder wall. The dimensions of the first ring differ from those of the other three identical rings, as shown in Table 3-2. The geometric details and configuration of the CFD model, including the dimensions for the crevice volume model, are also provided in Table 3-2.

Table 3-2 CFD Model Configuration and Dimensions in Converge Studio v3.0

Parameters	**Dimensions/Configuration**
Bore – in (mm)	14.00 (355.6)
Stroke – in (mm)	14.75 (374.7)
Connecting rod length – in (mm)	35.1 (892)
Crank speed (rpm)	299.8
PCC volume (in^3)	3.46
PCC nozzle diameter – in (m)	0.32 (0.008)
Number of intake ports	8
Intake bores height – in (m)	2.83 (0.072)

Intake bores set 1 width – in (m)	2.80 (0.071)
Intake bores set 2 width – in (m)	2.60 (0.066)
Intake bores set 3 width – in (m)	2.48 (0.063)
Intake bores set 4 width – in (m)	2.20 (0.056)
Number of exhaust ports	5
Exhaust ports height – in (m)	4.29 (0.109)
Exhaust ports width – in (m)	2.20 (0.056)
Fuel Injection Mode	High-pressure fuel injection
Prechamber design	OEM PCC
Chemical Mechanism	Berkeley
Baseline Injection Pressure (psi)	500
Baseline Injection Timing (deg ATDC)	-120 to -100
Ignition Timing (deg ATDC)	-1.5
Turbulent Prandtl number	0.9
Turbulent Schmidt number	0.78
Start time (deg ATDC)	-250
End time (deg ATDC)	-110
Maximum convection CFL limit	1

Maximum diffusion CFL limit	20
Maximum Mach CFL limit	500
Droplet motion time-step control multiple	1.5
Sector Angle (deg)	360
Orifice Discharge Coefficient	0.86
Top Ring Height (m)	0.0196
Top Ring Width (m)	0.00022
Crankcase Pressure (Pa)	84116
Crevice Region Temperature (K)	480
Rings 2, 3, and 4 Width (m)	0.0117
Rings 2, 3, and 4 Thickness (m)	0.00635
Rings 2, 3, and 4 Mass (kg)	3.403
Rings 2, 3, and 4 Gap (m)	0.00643
Rings 2, 3, and 4 Initial Position (m)	0

The CFD model simulated a complete two-stroke cycle, encompassing both scavenging and combustion processes. For the baseline case, fuel injection was configured at a pressure of 500 psi and an injection timing of 120 degrees BTDC. This setting, identified as the nominal point from previous engine operations, demonstrated minimized fuel consumption, formaldehyde, and NOx emissions at an SOA

value of -120 degrees [40]. The combustion pressure in the main cylinder was calibrated based on the LoPP from prior experimental data [2] by adjusting the ignition timing. A stable grid of 8 mm was employed along the Cartesian x, y, and z axes. The Courant-Friedrichs-Lewy (CFL) conditions for the two-stroke cycle of the engine model were determined and applied. The initial, minimum, and maximum time-steps used were 5e-07, 5e-07, and 2e-05 seconds, respectively.

The solver utilized successive over-relaxation (SOR) methods to resolve equations associated with momentum, pressure, density, energy, species, turbulent kinetic energy (TKE), dissipation rate, elliptic relaxation function, velocity scale ratio, radiation, wall distribution [41]. Berkeley's GRI 3.0 chemical mechanism was incorporated into this model, encompassing 5 elements, 53 species, and 325 reactions [42], [43], [44].

3.2.2.2 Late Cycle High-Pressure Fuel Injection

The subsequent CFD cases conducted after the baseline aimed to evaluate the effects of late-cycle high-pressure fuel injection on methane presence in the ring pack and blowby. The injection pressures and timing configurations were consistent with those used in the experimental study detailed in the preceding sections, focusing on 500 psi and 650 psi fuel injection. For each pressure, the start of admission was assessed at 120, 100, 80, and 60 degrees BTDC.

The injection duration for the 650-psi fuel injection was calculated under the assumption that it is inversely proportional to injection pressure, based on a given duration of 20 degrees for the 500-psi case. The mixing level in the main cylinder was quantified using $\emptyset_{SD}$, a measure of heterogeneity that reports the standard deviation of the equivalence ratio across all spatial points in the main combustion cylinder. This parameter, described by Equation 1, ranges between 0 and 1.

3.2.2.3 Quantifying Sources of Methane Emissions

The sources of methane emissions analyzed in this study included the main combustion chamber (MCC), the ring pack, and the blowby. To quantify the methane emissions from the MCC, the amount of methane left in the MCC at the end of the combustion cycle (110 degrees ATDC) was multiplied by the scavenging efficiency. This assumption was made to account for any remaining residual methane from a previous cycle that remained in the MCC after scavenging. The scavenging efficiency was assumed to be equal to the complement of the water percentage in the MCC after the scavenging process (from 131.2 to 233.7 degrees ATDC). It is described mathematically in equation 3 below:

$$Scavenging\ efficiency = 1 - \frac{H_2O_{233.7degATDC}}{H_2O_{131.2degATDC}} \qquad \text{Equation 3}$$

Where:

$H_2O_{233.7degATDC}$ = mass of water in the MCC at the beginning of scavenging

$H_2O_{131.2degATDC}$ = mass of water in the MCC at the end of scavenging

The methane emissions from the ring pack was quantified using the amount of methane remaining in the ring pack crevice volume after a complete cycle and obtained from the simulation output files. To quantify the amount of methane blowby through the ring pack to the crankcase vent, the mass fraction of methane in the ring pack (quotient of mass of ring pack methane by the mass of all species in the ring pack) was multiplied by the total amount of blowby through the ring pack. This assumption was made after the actual amount was calculated from the simulation results in terms of time from the given values at every crank angle degree, using the engine speed and time conversion factors.

3.3 Results

3.3.1 Experimental Results

3.3.1.1 Pressure Traces, LoPP, and COVs of Peak Pressures and IMEP

The results from the experiments on the GMV-4TF engine demonstrate its performance and emission characteristics. Table 3-3 summarizes the average peak pressures and their locations for all data points. The peak pressure locations for all data points were consistently at 18 ± 1 degrees ATDC, except for an outlier with fuel injection at 150 psi and 95 degrees BTDC, where the peak pressure occurred at 15.2 degrees ATDC. This deviation was due to less control of the peak pressure because of poor combustion performance. For the nominal condition of fuel injected at 500 psi and 120 degrees BTDC, the cylinder pressure trace during the experimental tests is shown in Figure 3-9, along with the mean cycle. The mean cycle is a calculated representation, and the cycle closest to this mean in terms of LoPP (Location of Peak Pressure) is referenced. The LoPP for this cycle is 17.1 degrees, with a peak pressure of 535.3 psi, which falls within the typical range for the engine.

The initial pre-combustion chamber sweep done on the engine yielded an optimal (minimum) COV of peak pressure of 5.33% at the operating pre-chamber supply pressure of 17.8 ± 2.0 psi. This range of PCC pressure was used at all data points while testing. The COVs of peak pressure are shown in Figure 3-10 against the start of admission values. The SOA values get later in the cycle, going from left to right. All the points are well below the acceptable maximum value of 10% and indicate acceptable engine stability during the experiments. Figure 3-11 shows the COV of indicated mean effective pressure (IMEP), and all points are below the maximum acceptable COV of IMEP (3%). The outliers are extreme points for very early injection of fuel at 500 psi and 140 degrees BTDC and very late injection of fuel at 150 psi and 95 degrees BTDC.

Table 3-3 Summary of engine average peak pressures, COVs of peak pressures, and location of peak pressures

Injection Pressure (psi)	Start of Admission (degrees)	Engine Average COV PP (%)	Average Peak Pressures (psi)	Average Location of Peak Pressures (degrees)
150	-145	6.31	539	18.0
	-135	5.43	556	17.8
	-115	5.97	558	18.2
	-95	7.28	583	15.2
300	-135	7.03	527	18.6
	-115	5.38	535	18.0
	-95	4.59	553	17.0
	-75	8.35	565	18.6
500	-140	8.10	524	18.9
	-120	5.59	539	17.8
	-100	5.80	522	18.6
	-80	4.83	574	17.3
	-60	8.46	557	18.6

650	-120	6.00	538	18.0
	-100	5.83	526	18.5
	-80	4.96	573	17.5
	-60	7.47	567	18.2

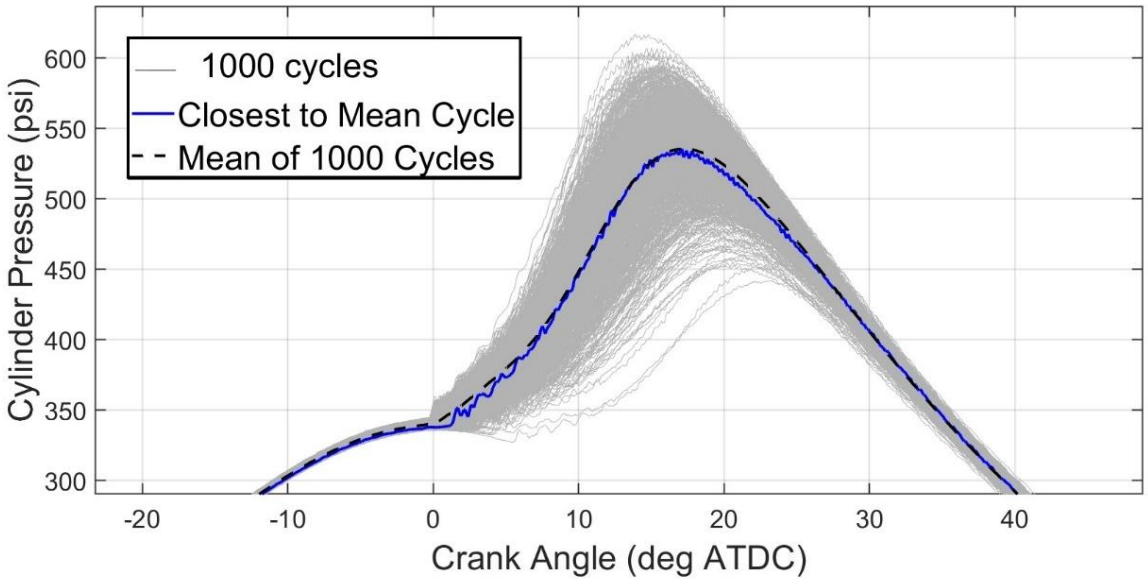

Figure 3-9 Cylinder Pressure Trace for Nominal Point (500 psi Injection Pressure, -120 degrees Start of Admission) at 300 rpm, 440 bhp (330 bkW)

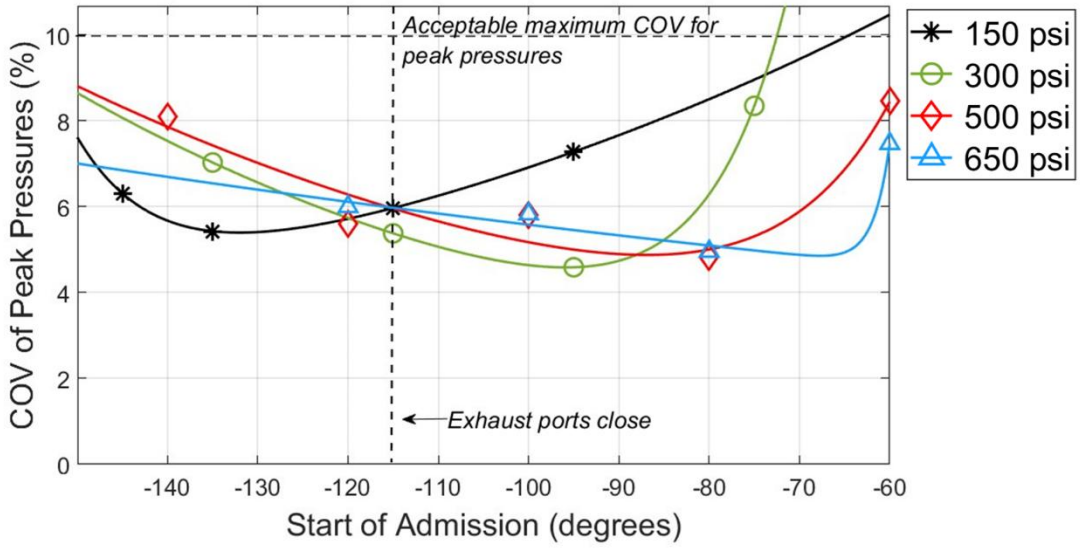

Figure 3-10 COV of Peak Pressures versus Start of Admission Values at 300 rpm, 440 bhp (330 bkW)

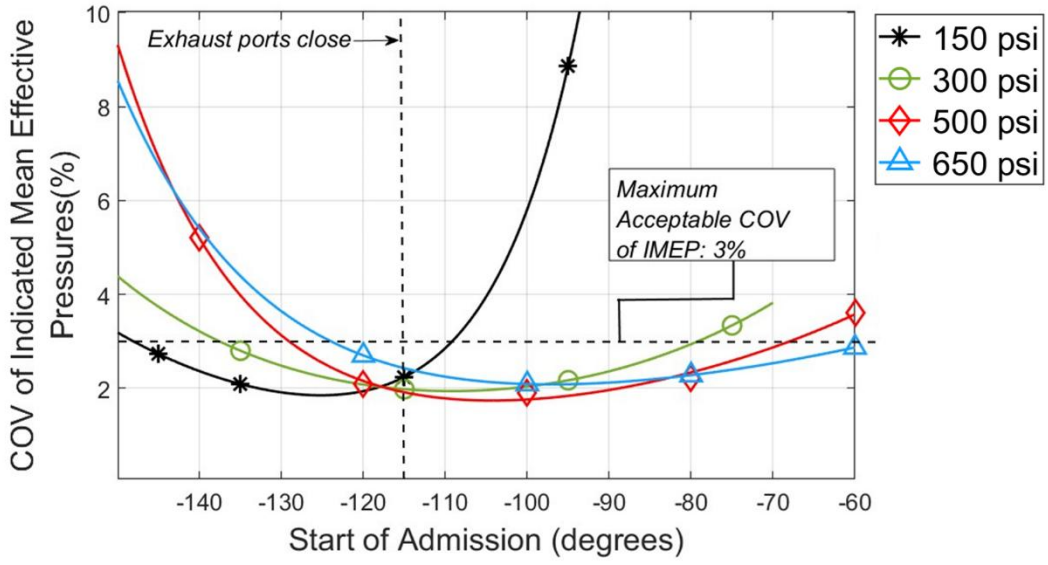

Figure 3-11 COV of IMEP versus Start of Admission Values at 300 rpm, 440 bhp (330 bkW)

The injection duration decreased as the pressure increased, as illustrated in Figure 3-12. At 150 psi, the

injection duration seems excessively long, whereas at 650 psi, it appears too short. These extreme durations at 150 psi and 650 psi are due to the closed-loop engine speed feedback control system regulating the injection duration. The poor combustion performance at 150 psi causes the duration to be longer than anticipated when compared to the baseline pressure of 500 psi, deviating from the expected inverse relationship between injection pressure and duration.

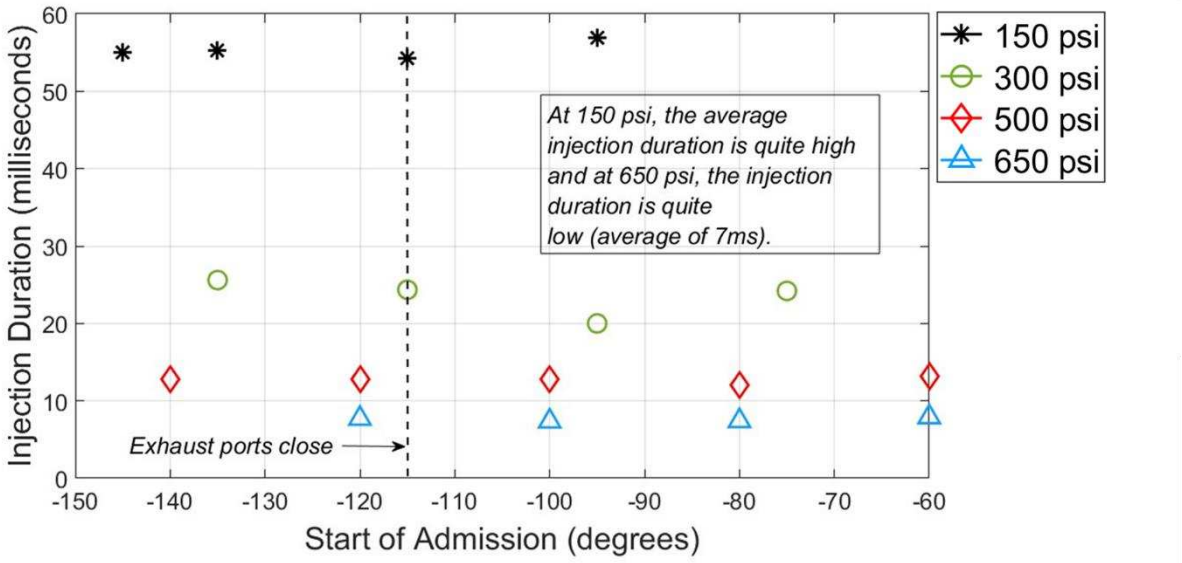

Figure 3-12 Injection Duration versus Start of Admission Values at 300 rpm, 440 bhp (330 bkW)

3.3.1.2 Brake Specific Fuel Consumption and Thermal Efficiency

Figure 3-13 illustrates the brake-specific fuel consumption (BSFC) under varying fuel injection conditions. For fuel injected at 150 psi, BSFC slightly decreases with later injection timings and then sharply declines at the start of admission (SOA) value of 95 degrees BTDC. Generally, BSFC is significantly higher at 150 psi compared to other pressures, corroborating the earlier observation of poor

combustion performance at this pressure. The BSFC values for 300 and 650 psi show a slight decreasing trend with later fuel injection at all SOA values. For 500 psi, BSFC initially decreases and then stabilizes with late-cycle fuel injection.

Figure 3-14 shows brake thermal efficiency (BTE), which follows an inverse trend to BSFC. Both fuel consumption and brake thermal efficiency trends with late-cycle fuel injection result from more effective fuel conversion when fuel is injected after exhaust ports close, allowing more time for fuel and air mixing. As injection pressure increases, overall performance improves (lower BSFC and higher BTE) due to increased fuel jet momentum and enhanced mixing. However, the performance at 650 psi is not as good as at 300 and 500 psi, likely due to the extremely short injection duration at 650 psi. When injection durations are below 10 ms, the time required to open and close the fuel valve constitutes a significant portion of the duration, leading to increased variability in fuel delivery (injected mass per event) and greater combustion instability.

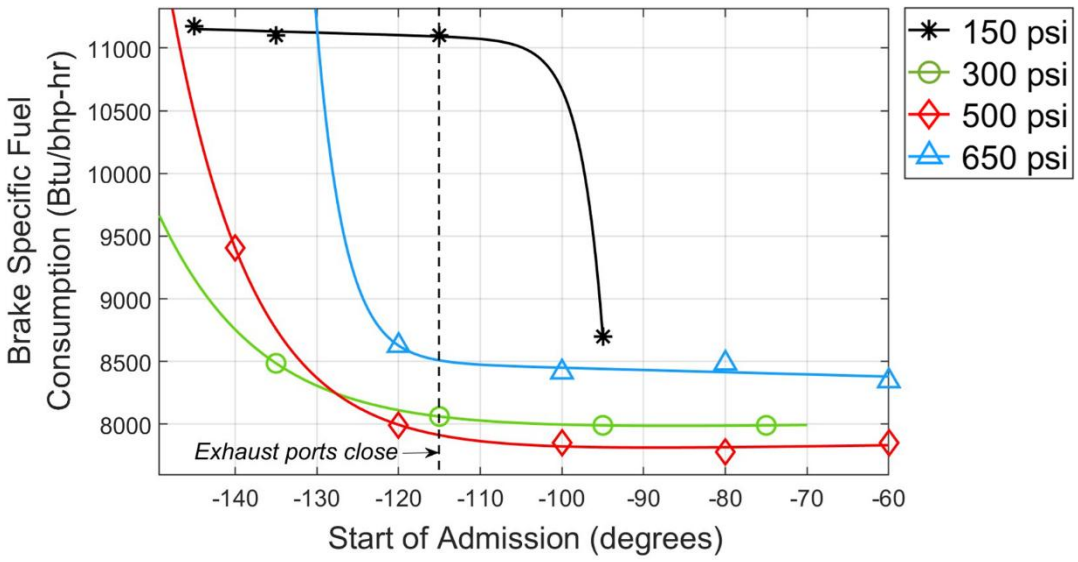

Figure 3-13 Brake Specific Fuel Consumption versus Start of Admission Values at 300 rpm, 440

bhp (330 bkW)

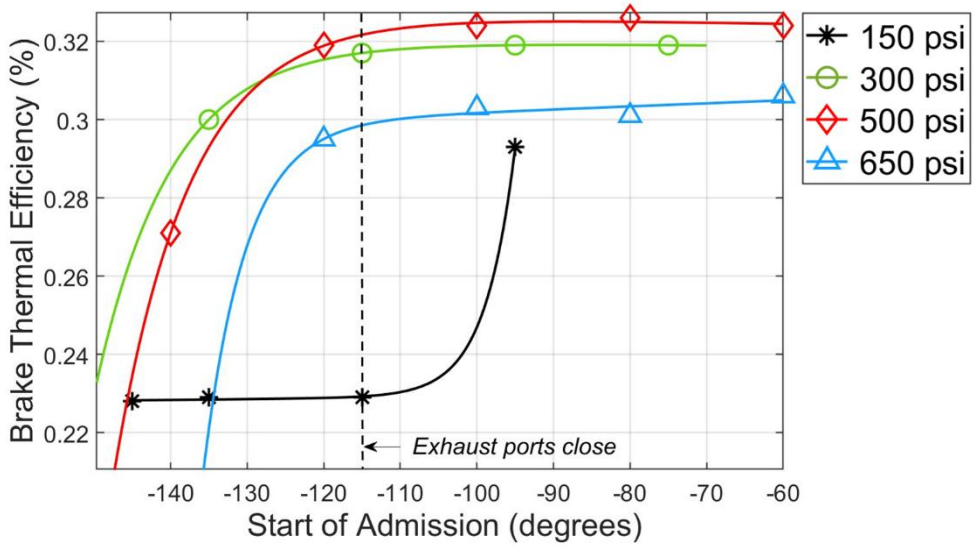

Figure 3-14 Brake Thermal Efficiency versus Start of Admission Values at 300 rpm, 440 bhp (330 bkW)

3.3.1.3 Emissions

Figure 3-15 presents methane emissions versus injection SOA for four different injection pressures. The general trends mirror those observed for BSFC, except for the 150 psi cases, which exhibit emissions levels more comparable to the other pressures. Overall, methane emissions are minimized at the earliest injection timing when fuel delivery occurs after the exhaust ports close.

Figure 3-16 shows the optimal points for all injection pressures where the minimum exhaust methane emissions are recorded. The optimal points are at -115 degrees for 150 and 300 psi fuel injection and -100 degrees for 500 and 650 psi. The lowest methane emissions occur at a fuel injection pressure of 500 psi with an SOA of -100 degrees.

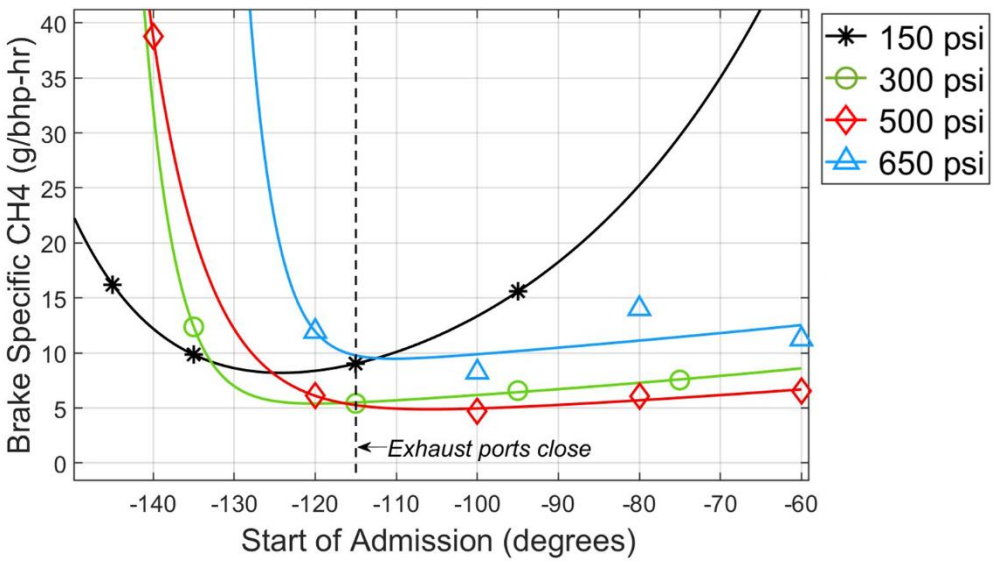

Figure 3-15 Brake Specific Exhaust Methane Emissions versus Start of Admission Values at 300 rpm, 440 bhp (330 bkW).

Figure 3-17 displays the crankcase vent methane concentration, measured in ppm, at various test points. When fuel is injected at 500 psi, the methane concentration in the crankcase decreases steadily at later SOA values. Similarly, for 150, 300, and 650 psi, there is a reduction in crankcase methane concentration with later fuel injection in the cycle. This trend contrasts with the exhaust methane emissions, which showed a minimum near exhaust port closure. Figure 3-18 presents the brake-specific crankcase methane emissions. For 500 psi, there is an initial decrease in crankcase methane emissions, followed by a slight increase at -80 degrees, and a further slight decrease at -60 degrees. The minimum brake-specific crankcase methane concentration occurs at -60 degrees for 500 psi fuel injection. Compared to the exhaust, brake-specific crankcase methane emissions are relatively small due to the smaller crankcase mass flow. However, the concentration (ppm) of crankcase methane emissions is higher than that of the exhaust methane concentration.

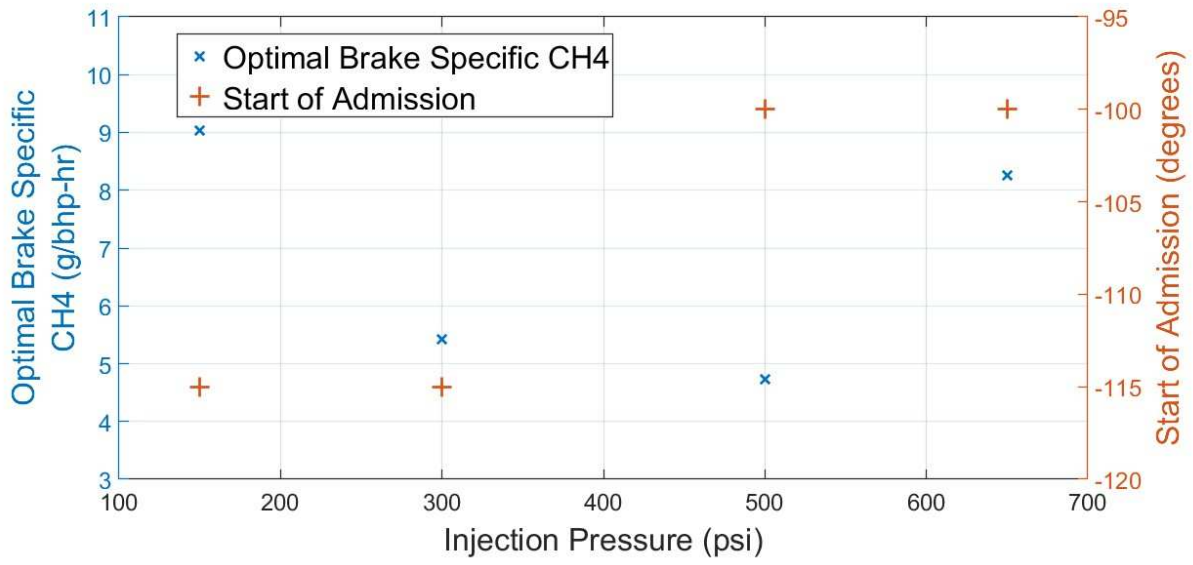

Figure 3-16 Optimal Methane Emissions for each Injection Pressure and their corresponding Start of Admission Values at 300 rpm, 440 bhp (330 bkW)

Figure 3-19, Figure 3-20, Figure 3-21, and Figure 3-22 present the trends of other emissions – carbon monoxide, formaldehyde, total hydrocarbons, and volatile organic compounds respectively. The carbon monoxide and formaldehyde emissions show a similar trend with an initial decrease in the emissions and an increase after the optimal points for each pressure for SOA values after the exhaust ports close at -115 degrees. The trends for total hydrocarbons and VOCs indicate an initial decline but stabilize for SOA values after the exhaust ports closed except for the 150 psi cases which start to increase with late-cycle fuel injection (injection after the exhaust ports close).

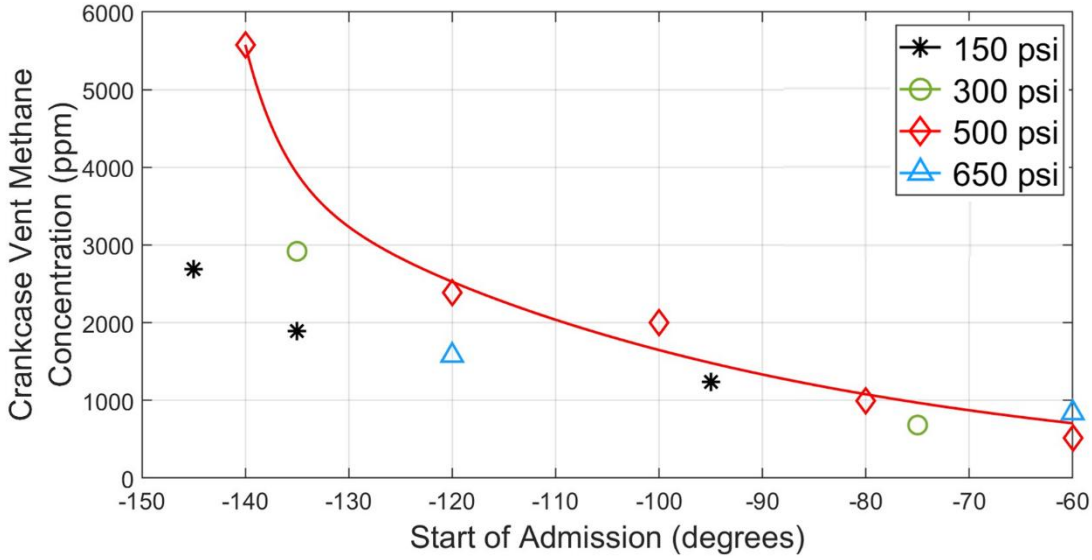

Figure 3-17 Crankcase Vent Methane Concentration versus Start of Admission Values at 300 rpm, 440 bhp (330 bkW)

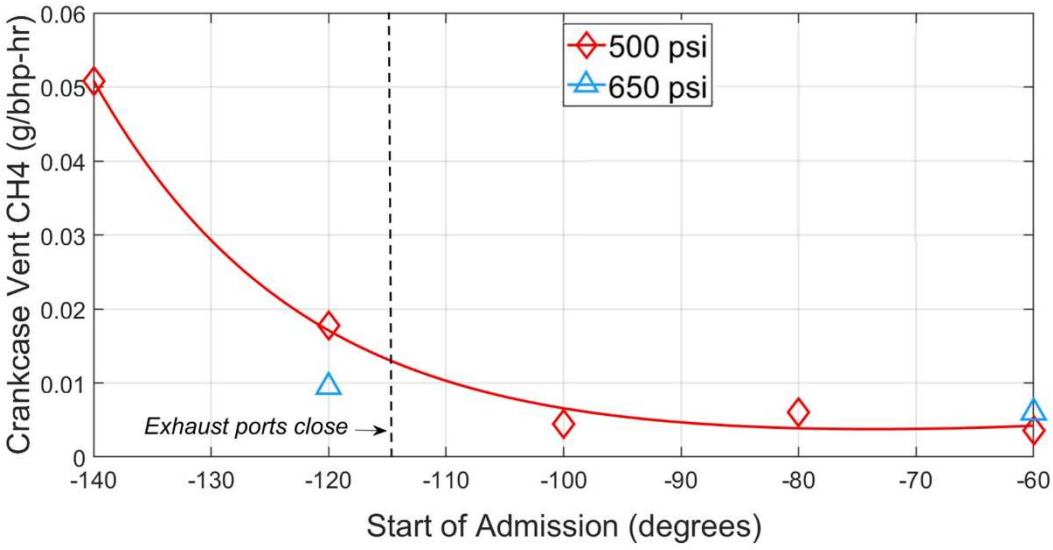

Figure 3-18 Brake Specific Crankcase Vent Methane versus Start of Admission Values at 300 rpm,

440 bhp (330 bkW)

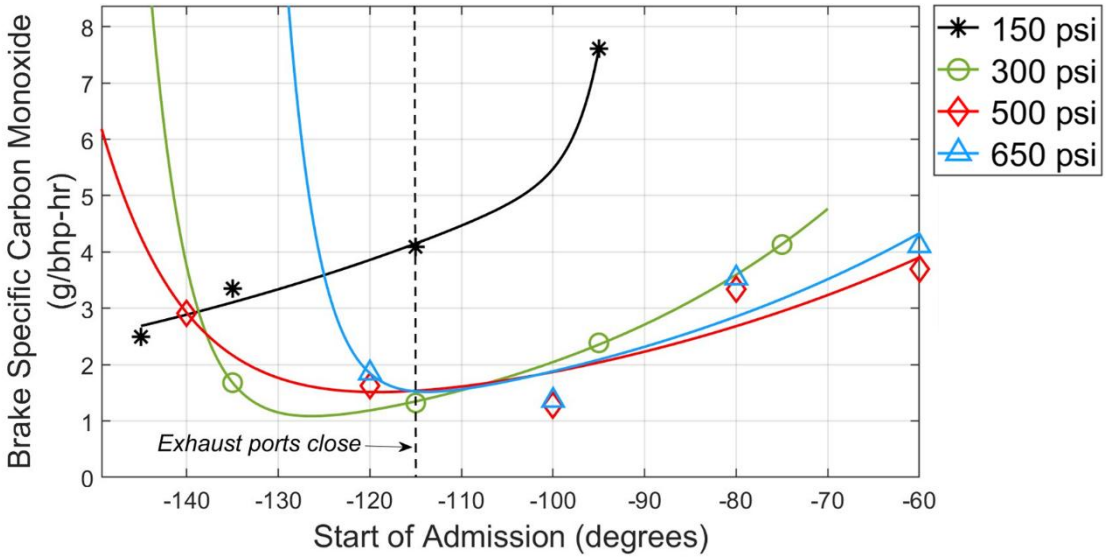

Figure 3-19 Brake Specific Carbon Monoxide versus Start of Admission Values at 300 rpm, 440 bhp (330 bkW)

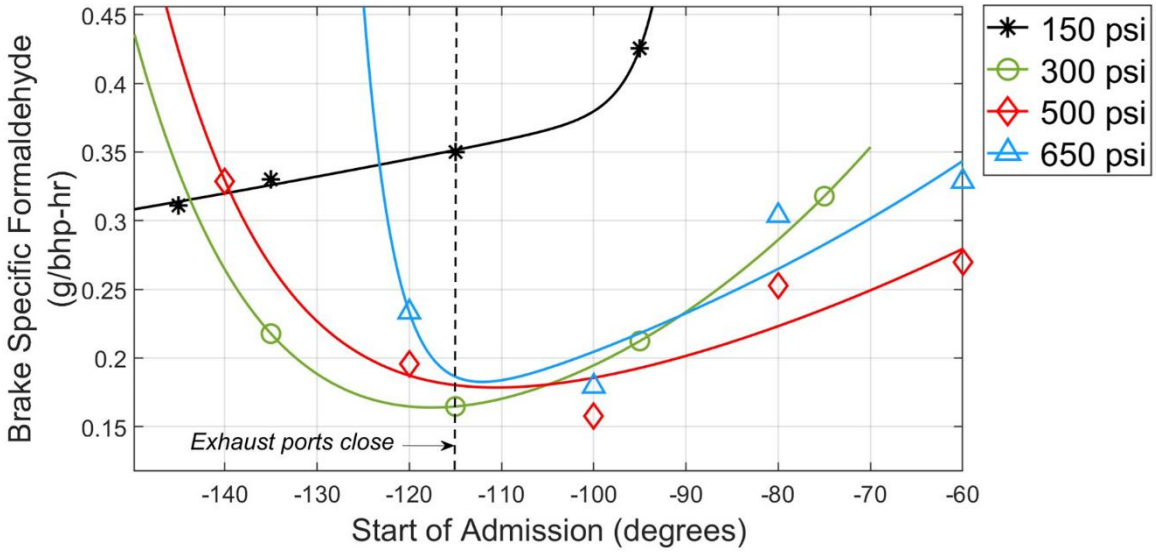

Figure 3-20 Brake Specific Formaldehyde versus Start of Admission Values at 300 rpm , 440 bhp

(330 bkW)

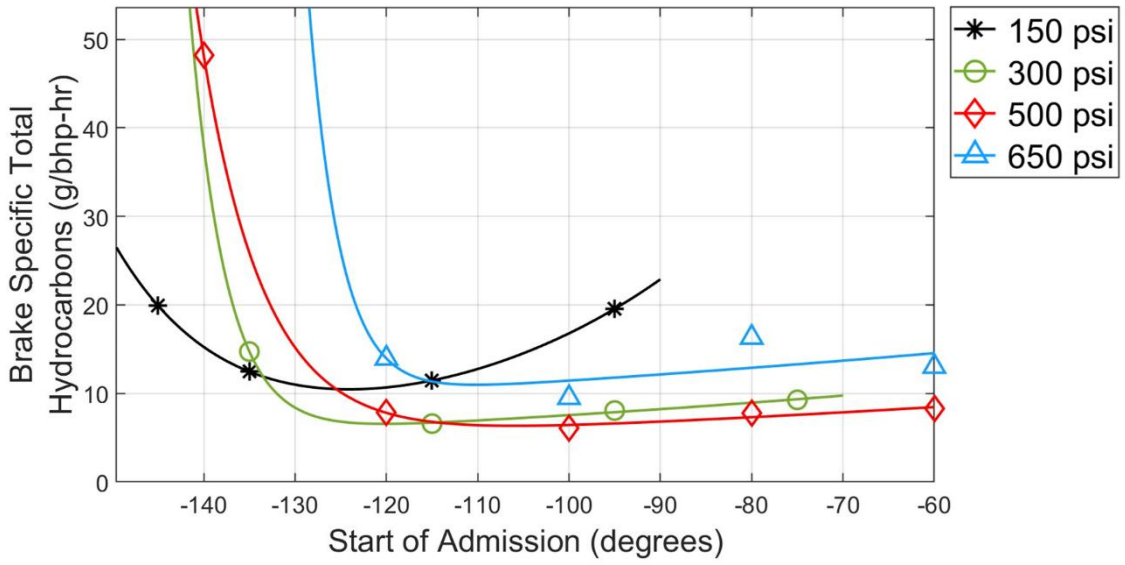

Figure 3-21 Brake Specific Total Hydrocarbon versus Start of Admission Values at 300 rpm , 440 bhp (330 bkW)

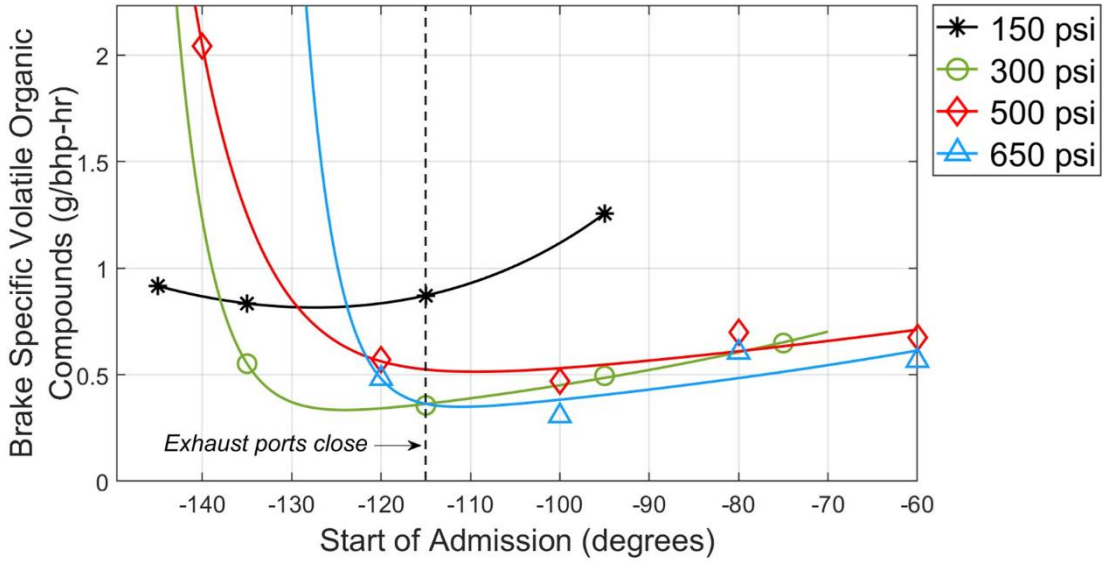

Figure 3-22 Brake Specific Volatile Organic Compounds versus Start of Admission Values at 300

rpm, 440 bhp (330 bkW)

3.4 CFD Results

The baseline CFD simulation was performed using Converge Studio, incorporating the crevice volume model for an injection pressure of 500 psi and an SOA value of -120 degrees, as used in the experimental study. Figure 3-23 shows the cylinder pressure trace, which was validated against experimental data based on the peak pressure location. The trapped air volume depends on the pressure drop assumptions between the intake air pressure sensor and the intake system boundary, as well as between the exhaust system boundary and the exhaust manifold pressure sensor. Ignition timing was adjusted to match the peak pressure location and amplitude. Other key parameters, such as the fuel delivered per cycle, manifold pressures and temperatures, and engine speed, were sourced from experimental data. The peak pressure for the CFD baseline was 477.84 psi, occurring at 17.9 degrees. While the CFD baseline trace falls within the experimental data range, its peak pressure is below average. Despite this, the baseline case was deemed sufficient, as the primary aim of the study was to examine the relative effects of different fuel injection pressures and timing values, rather than fine-tuning the baseline case.

The equivalence ratio standard deviation values range from 0 to 1, with 0 indicating perfect mixing and 1 indicating the worst level of mixing. Figure 3-24 illustrates the level of in-cylinder mixing at the ignition point (-1.5 degrees) for each CFD case at 500 and 650 psi. The 650 psi cases demonstrate better mixing compared to the 500 psi cases across all SOA values, confirming the beneficial impact of high-pressure fuel injection on mixing. However, for both 500 and 650 psi fuel injections, mixing quality deteriorates as the SOA values become later in the cycle. This decline in mixing quality is attributed to the reduced time between injection and spark in late-cycle fuel injection scenarios.

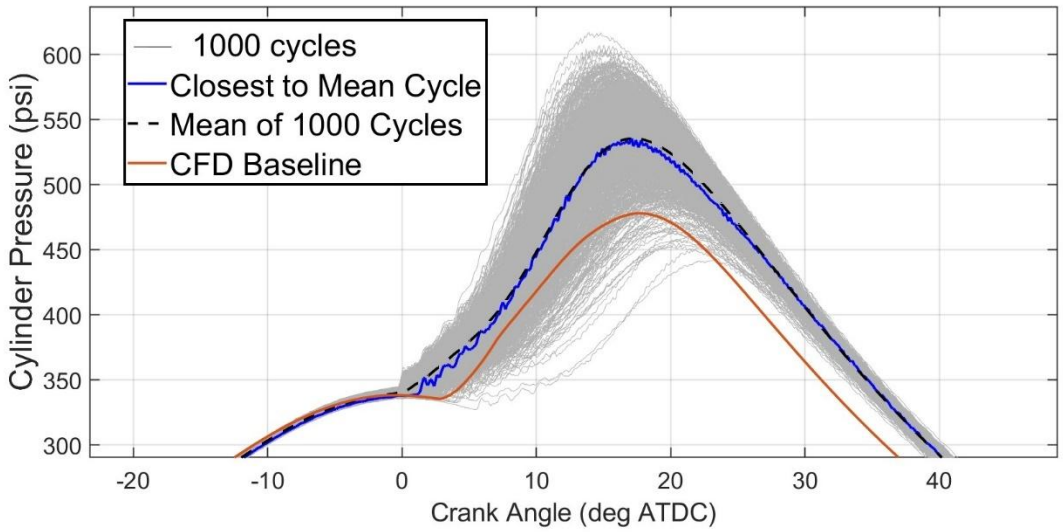

Figure 3-23 Cylinder Pressure Trace of the CFD Baseline (fuel injection pressure of 500 psi, SOA value of -120 degrees) in Converge CFD model at ~300 rpm, 440 bhp (330 bkW) for one cylinder compared with Experimental Data (Cylinder #2).

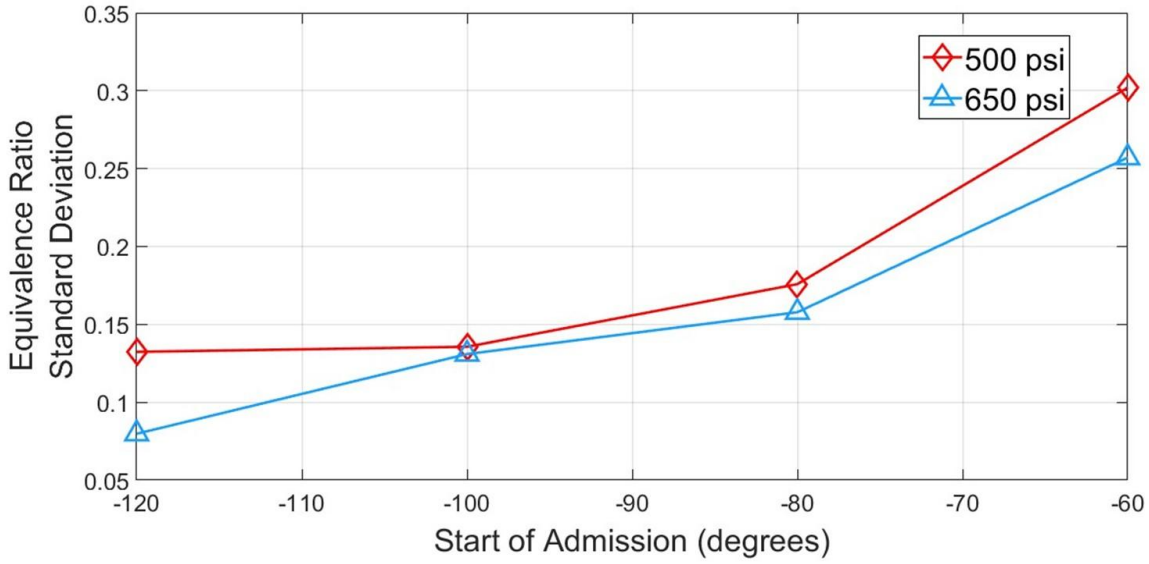

Figure 3-24 Equivalence Ratio Standard Deviation vs Start of Admission at 500 and 650 psi fuel

injection in Converge CFD model at ~300 rpm, 440 bhp (330 bkW).

Figures 3-24 to 3-28 shows the methane mass fraction distribution in the main combustion chamber (MCC) at five (5) crank angle degrees during the engine cycle up to 110 crank angle degrees, reflecting the mixing levels and amount of methane residual in the MCC. Figure 3.29 illustrates the methane flow to the exhaust from the MCC for each simulation. This value was determined by multiplying the methane residual in the MCC at the end of a combustion cycle by the scavenging efficiency. For the 500 psi cases, the exhaust methane emissions from the MCC decrease as the SOA moves later in the cycle, with an increase observed at -60 degrees. The 650 psi cases exhibit a similar trend, increasing initially and then decreasing steadily at -100 degrees. At SOA values of -120 and -60 degrees, the 650 psi case results in lower methane emissions from the MCC compared to the 500 psi case. However, for SOA values of -100 and -80 degrees, the 500 psi cases outperform the 650 psi cases by producing lower methane emissions from the MCC.

The ring pack, comprising four compression rings on the piston of the GMV-4TF engine model in Converge, creates crevice volumes in the engine, as depicted earlier in Figure 3-8. Figure 3-31 illustrates the movement of the rings compared to the methane within the ring pack throughout a complete cycle for the baseline scenario. Ring 1, the topmost ring, exhibits negligible motion until 62 crank angle degrees, at which point it displaces by 7.62×10^{-5} m. According to the sign convention, zero displacement signifies the ring is positioned at the bottom of the piston, while a positive displacement indicates movement towards the top of the piston. Ring 2 shows oscillation, reaching a maximum displacement of 7.62×10^{-5} m between -61 and -13 crank angle degrees as it moves within its slot in the ring pack. Ring 3 also oscillates, reaching a maximum displacement of 7.62×10^{-5} m between -70 and 39 crank angle degrees. Similarly, ring 4 oscillates to the same maximum displacement from -70 to 67 crank angle degrees. Within these oscillation ranges, the amount of methane in the ring pack increases rapidly. Both the ring

movements and the increased methane accumulation are attributed to the pressure differential between the main combustion chamber (MCC) and the ring pack. The peak pressure region in the MCC corresponds to where the highest volumes of methane are pushed into the ring pack.

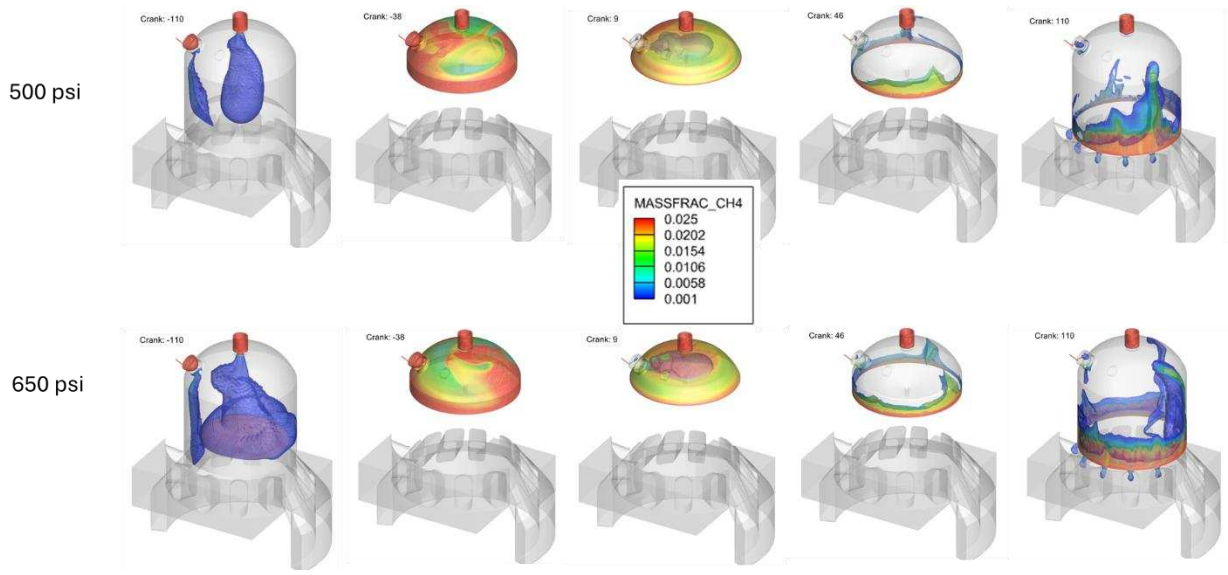

Figure 3-25 MCC Methane Mass Fraction for Fuel Injection with Start of Admission at -120 degrees (Injection Pressures: 500 and 650 psi): -110, -38, 9, 46, and 110 Crank Angle Degrees.

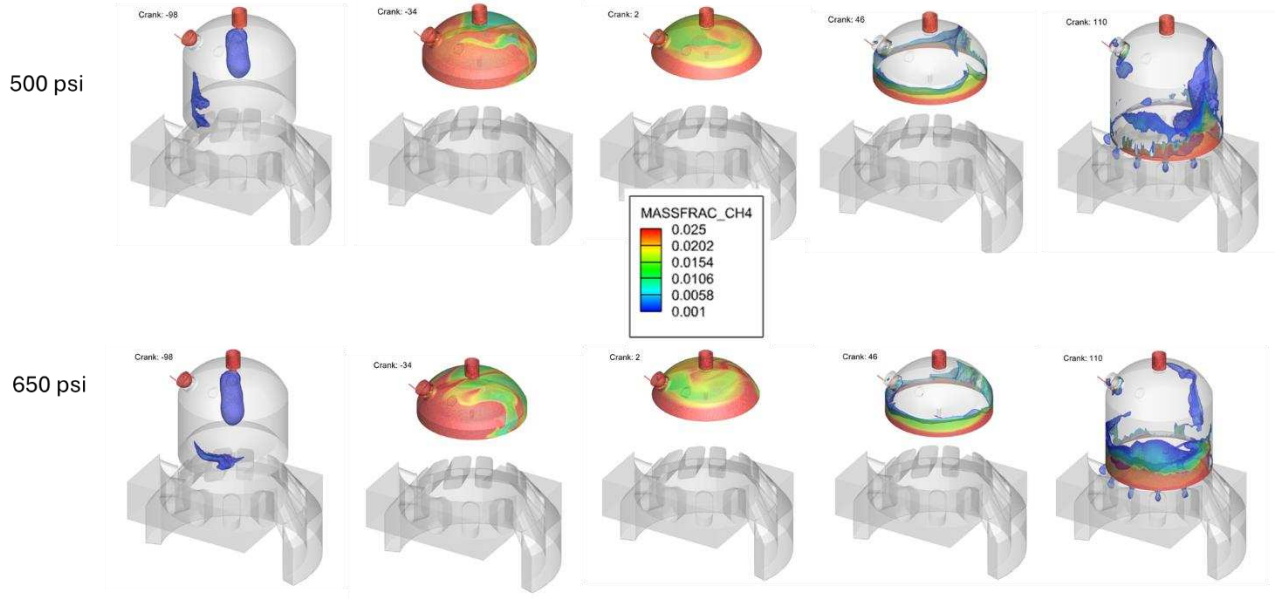

Figure 3-26 MCC Methane Mass Fraction for Fuel Injection with Start of Admission at -100 degrees

(Injection Pressures: 500 and 650 psi): -98, -34, 2, 46, and 110 Crank Angle Degrees.

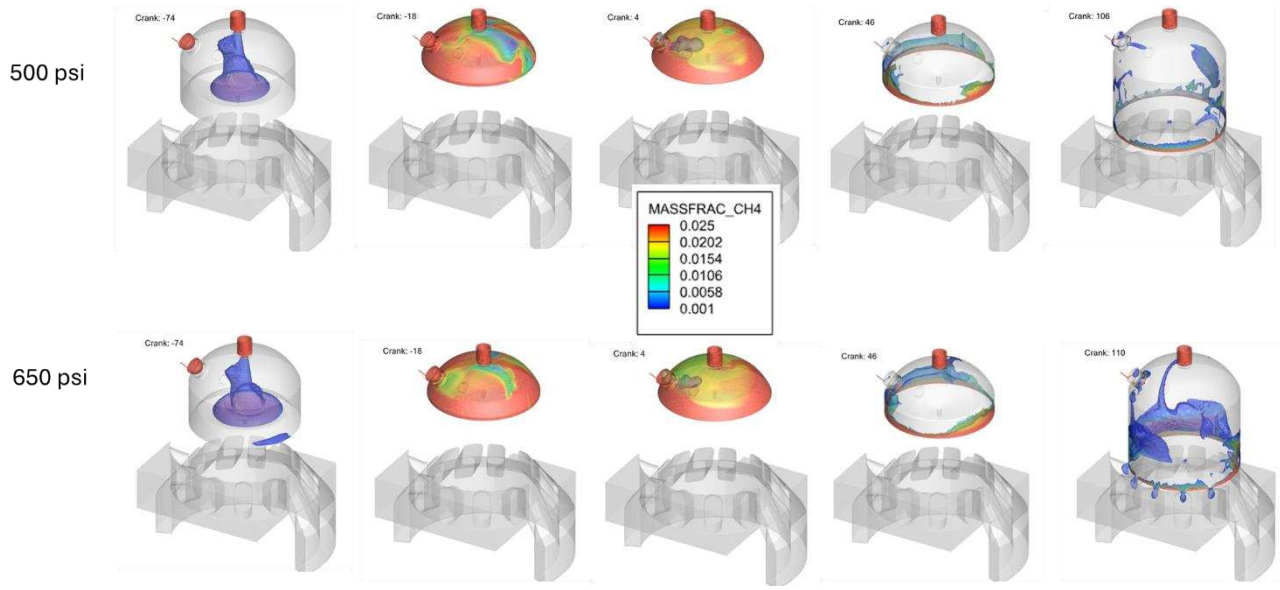

Figure 3-27 MCC Methane Mass Fraction for Fuel Injection with Start of Admission at -80 degrees

(Injection Pressures: 500 and 650 psi): -74, -18, 4, 46, and 110 Crank Angle Degrees.

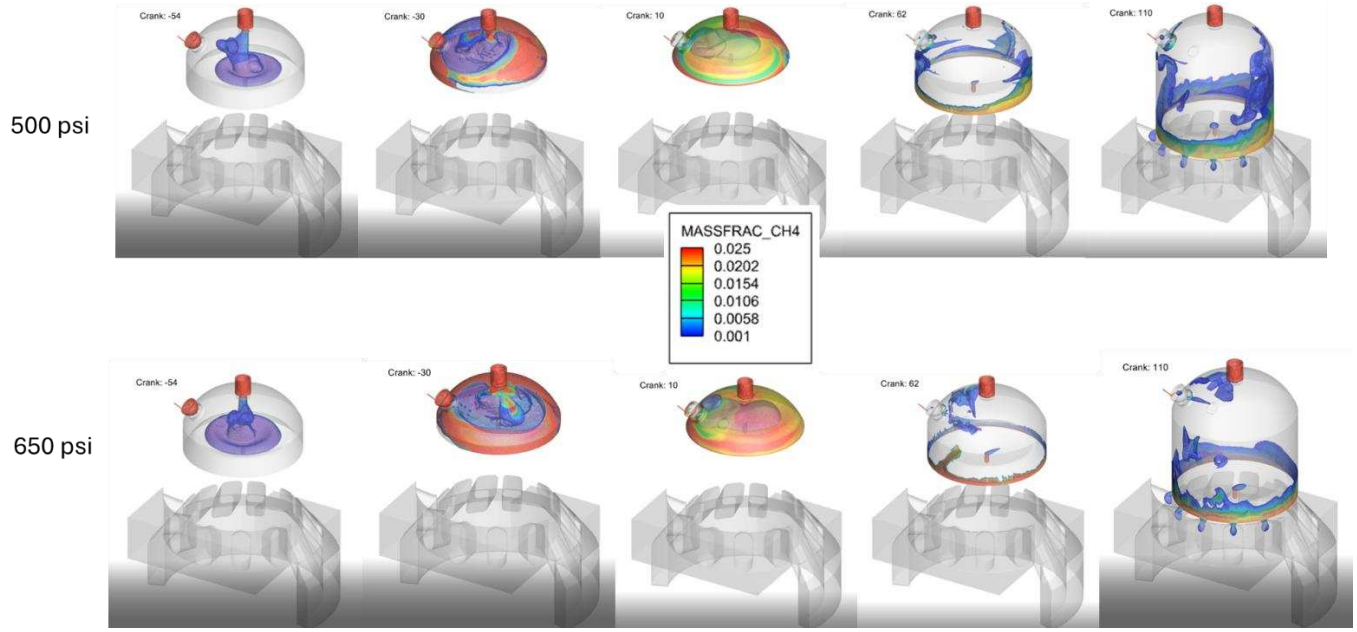

Figure 3-28 MCC Methane Mass Fraction for Fuel Injection with Start of Admission at -60 degrees

(Injection Pressures: 500 and 650 psi): -54, -30, 10, 62, and 110 Crank Angle Degrees.

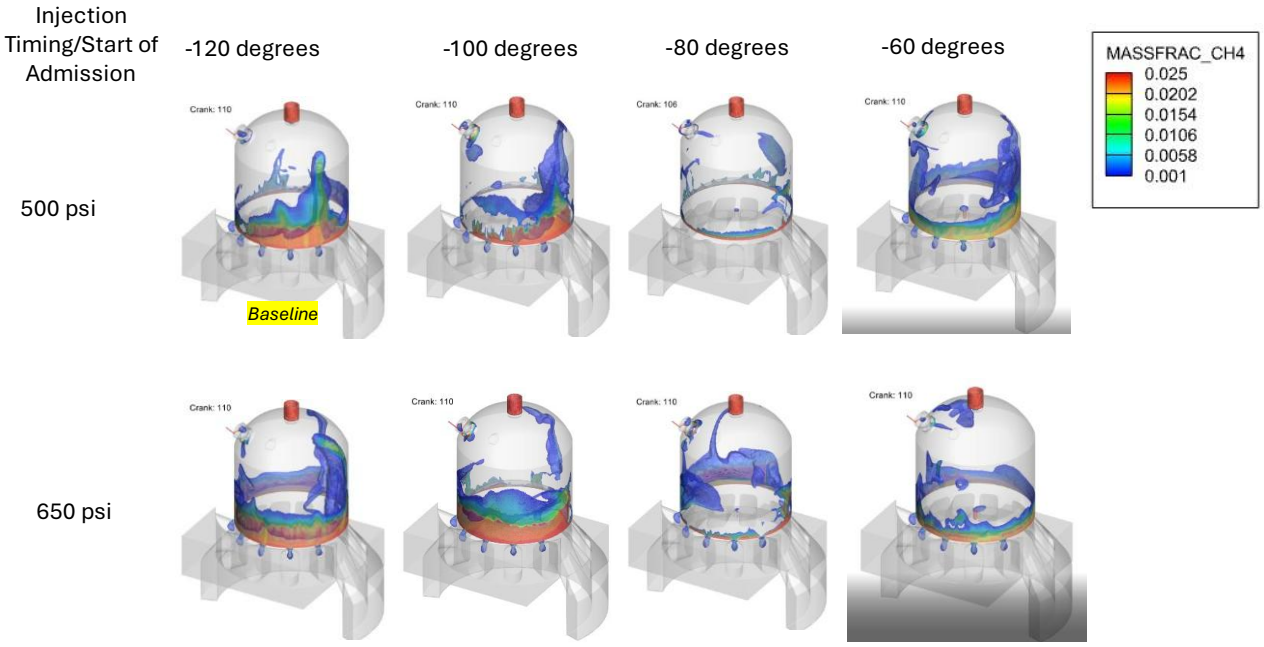

Figure 3-29 MCC Methane Residual Mass Fraction at the end of Engine Cycle at 110 Crank Angle Degrees with Start of Admission ranging from -120 to -60 degrees (Injection Pressures: 500 and 650

psi).

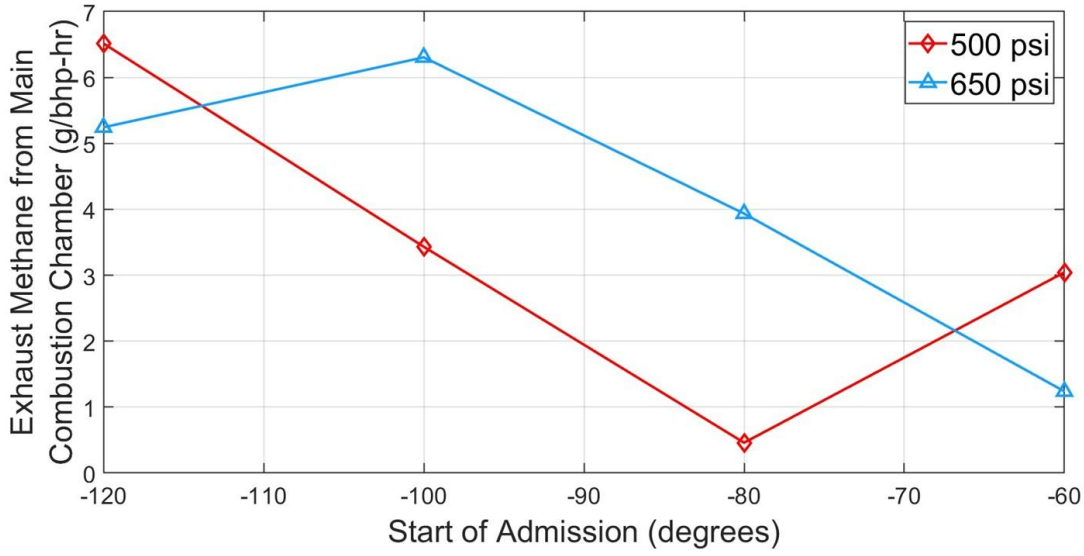

Figure 3-30 Methane Outflow from Main Combustion Chamber to Exhaust vs Start of Admission at 500 and 650 psi fuel injection in Converge CFD model at ~300 rpm, 440 bhp (330 bkW).

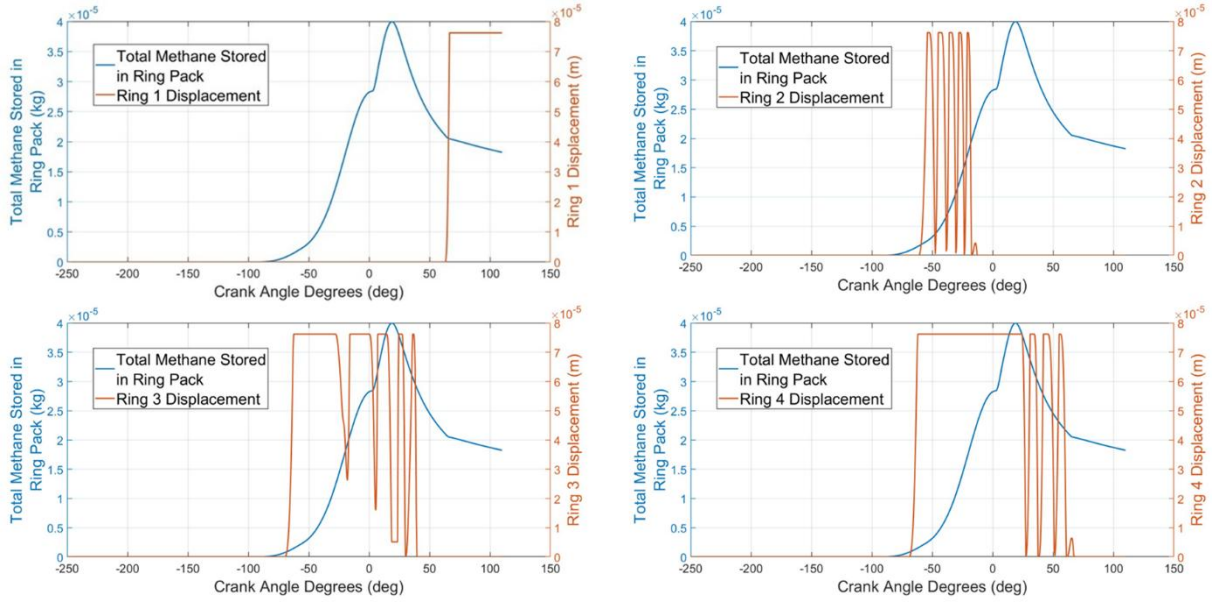

Figure 3-31 Piston Compression Rings Movements relative to Total Methane Stored in the Ring

Pack as the piston moves from -250 CAD to 110 CAD at an injection pressure of 500 psi and SOA of -120 degrees in Converge CFD model at ~300 rpm, 440 bhp (330 bkW).

Figure 3-32 shows the amount of methane remaining in the ring pack at the end of a combustion cycle (at 110 degrees). For fuel injection at 500 psi, the methane residue in the ring pack initially decreases at an SOA value of -100 degrees, peaks at -80 degrees SOA, and then reaches its lowest value at -60 degrees SOA. In the case of 650-psi fuel injection, the methane residue first increases at -100 degrees SOA but follows a decreasing trend for the subsequent cases. Overall, for both 500 and 650 psi fuel injection, the minimum methane residue in the ring pack occurs at -60 degrees SOA, which is late in the cycle.

Figure 3-33 illustrates the amount of methane flowing through the ring pack (blowby) into the crankcase for all the CFD cases. For 500 psi fuel injection, methane blowby initially decreases at -100 degrees SOA, increases at -80 degrees SOA, and then decreases to its minimum value at -60 degrees SOA. For 650 psi fuel injection, methane blowby slightly increases at -100 degrees SOA before steadily decreasing. In both 500 psi and 650 psi cases, the minimum methane blowby through the ring pack occurs at -60 degrees SOA.

Figure 3-34 presents a flowchart detailing the flow of the methane portion of the injected fuel in the main combustion chamber for the baseline case. It indicates that 92.3% (by mass) of the methane introduced into the engine combustion system undergoes complete combustion. The remaining 7.7% is emitted through various pathways: 4.9% (by mass) through the MCC, 2.6% (by mass) through the ring pack, and 0.2% (by mass) through the crankcase vent.

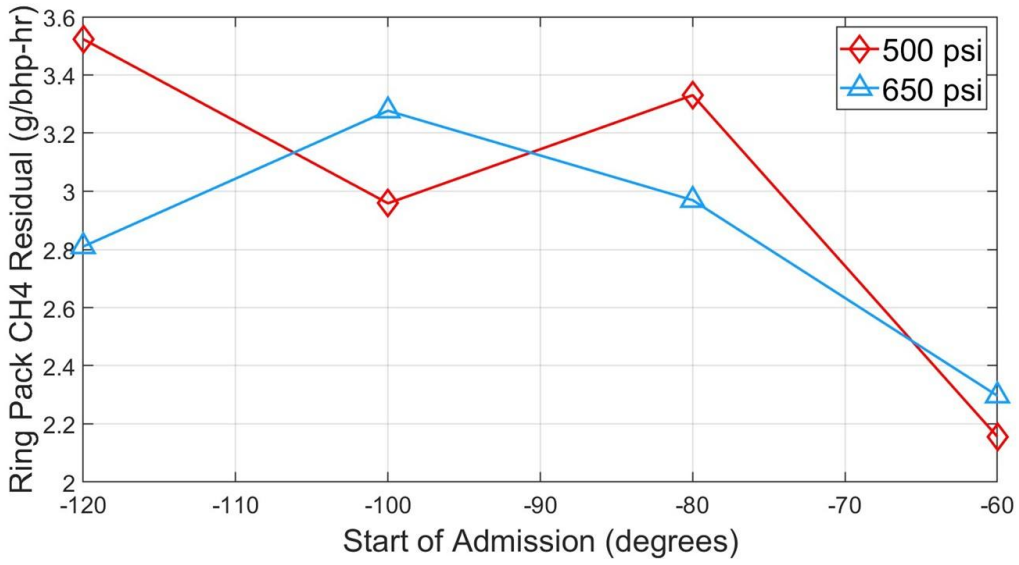

Figure 3-32 Ring Pack Methane Residual at the end of a cycle (110 CAD) vs Start of Admission at 500 and 650 psi fuel injection in Converge CFD model at ~300 rpm, 440 bhp (330 bkW).

The contributions of the MCC, ring pack, and crankcase vent (blowby) to methane emissions from the engine for the baseline case are illustrated in Figure 3-35. These percentages are derived from the brake-specific values for the various sources of methane emissions. The methane residual in the ring pack, caused by the pressure differential between the main combustion chamber and the ring pack (trapped between the rings and the piston wall), leads to methane outflow to the exhaust during expansion, contributing to overall methane emissions. The results indicate that the ring pack significantly contributes 33.7% of the engine's total methane emissions.

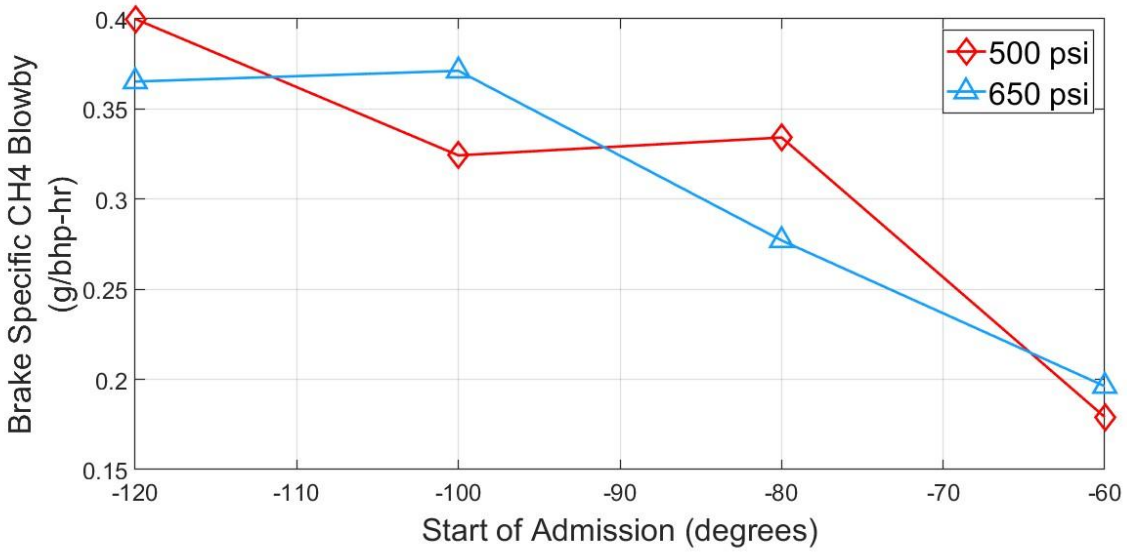

Figure 3-33 Methane Blowby Across the Ring Pack to Crankcase Vent vs Start of Admission at 500 and 650 psi fuel injection in Converge CFD model at ~300 rpm, 440 bhp (330 bkW).

The CFD results predicted that 0.2% of the injected methane in the GMV engine is emitted as blowby across the ring pack to the crankcase vent. During the experimental study, the fuel flow into the GMV engine at the nominal point (injection pressure: 500 psi, SOA: -120 degrees) was 199.8 lb/hr at 439.9 bhp. With 77.6% of the natural gas by mass being methane, as indicated by gas chromatography (GC) data, the injected methane was 182.3 g/bhp-hr. As shown in Figure 3-17 and Figure 3-18, the methane concentration and brake-specific value of methane gas in the crankcase vent were 2383 ppm and 0.02 g/bhp-hr, respectively, accounting for only 0.01% of the injected methane.

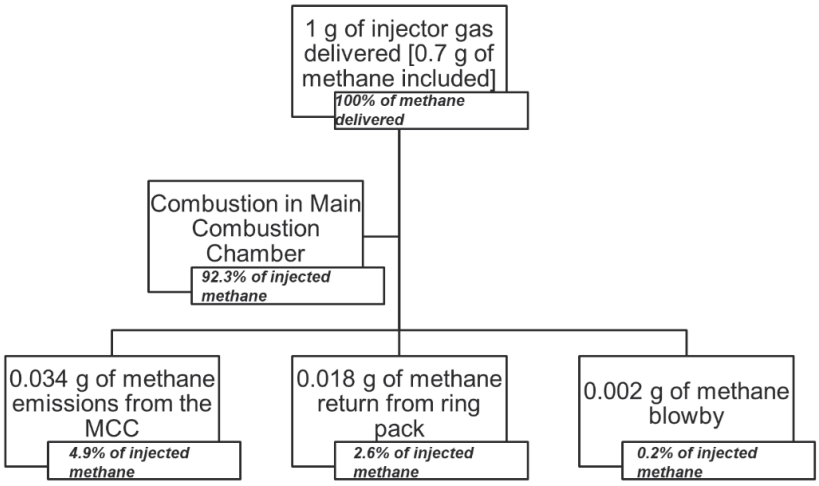

Figure 3-34 Methane Emissions Relative to Mass of Methane Delivered to the main combustion chamber at an injection pressure of 500 psi and SOA of -120 degrees in Converge CFD model at ~300 rpm, 440 bhp (330 bkW) for one cylinder.

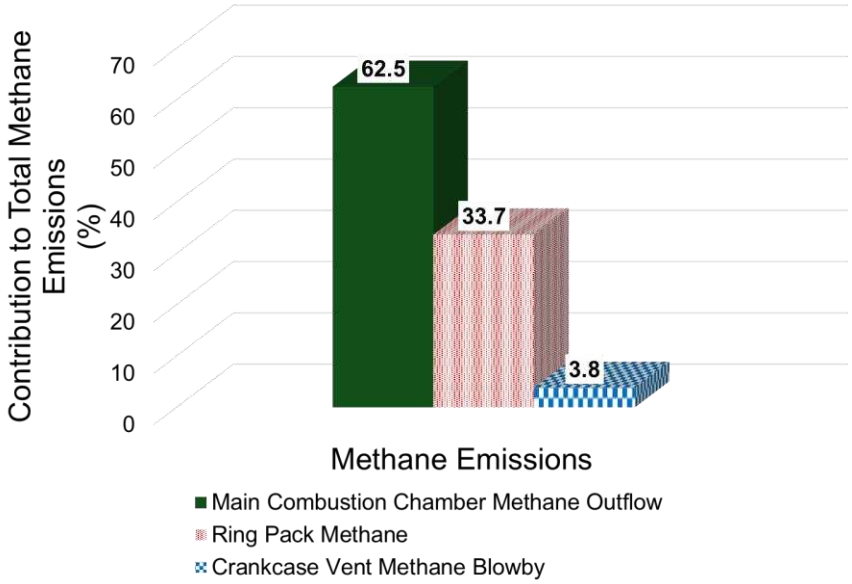

Figure 3-35 Contribution of the MCC, Ring Pack, and Crankcase Vent to Methane Emissions at an injection pressure of 500 psi and SOA of -120 degrees in Converge CFD model at ~300 rpm, 440 bhp

(330 bkW) for one cylinder.

Figure 3-36 presents the total methane emissions observed in both experimental and computational studies for fuel injection pressures of 500 and 650 psi at SOA values ranging from -120 to -60 degrees. The experimental data encompasses methane emissions from the exhaust and the crankcase vent gas, while the computational data includes emissions from the MCC, the ring pack, and the blowby. For 500 psi fuel injection, the optimal points for total methane emissions occur at -100 degrees SOA in the experimental study and -60 degrees SOA in the computational study. At the nominal point (injection pressure: 500 psi, SOA: -120 degrees), CFD predicts that 7.7% of the injected methane escapes complete combustion, while experimental results show only 4% of the injected methane as emissions. The higher predicted percentage of unburned methane in the CFD simulations, compared to the lower percentage observed in the crankcase vent, is attributed to oxidation in the exhaust ports and exhaust manifold, which is not accounted for in the CFD model.

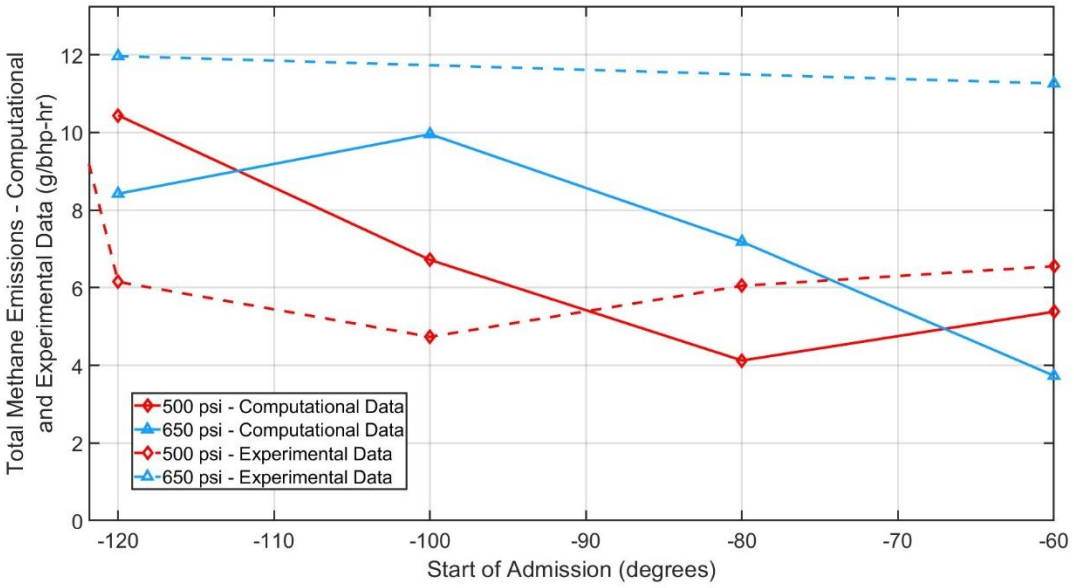

Figure 3-36 Total Methane Emissions at an injection pressure of 500 psi and SOA of -120 degrees in Converge CFD model at ~300 rpm, 440 bhp (330 bkW) for one cylinder. Experimental data comprising of exhaust methane emissions and crankcase vent methane gas; Computational data comprising of MCC outflow to exhaust, ring pack methane and blowby.

3.5 Discussion

The exploration of fuel injection pressure and timing, conducted in this chapter, showed that fuel injection timing has a strong impact on methane emissions in the exhaust and crankcase of large-bore engines. The experimental data showed the effects of low-pressure fuel injection and the advantages of high-pressure fuel injection, as well as late-cycle fuel injection. The computational results were all based on the baseline case set up for CFD simulations. All the results in this study are relevant to understanding the mechanisms of methane emissions in large bore engines and are critical to mitigating these emissions.

There is an optimal point for exhaust methane emissions based on injection timing for every injection pressure, and it occurs at the first injection timing encountered after the exhaust ports close. This can be

attributed to the varying mixing levels, which result from turbulence levels and the time available for mixing [25], [26]. This behavior is consistent with the unburned hydrocarbons (UHC), both measured and from simulations, observed in a previous study, which also showed a trend of UHC reducing as the port injection timing went later in the cycle and eventually increasing after the optimal point [14]. The lowest methane emissions are encountered with fuel injection at a pressure of 500 psi and an SOA value of -100 degrees, which constitutes a 22.4% decrease from the nominal point (500 psi, -120 degrees SOA) methane emissions. There are no performance penalties or emission penalties for this methane emission reduction at the optimal point, as the COVs are minimized and fuel consumption is reduced. There are also no NOx emissions penalties due to the NOx control loop [34] employed, keeping NOx constant. There are also reduced CO, THC, VOCs, and Formaldehyde emissions at the optimal points for 500 and 650 psi, but it is not necessarily so for the cases at 150 and 300 psi, where these emissions tend to increase with late-cycle fuel injection due to the lower pressure levels not being enough for adequate mixing in the short time available for late-cycle fuel injection.

Late-cycle fuel injection reduces crankcase methane emissions. Crankcase methane emissions are influenced by fuel injection timing as shown by both experimental results and results from computational simulations. The measured crankcase vent methane in the experimental study has a constant decline at 500 psi as the SOA values move later in the cycle. The amount of methane blowby through the ring pack also declines with late-cycle fuel injection, as shown through the simulation results. The percentage of crankcase gas emissions to total methane emissions measured from the engine (0.3%) is slightly less than the percentage obtained in a similar study [35] on the same engine (0.5%). However, the constant decrease in the same measurement environment validates the impact of late cycle fuel injection on reducing methane emissions.

The ring pack contributes a significant portion to methane emissions. Approximately one-third of the

methane emissions from large bore engines come from methane residuals in the crevice volumes in the compression ring pack of the engine. In a different study that examined how significant the inter-ring crevice HC emissions were relative to total HC emissions, it was discovered to contribute 10-30% of the total unburned HC emissions over a range of speeds and loads [45]. Another study also showed that when the top land was minimized, the total hydrocarbons for high compression ratio (CR) pistons were minimized [46].

Though the percent reduction of crankcase methane emissions is impressive (93%), crankcase methane constitutes a small portion of total methane emissions from the engine (< 0.5%). The late-cycle exhaust methane reduction of 23% is dependent on the nominal HPFI injection timing and duration [17]. The result suggests that operators with HPFI systems should re-optimize injection timing in the context of minimizing methane emissions, which most likely was not a consideration when the HPFI system was commissioned.

Future studies will evaluate the limits of existing fuel injection systems for high-pressure and investigate better ways of achieving high-pressure fuel injection with sufficient injection durations. To further explore the benefits of late-cycle high-pressure fuel injection, the concept will also be implemented in the field.

4. Impact of Top-land Crevice Modeling Approach on Methane Emissions

4.1 Overview

Some unburned natural gas of lean-burn natural gas engines flows to the piston ring-pack crevices during compression when the cylinder pressure exceeds that of the crevice volume regions and escapes complete combustion in the cylinder [47]. After getting trapped in the ring-pack, methane returns to the cylinder during the latter part of the expansion stroke and eventually gets released through the exhaust.

Previous studies have confirmed the ring-pack contribution to methane emissions in various spark-ignited engines, mostly using the model that describes the side clearance flow as a laminar channel flow and the flow through the top ring end gap as a jet flow [30], [32], [48]. It was initially developed in 1982 by Namazian and Heywood [42]. A study based on it modeled two compression rings and one oil ring in an engine ring-pack crevice model using a KIVA-II program [47]. The authors discovered that an increase in the piston-cylinder side clearance resulted in increased hydrocarbon (HC) emissions and concluded that a decrease in the piston-cylinder side clearance should concurrently lead to reduced HC emissions, and that a reduction in the ring-end gap area had no significant influence on unburned HC emissions at the end of expansion. Another study used an Xybion Model ISG-350 camera to acquire Planar Laser Induced Fluorescence (PLIF) images from an SI engine piston-cylinder setup [49]. Unburned fuel leaving the upper ring-land crevice was observed, and it was concluded that the process controlling such escape of HC emissions is a function of the azimuthal location around the piston circumference.

More recent studies have also considered the impact of the crevice volume on methane emissions and have used modern technology to examine the action of the ring-pack to find a solution to reducing methane emissions from the angle of the crevice volume. Piston rings have been instrumental in pressure-sealing the combustion chamber and oil control, but the dynamics of gas flow through the crevice is yet to be fully

understood [50]. An approach to evaluating complicated details in engines without having to run the physical engine has been the use of computational fluid dynamics (CFD) [51]. This can be applied to each attempt at understanding or modifying the crevice volume. A study using experimental PLIF and computational methods to evaluate the effects of piston crevice-trapped HC emissions in early-injection compression ignition (CI) engines revealed that the squish zone and crevice had more significant amounts of unburned HC emissions trapped for early injection timing cases [52]. Another numerical study was conducted using CONVERGE, a commercially available CFD software, on a stoichiometric 6.87 L SI natural gas engine converted from a diesel engine with the same displacement volume [53]. It was discovered that a 50% reduction in the piston crevice volume led to a reduction in methane emissions by 57.1% and a reduction in incomplete combustion by 1.85%. These studies have examined the impact of combustion technologies and design modifications to reduce crevice-trapped methane emissions.

One of the combustion technologies that has proven to reduce methane emissions is high-pressure fuel injection and late cycle fuel injection, as it improves the mixing levels in the cylinder and prevents unburned methane from getting into the crevices [27], [29], [54], [55]. In this chapter, the flow through piston ring-pack crevice volumes is examined with different allocations of the top-land crevice with CFD in CONVERGE Studio and visualized using Tecplot for CONVERGE. The grid size for CFD modeling is also optimized to improve accuracy and insight from previous simulations [56] is used to study the crevice-related methane emissions.

4.2 Approach

For this study, the GMV-4TF engine is modeled in SolidWorks and imported into CONVERGE Studio v3.1 for simulations using the built-in crevice model. The built-in crevice model allocates the top-land crevice to the ring pack region. To further evaluate the impact of crevice volume on methane emissions, this study considers two sets of cases where the top-land crevice volume is allocated differently. It also

evaluates the base grid cell size for the second case classification. For all cases, fuel is injected at -120 degrees and an injection pressure of 500 psi. The geometry for all cases remains the same as in Chapter 3, but with different case setup characteristics and top-land crevice allocations. The two sets of cases considered are as follows:

1. Top-land Crevice Modeled in Ring-Pack Region Case (Baseline),
2. Top-land Crevice Modeled in Main Combustion Chamber (MCC) Cases.

4.2.1 Top-land Crevice Modeled in Ring-Pack Region Case (Baseline)

The baseline case for this study was modeled exactly as the baseline in the computational study in chapter 3, but in a more updated version of CONVERGE Studio (version 3.1 as opposed to version 3.0 used in the previous chapters). The ring pack model in the newer version allows for more than two rings and enables inputting details of the four (4) rings of the GMV-4TF engine directly into the CFD simulation case setup, rather than the editing of the *"crevice.in"* input file needed for it to run in CONVERGE Studio v3.0.

The CFD parameters as described in Table 3-2 remain the same for this case, but fuel injection is maintained at a pressure of 500 psi and -120 degrees. The stable base cell grid size for this CFD case is set at 8 mm as previously determined in Chapters 3 and 4 [54], [56]. The level of mixing in the main combustion chamber (MCC) is characterized using the standard deviation of the equivalence ratio of the air-fuel mixture at the ignition point (10 degrees BTDC).

4.2.2 Top-land Crevice Modeled in Main Combustion Chamber (MCC) Cases

The second classification of cases is further modified from the baseline case, with the top-land crevice allocated to the MCC rather than the ring pack region in the engine model. The crevice volume model was used for these cases, but to achieve the allocation of the top-land crevice to the MCC, the top-land crevice height is set to 1 mm, a negligible value compared to the engine bore and stroke, rather than the actual

top-land height of 19.6 mm from the engine measurements and used in the baseline. Proper visualization of the crevice volume was achieved by varying the base grid size across three cases: 8 mm, 6 mm, and 4 mm, and evaluating the effects on methane emissions from the engine. This also provides an assessment of grid independence. Fuel is injected at an injection pressure of 500 psi at -120 degrees, like the fuel injection parameters from the baseline.

4.3 Results from CFD Simulations

4.3.1 Power output

Figure 4-1 shows the pressure-volume plot for the baseline top-land-in-ring-pack case, the 8 mm, 6 mm, and 4 mm grid top-land-in-MCC cases. The area within the curve gives the power output for each case. The results show that the power output for the top-land-in-MCC cases are all slightly (3 to 5%) greater than the baseline, as seen in Figure 4-1. This could be attributed to the reduced crevice volume leakage in the top-land-in-MCC configuration compared to the baseline top-land-in-ring-pack case. By including the top-land crevice in the main combustion chamber (MCC) region, more of the trapped charge is exposed to combustion, leading to more complete fuel burn and increased pressure during the power stroke. Additionally, the finer grid resolutions (8 mm, 6 mm, and 4 mm) improve the resolution of pressure gradients and flame propagation, slightly enhancing the predicted power output.

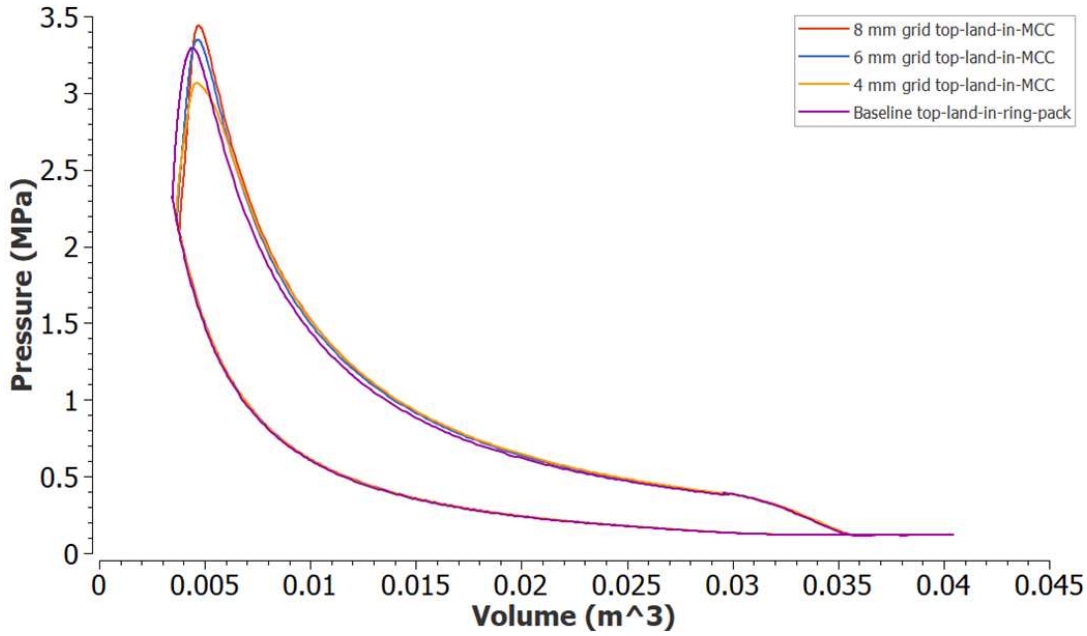

Figure 4-1 P-V Diagram for the Baseline and Top-Land-in-MCC Cases showing Power Output for all the Cases.

Table 4-1 Power Output for the Baseline and Top-Land-in-MCC Cases.

CFD Cases	**Brake Power (bhp)**
8 mm grid top-land-in-MCC	409
6 mm grid top-land-in-MCC	405
4 mm grid top-land-in-MCC	402
Baseline top-land-in-ring-pack	391

4.3.2 MCC Air-Fuel Mixing Levels, Methane Residual and Methane Flow to Exhaust

At the end of the combustion cycle, unburned gases flow out through the exhaust from the MCC along with other exhaust gases. Unburned methane forms part of this outflow because of poor combustion efficiency. Results from the simulations in this study are shown in Figure 4-3, with the methane outflow from the exhaust and mixing levels indicated on the same plot. The methane outflow to the exhaust calculated based on the methane residual in the MCC seen in Figure 4-4 and Figure 4-5, and the scavenging efficiency as explained in Chapter 3, is seen to be lower for the top-land-in-MCC cases than the baseline case, and continues to reduce as the resolution of the CFD case gets finer. The mixing levels also show improvement with reduced heterogeneity for the 8 mm grid top-land-in-MCC case. However, the 4 mm and 6 mm cases show poorer mixing than the 8 mm grid top-land-in-MCC case, but not as poor as the baseline case. The reason for this behavior in mixing quality could be attributed to the complex relationship between mesh resolution and turbulent flow structures in the main combustion chamber. While finer grid resolutions (such as 4 mm and 6 mm) generally allow for better resolution of flow features, they can also alter the numerical dissipation and turbulence representation in a way that does not always enhance mixing uniformly. The 8 mm grid may strike an optimal balance by capturing key bulk flow and swirl motions that promote better fuel-air mixing, while the finer grids might over-resolve small-scale eddies that disrupt coherent mixing patterns or do not contribute significantly to large-scale homogenization.

Moreover, numerical artifacts or under-resolved turbulence in the finest meshes may lead to localized regions of poor scalar transport, particularly in crevice or near-wall regions [57]. The improvement in methane outflow reduction with grid refinement, despite mixing degradation in the 4 mm and 6 mm cases, suggests that mixing quality alone is not the sole driver of methane emissions. The inclusion of the top-land crevice in the MCC plays a more dominant role by exposing more trapped fuel to combustion.

The results show that the simulations are not grid independent. In general, a smaller mesh size yields more

accurate solutions. However, the model was tuned using an 8 mm mesh, so it likely yields the most accurate prediction of bulk parameters like engine power and blow-by flowrate. The motivation for exploring smaller mesh sizes is to gain more insight into top land crevice volume flow phenomena. The use of smaller mesh sizes results in long simulation times, likely making them impractical for most scenarios. Figure 4-2 shows the computational time taken to run each of the cases in this study. The finest case took about 67 days to run, indicating that further evaluation would take a very long time.

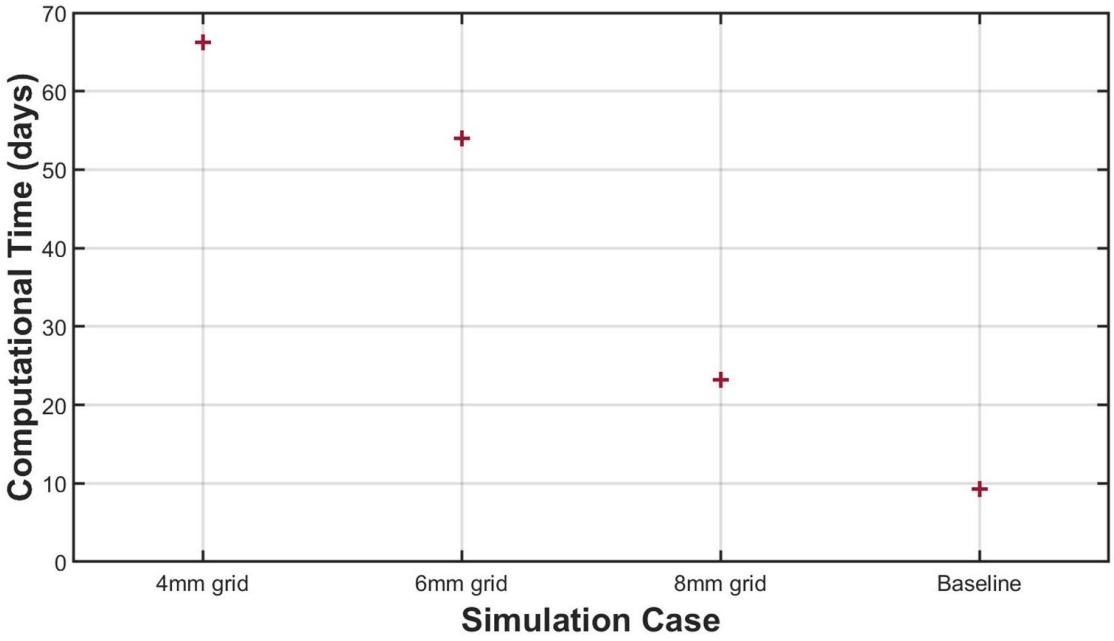

Figure 4-2 Computational Time for the Baseline Top-Land-in-Ring-Pack Case, 8 mm, 6 mm, and 4 mm grid size Top-Land-in-MCC Cases

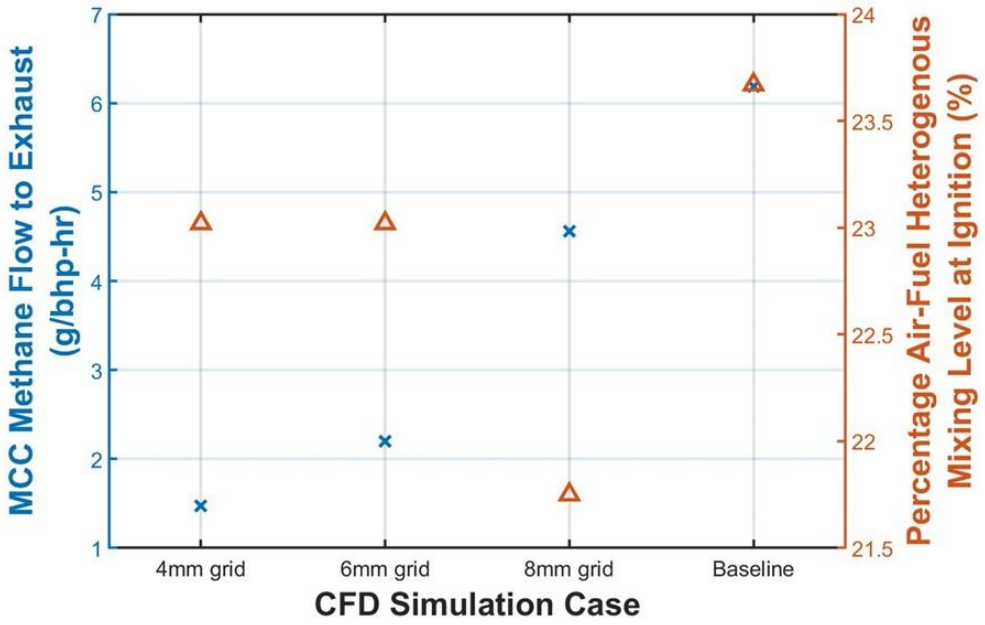

Figure 4-3 MCC Methane Outflow to Exhaust and Percentage of Heterogeneity Measured using the Standard Deviation of the Equivalence Ratio.

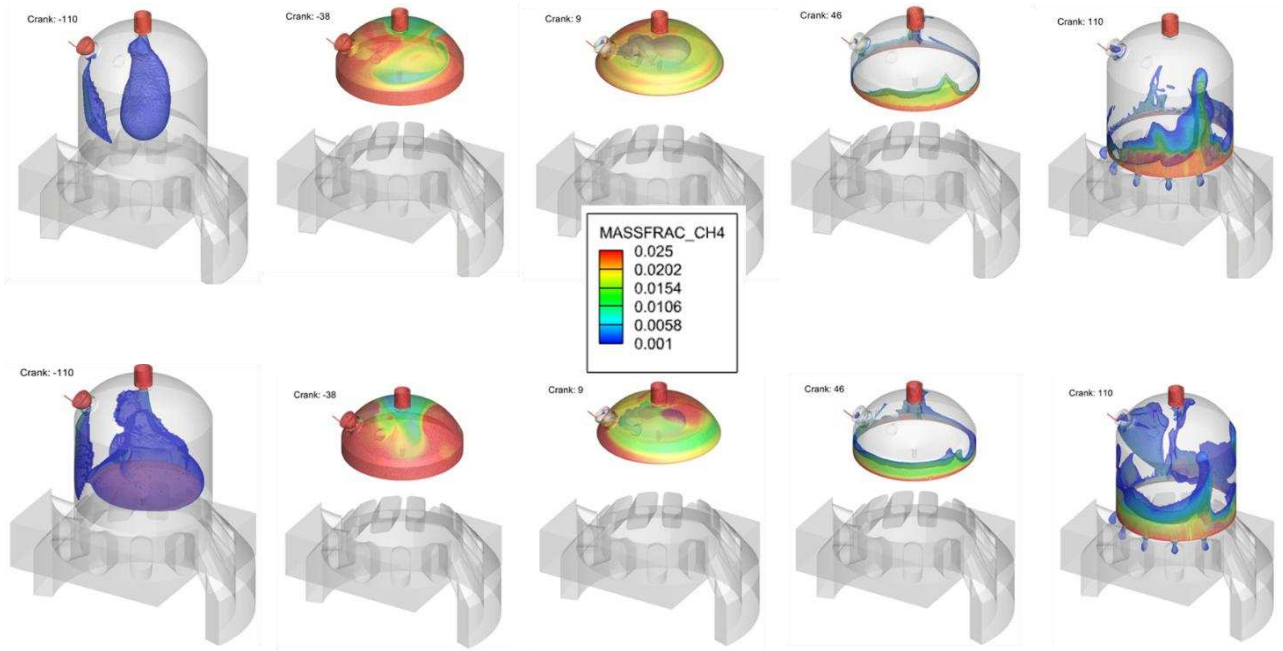

Figure 4-4 3D Contour Plots of MCC Methane Fraction Distribution at -110, -38, 9, 46, and 110

Crank Angle Degrees for the Baseline (Top) and 8mm Grid Top-Land-in-MCC Case (Bottom).

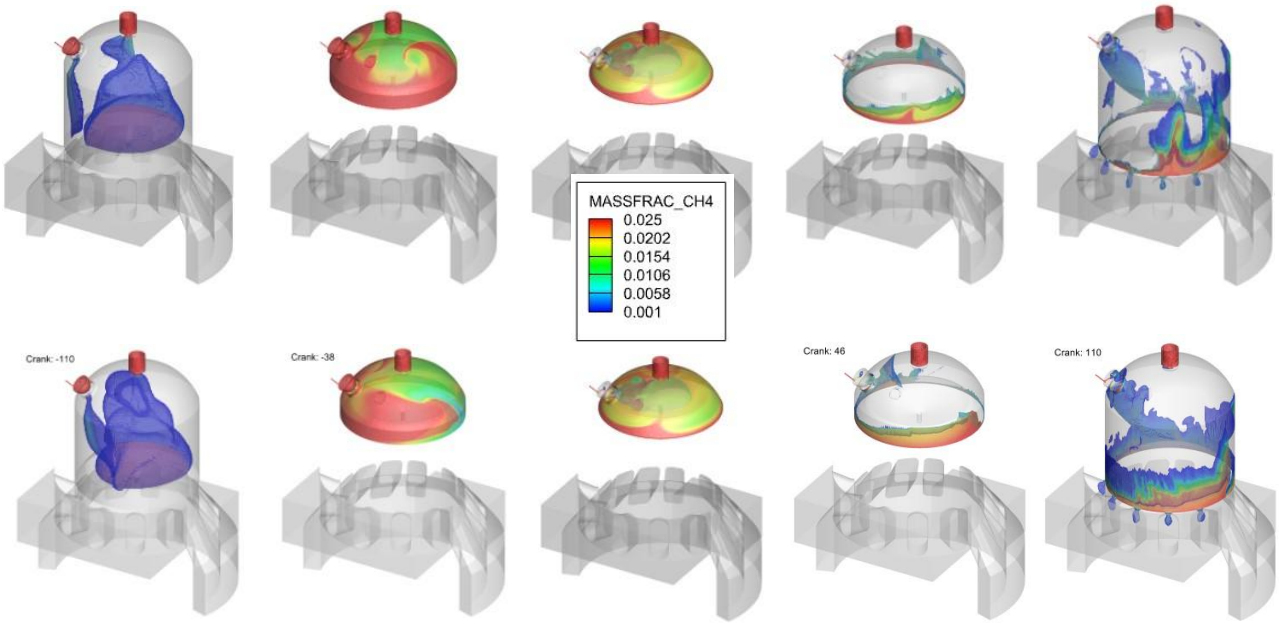

Figure 4-5 3D Contour Plots of MCC Methane Fraction Distribution at -110, -38, 9, 46, and 110 Crank Angle Degrees for the 6 mm (Top) and 4 mm Grid Top-Land-in-MCC Cases (Bottom).

4.3.3 Ring Pack Methane Residual and Blowby

The ring pack model in CONVERGE Studio v3.1 allows for calculating the amount of residual methane in the ring pack as well as the total and methane blowby through the ring pack crevice volume. Figure 4-6 shows the amount of methane trapped in the ring pack after the combustion cycle is completed. Some of this methane has the potential to return to the MCC and get released to the atmosphere through exhaust. Methane blowby that inevitably leaks past the piston rings into the crankcase is also shown in Figure 4-6. The results show the same trend for the ring pack methane residual and blowby for all four cases. The baseline case shows the least amount of methane residual and blowby, while they increase for both the 8 mm and 6 mm grid top-land-in-MCC cases before reducing for the finest resolution case, the 4 mm top-land-in-MCC case. This non-monotonic trend highlights the importance of mesh resolution in capturing

crevice gas behavior and suggests that coarse grids may misrepresent the magnitude of blowby and unburned methane retention, while finer grids improve the fidelity of crevice gas transport modeling.

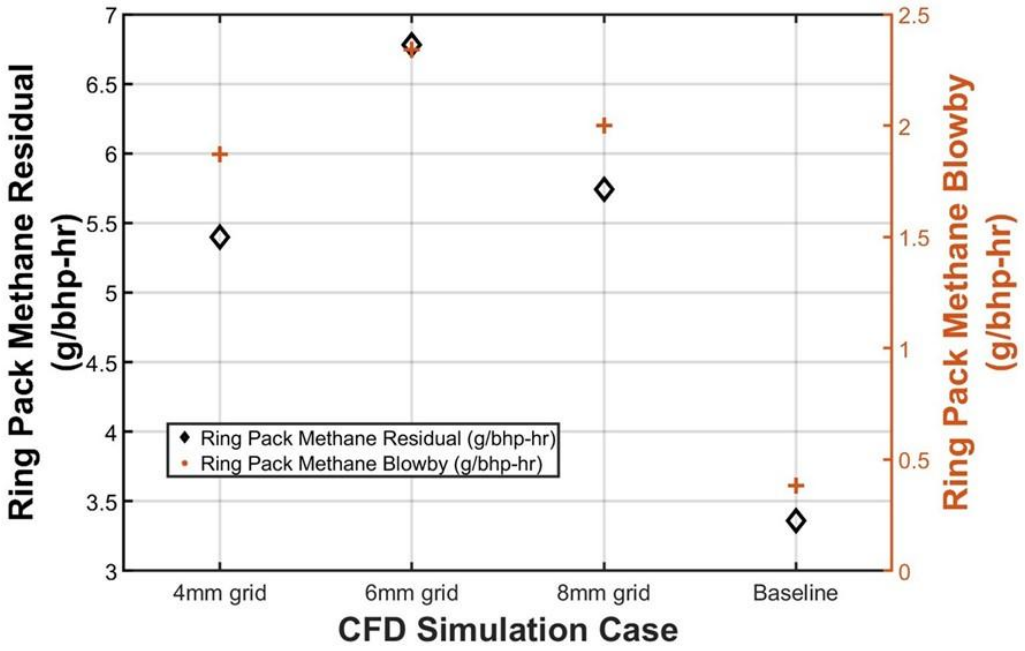

Figure 4-6 Ring Pack Methane Residual at 110 Crank Angle Degrees and Ring Pack Blowby throughout the Engine Cycle (-250 to 110 Crank Angle Degrees)

4.3.4 Velocity Profile and Methane Profile in Top-land Crevice (6 mm grid top-land-in-MCC case) study)

To understand the flow in the top-land-in-MCC cases near the ring pack, 3D contour plots and cross sections at 30, 50, 70, 90, and 110 crank angle degrees are shown in Figure 4-7 and Figure 4-8 for the 6 mm grid top-land-in-MCC case. From Figure 4-7, we observe layered distributions of methane concentration increasing toward the exhaust port and the region corresponding to the physical location of the ring pack. The rings of highly concentrated methane near the bottom of the MCC suggest that methane trapped in the top-land crevice migrates toward the exhaust side during the scavenging process, especially as pressure gradients and piston motion drive flow along the cylinder wall. This also indicates incomplete

mixing or flame quenching near the crevice region, leaving residual unburned methane.

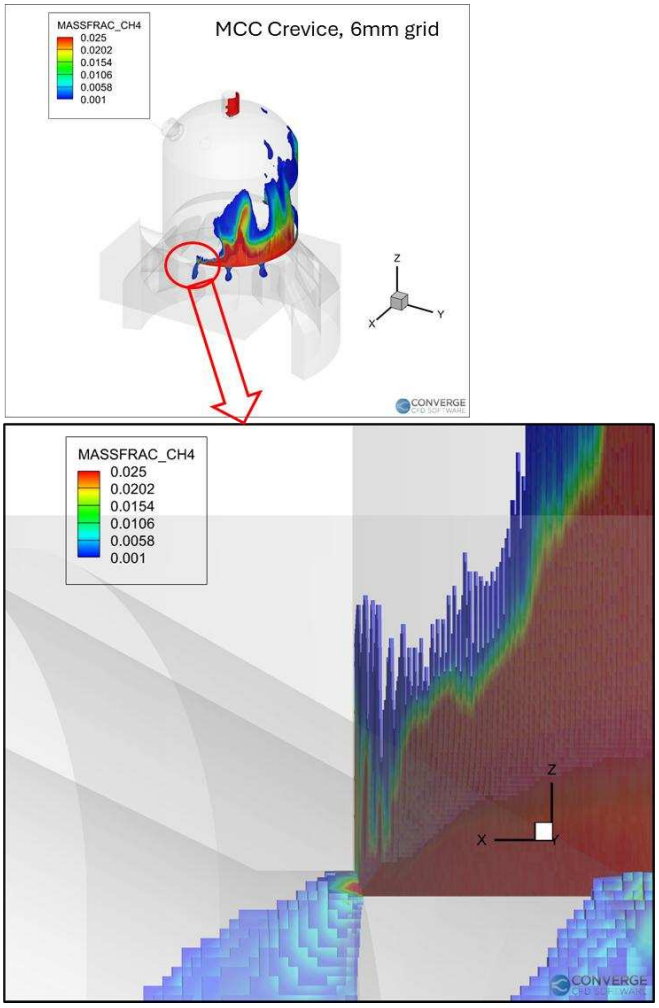

Figure 4-7 MCC Methane Mass Fraction Distribution at 110 degrees for 6 mm Grid Top-Land-in-MCC Case for a Cross Section along the X-Axis at Y=0 in the XYZ Plane and Enhanced Shades for Contour.

The direction of motion of the gases shown in Figure 4-8 is consistently downward due to the piston motion. However, the flow of methane out of the ring pack back to the MCC is shown in Figure 4-9 and indicates that the relative flow direction of methane from 22 crank angle degrees is in the upward direction (into the MCC). The derivative is shown to be negative from that point till the end of the cycle at 110 crank angle degrees, showing that methane flows into the main combustion chamber and escapes through

the exhaust as methane emissions at the end of the engine cycle.

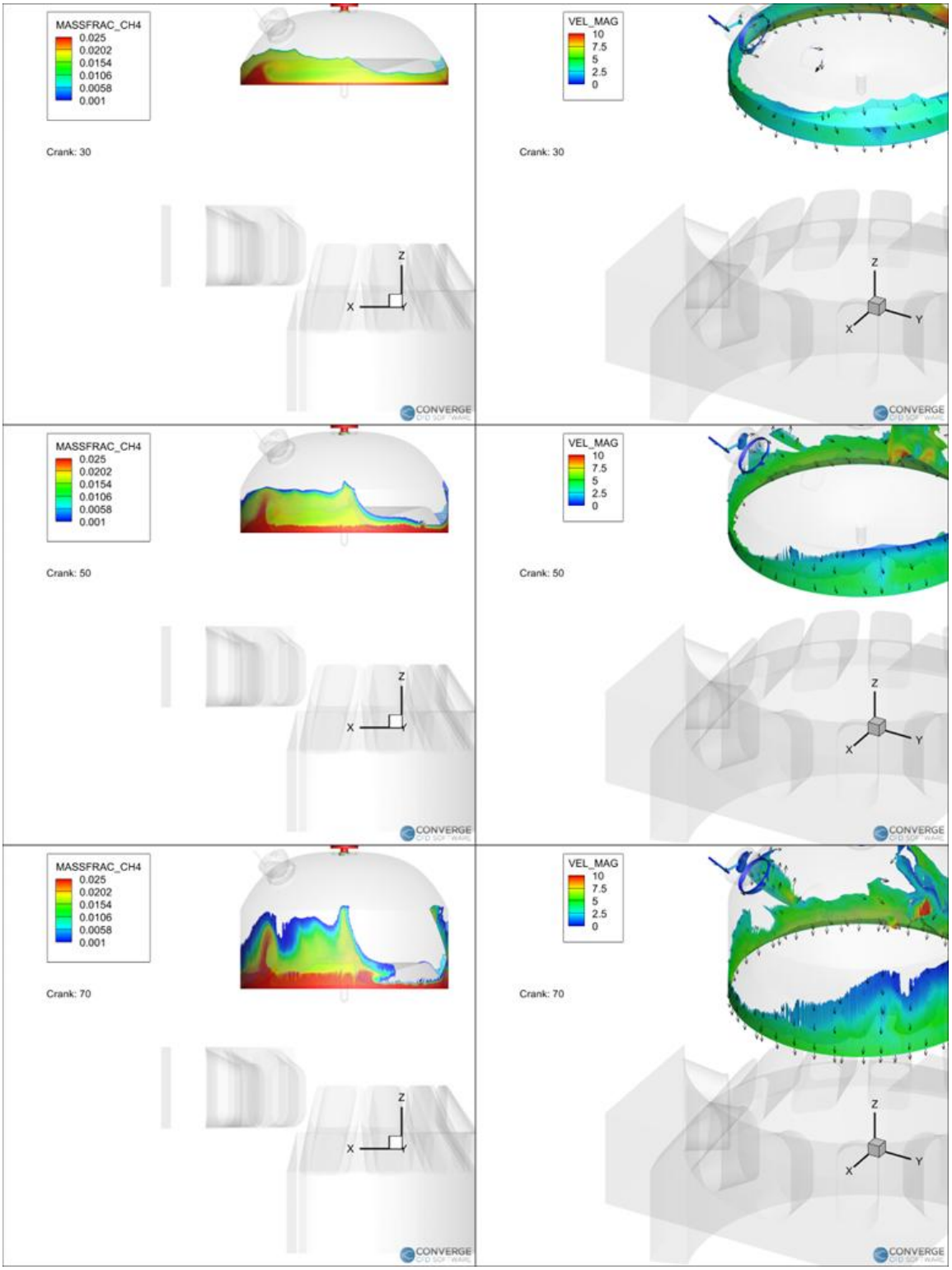

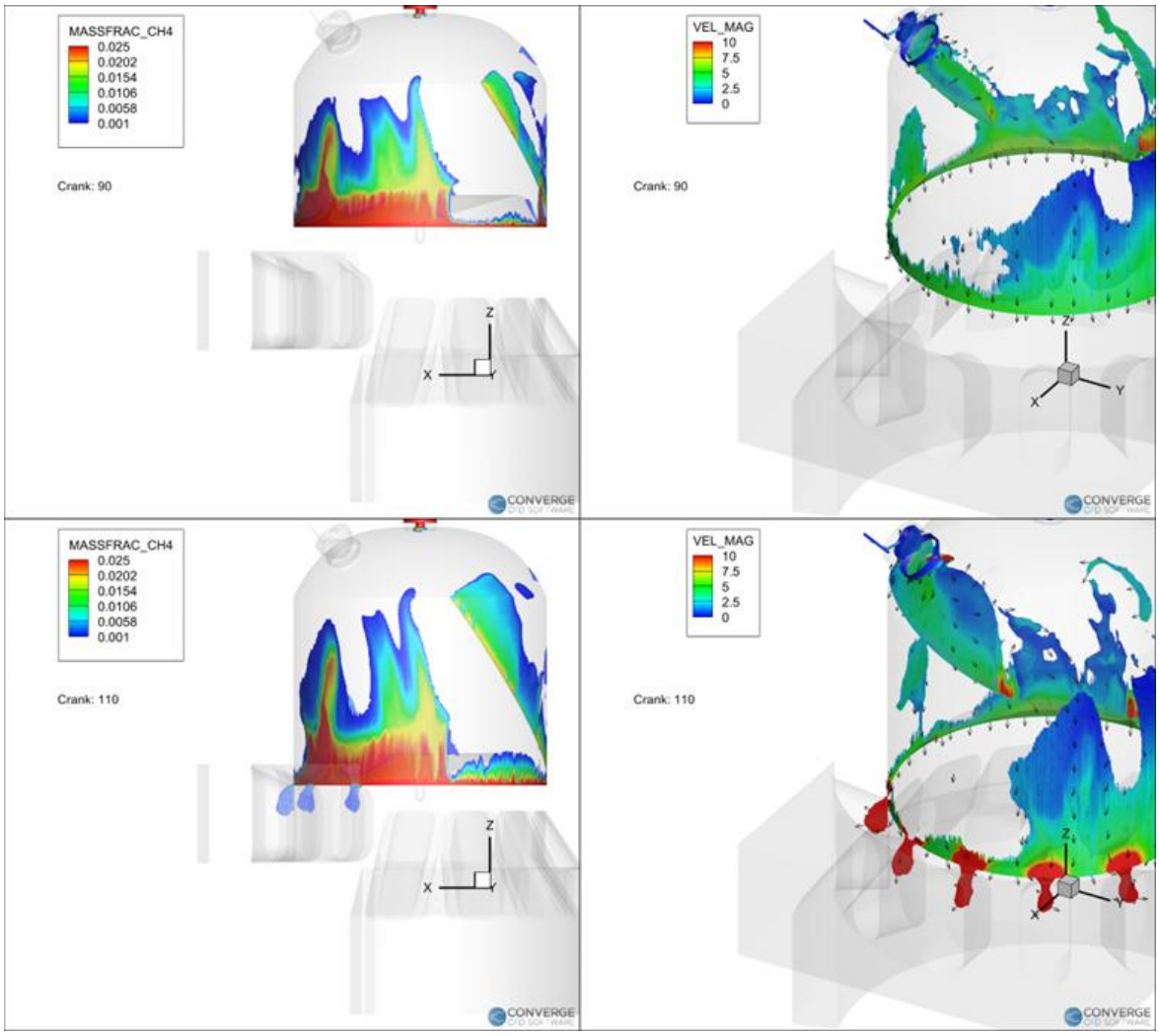

Figure 4-8 2D Contour Plots of MCC Methane Mass Fraction Distribution and 3D Contour Plots of the Velocity Profile of the MCC and Exhaust Ports at 30, 50, 70, 90, and 110 Crank Angle Degrees.

The methane that flows out of the ring pack to the main combustion chamber is likely concentrated around the top-land crevice along with other combustion gases. When methane undergoes oxidation, some intermediate and final products include methyl (CH_3), formaldehyde (CH_2O), formyl radical (HCO), carbon monoxide (CO) and carbon dioxide (CO_2) [15]. Figure 4-10 shows the levels of three methane oxidation products in the main combustion chamber for the 8 mm grid top-land-in-MCC case from the point where methane starts to exit the ring pack. This indicates that some of the methane concentrated at

the entrance of the ring pack undergoes oxidation to products such as formaldehyde (CH_2O), carbon monoxide (CO) and carbon dioxide (CO_2) though at different rates. Consequently, some of the methane trapped in the ring pack oxidizes as it exits and does not contribute to engine-out methane emissions.

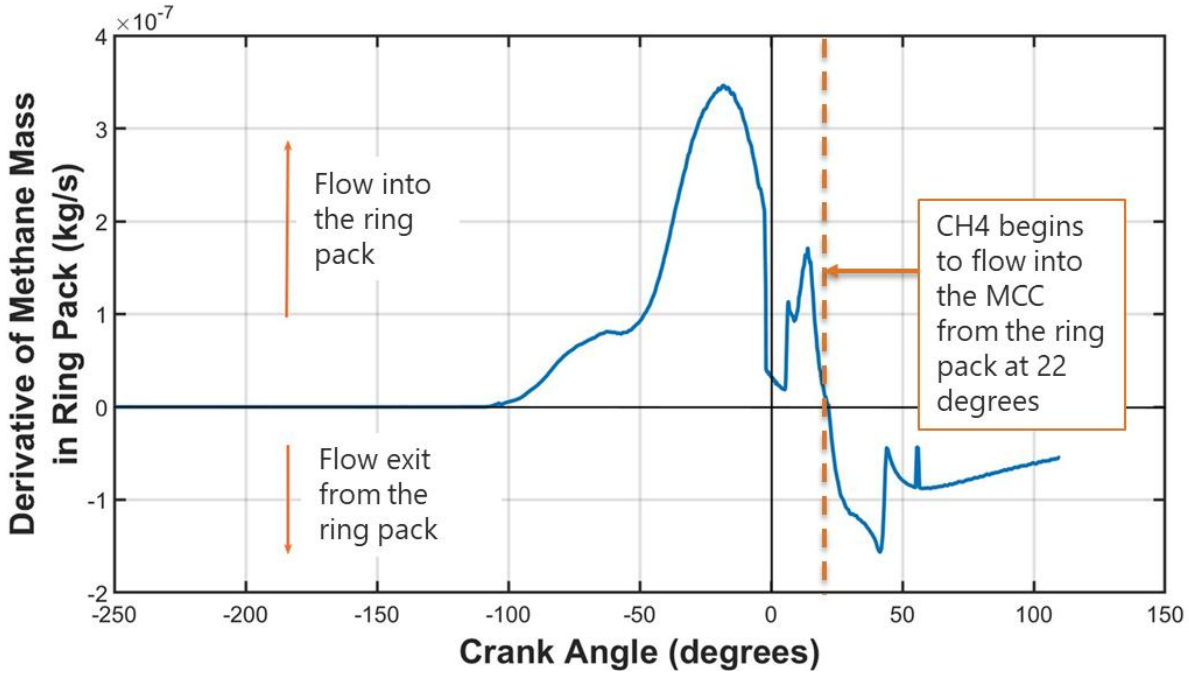

Figure 4-9 Derivative of Methane Mass in the Ring Pack indicating Flow in and out of the Ring Pack.

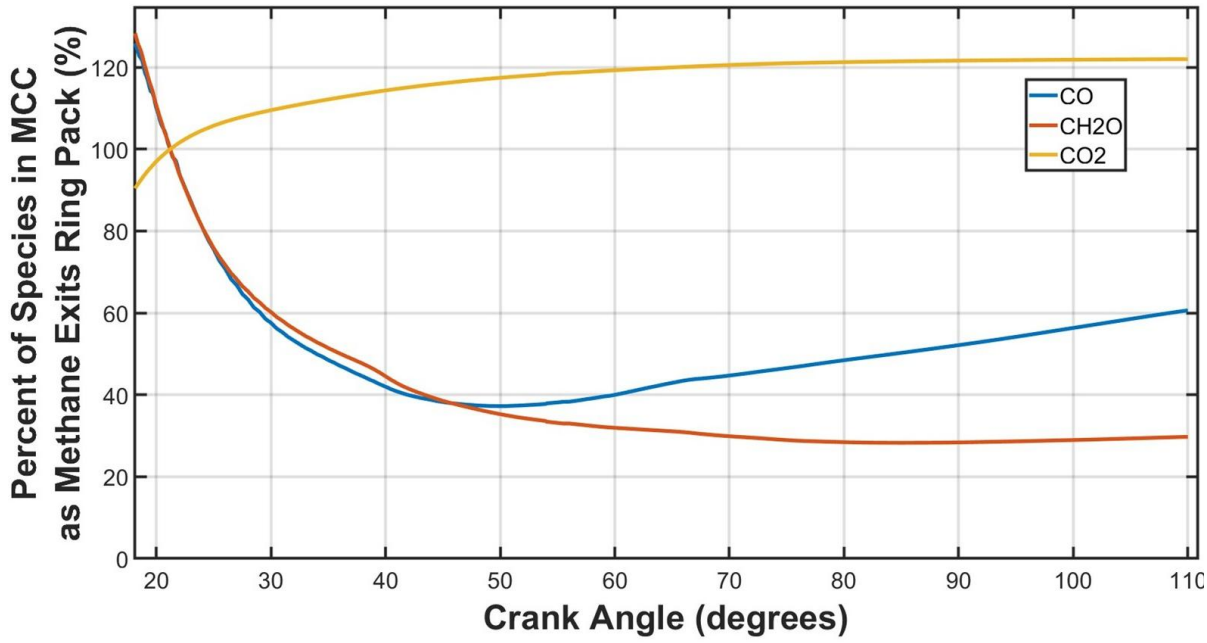

Figure 4-10 Methane Oxidation Products in MCC as Methane exits Ring Pack in 8 mm Grid Top-Land-in-MCC Case.

4.4 Discussion

This chapter investigated the impact of top-land crevice allocation on in-cylinder methane emissions and engine performance using CFD simulations of the GMV-4TF engine in CONVERGE Studio v3.1. Two configurations were compared: one where the top-land crevice volume was assigned to the ring pack region (baseline case), and another where it was assigned to the main combustion chamber (MCC) by reducing the top-land height to 1 mm (top-land-in-MCC cases). The top-land-in-MCC configuration was further evaluated across three grid resolutions (8 mm, 6 mm, and 4 mm) to assess the sensitivity of results to mesh size.

Flow visualizations and contour plots further confirmed that methane accumulation occurs near the crevice and exhaust regions, highlighting the role of top-land crevice geometry and scavenging dynamics in emission formation. Velocity vectors supported the directional movement of trapped gases toward the exhaust during blowdown and scavenging phases, but the flow in and out of the ring pack is consistent with the result of the planar laser-induced fluorescence (PLIF) study that visualized the escape of unburned fuel from the ring pack to the main combustion chamber [49]. Partial oxidation products observed in the main combustion chamber from when methane starts to flow from the ring pack to the MCC till the end of the combustion also validate the description by a previous study on the rapid formation of formaldehyde due to partial oxidation when the pressures and temperatures drop rapidly as a result of the piston motion during the expansion stroke [58].

Methane emissions were evaluated through exhaust outflow and residual methane in the MCC. Results showed that methane outflow consistently decreased with finer grid resolution in the top-land-in-MCC cases. Interestingly, the 8 mm case showed the best mixing performance, and the 6 mm and 4 mm cases, while superior to the baseline, exhibited slightly poorer mixing. Analysis of the ring pack methane residual and blowby, using CONVERGE's ring pack sub-model, revealed a non-monotonic trend across cases. Although none of the simulations explicitly modeled the physical ring pack geometry, the top-land-in-MCC cases, despite having a negligible top-land height, showed higher ring pack methane predictions in the coarser grids. These results show that the results are not grid independent. Grid independence remains largely unverified in ring-pack crevice allocation studies, and this verification provides a starting point for a future, more comprehensive grid-independent study.

5. Conclusions and Recommendations

5.1 Overview

This work explored various approaches geared at improving the performance, combustion, and emissions characteristics of the Cooper Bessemer GMV-4TF engine using experimental and computational methods, particularly to reduce methane emissions in over 7000 large-bore two-stroke natural gas engines used for natural gas compression along over 1700 compression stations in the United States. The objectives of the work, as stated earlier, have been met using different techniques. The first part of this work used CONVERGE Studio v3.0 for CFD simulations to evaluate how sensitive injection pressure is to in-cylinder mixing and explored ideal uniform mixing as well as different injection pressures to determine the best mixing cases and the effect of high-pressure fuel injection on the mixing levels in the MCC. The flow area design for the fuel injector was also modified to explore the possibility of improving medium-pressure fuel injection (150 psi), which is already used in the field. This was an investigation that would provide a cost-effective solution to methane emissions that stem from poor mixing and low combustion efficiency in large-bore two-stroke natural gas engines for natural gas compression stations, operators, and stakeholders. The second aspect of this work focused on late-cycle high-pressure fuel injection using both experimental and computational studies, using the physical engine test bed with piezoelectric combustion pressure sensors, and CONVERGE Studio v3.0 for CFD simulations. The study explored different injection pressures and timings to evaluate how late-cycle high-pressure fuel injection can affect methane emissions and engine performance. The third aspect of the study evaluates the CFD study of the GMV-4TF engine to investigate the effect of allocating the top-land crevice to the MCC and the ring pack using the built-in CFD model in CONVERGE Studio v3.1. It also explores grid optimization for the study and examines the effects and limitations of different base cell grid sizes.

5.2 Conclusions

The studies resulted in conclusions stated in each chapter of this dissertation, and the most interesting findings from the different sections of the study include the following:

1. Improved In-Cylinder Mixing – Injection Pressure Sensitivity: This study demonstrated that in-cylinder mixing in large-bore engines significantly influences methane emissions and is sensitive to changes in injection pressure. Using baseline CFD results for comparison, the study found that ideal mixing could reduce methane emissions by up to 50%. Two key strategies were identified for improving mixing: increasing injection pressure (up to 800 psi) and enlarging the injector flow area at lower pressures (e.g., 150 psi). While higher injection pressures generally improved mixing due to increased momentum, a slight decline was observed beyond 800 psi, warranting further investigation.
2. Late-Cycle High-Pressure Fuel Injection: This study showed that fuel injection timing strongly affects methane emissions in large-bore engines, with late-cycle injection significantly reducing both exhaust and crankcase methane. Key findings include:
    - Optimal injection timing for each pressure level minimizes methane emissions, with the best result at 500 psi and -100° SOA, reducing exhaust methane by 22.8% compared to the nominal case, without penalties to performance or other emissions (NOx, CO, THC, VOCs, formaldehyde).
    - Late-cycle injections consistently reduce crankcase methane, with simulations and experiments showing up to 93% reduction, although crankcase emissions are less than 0.5% of total emissions.
    - The ring pack crevice is a major contributor to total methane emissions, responsible for roughly one-third of the total.

- The study recommends re-optimizing injection timing in high-pressure fuel injection (HPFI) systems to target methane reduction. Future work will focus on enhancing HPFI system capabilities and testing late-cycle injection strategies in real-world engine applications.

3. Impact of Top-land Crevice Allocation on Methane Emissions in Engine CFD Simulations: This study used CFD simulations to examine how assigning the top-land crevice volume to the main combustion chamber (MCC)—rather than the ring pack region—affects methane emissions and engine performance in a large-bore two-stroke engine. Key findings include:
    - Methane Emissions and Ring Pack Behavior: Exhaust methane consistently decreased with finer grids in MCC cases, validating the benefit of improved crevice exposure. Interestingly, the 8 mm grid gave the best mixing, while finer meshes (6 mm, 4 mm) slightly disrupted mixing due to over-resolved turbulence. Methane blowby and residuals showed inconsistent trends across mesh sizes. Coarser grids in MCC cases overestimated ring pack emissions due to artificial crevice paths, while the 4 mm grid reduced these artifacts, showing the importance of mesh quality. Generally, the results show grid dependency.
    - Flow Visualization: Plots confirmed that methane accumulates near crevices and the exhaust, and that scavenging dynamics play a major role in emission formation. Methane in the ring pack is observed to begin leaving the ring pack at 22 degrees. Initial methane exiting the ring pack gets oxidized. However, later in the expansion process when cylinder gases are cooler unburned methane that exits the ring pack to the MCC does not oxidize and flows out through the exhaust.

5.3 Recommendations

Based on this study, some recommendations for future work can be made. High-pressure fuel injection (HPFI) systems can be re-optimized to use late-cycle injection (at SOA values of -100 degrees and beyond)

to reduce exhaust methane emissions by more than 22% without NOx emissions or performance penalties. Field trials of late-cycle high-pressure injection are recommended to validate findings in real engine environments. Collaborating with industry partners to explore the limits of existing fuel injection hardware, investigating the combined effects of improved mixing, optimized injection timing, and crevice design in a unified experimental setup, and cost-effective ways to upgrade to HPFI systems or improve injector designs is also recommended. Additionally, using larger injector flow areas for medium-pressure injection will boost fuel jet momentum and achieve mixing comparable to 500 psi systems, as well as aiming for ideal mixing conditions through design improvements.

For CFD studies, the top-land height and MCC geometry can be carefully designed to limit gas trapping in the ring pack. Simulation and modeling practices can also be improved by using high-resolution meshes (down to 4 mm) to accurately capture crevice flows and methane blowby. Considering the long simulation time it took for the 4 mm case, improved computational resources in the future would allow for full grid-independent study and improve accuracy. Being cautious of mesh-induced artifacts in coarser grids (e.g., artificial crevice flow paths) and balancing grid resolution and turbulence modeling to avoid over-resolving small eddies that may disrupt realistic mixing is also recommended. Lastly, a 45-degree or 60-degree sector of the full engine can be modeled instead of the full engine, and the ring pack can be physically modeled in the geometry rather than using the sub-models to improve accuracy on crevice volume simulations.

6. References

[1] U.S. Energy Information Administration, “Natural Gas Explained - Use of Natural Gas,” Apr. 2023, [Online]. Available: https://www.eia.gov/energyexplained/natural-gas/use-of-natural-gas.php

[2] B. Willson, G. Hutcherson, D. Olsen, and J. Holden, “Evaluation of High Pressure Injection of Fuel Gas in Large-Bore Natural Gas Engines,” 1999.

[3] D. B. Olsen and B. D. Willson, “The Effect of Retrofit Technologies on Formaldehyde Emissions from a Large Bore Natural Gas Engine,” *Energy Power Eng.*, vol. 03, no. 04, pp. 574–579, 2011, doi: 10.4236/epe.2011.34071.

[4] M. A. Patterson, N. Xie, K. Beurlot, T. Jacobs, and D. Olsen, “Analysis of Unburned Methane Emission Mechanisms in Large-Bore Natural Gas Engines With Prechamber Ignition,” *J. Eng. Gas Turbines Power*, vol. 146, no. 10, Oct. 2024, doi: 10.1115/1.4065313.

[5] European Commission, “Energy, Climate change, Environment - Methane emissions”, [Online]. Available: https://energy.ec.europa.eu/topics/carbon-management-and-fossil-fuels/methane-emissions_en

[6] A. J. Marchese *et al.*, “Methane Emissions from United States Natural Gas Gathering and Processing,” *Environ. Sci. Technol.*, vol. 49, no. 17, pp. 10718–10727, Sep. 2015, doi: 10.1021/acs.est.5b02275.

[7] “Global Methane Pledge.” Accessed: Jul. 10, 2023. [Online]. Available: https://www.globalmethanepledge.org/

[8] M. Omara *et al.*, “Methane Emissions from Natural Gas Production Sites in the United States: Data Synthesis and National Estimate,” *Environ. Sci. Technol.*, vol. 52, no. 21, pp. 12915–12925, Nov. 2018, doi: 10.1021/acs.est.8b03535.

[9] M. R. Johnson, D. R. Tyner, and B. M. Conrad, “Origins of Oil and Gas Sector Methane Emissions:

On-Site Investigations of Aerial Measured Sources," *Environ. Sci. Technol.*, vol. 57, no. 6, pp. 2484–2494, Feb. 2023, doi: 10.1021/acs.est.2c07318.

[10] John. Heywood, *Internal Combustion Engine Fundamentals 2E*. McGraw-Hill Education, 2019, p. 1056.

[11] A. A. Abdel-Rahman, "On the emissions from internal-combustion engines: A review," *Int. J. Energy Res.*, vol. 22, no. 6, pp. 483–513, 1998, doi: 10.1002/(SICI)1099-114X(199805)22:6<483::AID-ER377>3.0.CO;2-Z.

[12] C. P. Ranasinghe and W. Malalasekera, "Modelling combustion in spark ignition engines with special emphasis on near wall flame quenching," *Int. J. Engine Res.*, vol. 23, no. 1, pp. 20–32, Jan. 2022, doi: 10.1177/1468087420972903.

[13] T. E. Strand, "EXPERIMENTAL INVESTIGATION OF BULK FLAME QUENCHING IN A DIRECT-INJECTION SPARK IGNITION ENGINE," 2001.

[14] J. Hiltner, A. Loetz, and S. Fiveland, "Unburned Hydrocarbon Emissions from Lean Burn Natural Gas Engines-Sources and Solutions," presented at the CIMAC Congress, Helsinki, 2016. [Online]. Available: www.tcpdf.org

[15] S. Turns, *AN INTRODUCTION TO COMBUSTION*, 3rd ed. 2011.

[16] D. B. Olsen and B. D. Willson, "THE IMPACT OF CYLINDER PRESSURE ON FUEL JET PENETRATION AND MIXING," in *Proceedings of the ASME 2002 Internal Combustion Engine Division Fall Technical Conference. Design, Application, Performance and Emissions of Modern Internal Combustion Engine Systems and Components. New Orleans, Louisiana, USA*, 2002, pp. 233–240. doi: https://doi.org/10.1115/ICEF2002-502.

[17] B. Willson, G. Hutcherson, S. Hawley, and K. Willett, "Relative Performance of High-Pressure Fuel Gas Delivery," in *GMRC Gas Machinery Conference, Austin, Texas, Oct. 6-8*, 1997.

[18] D. B. Olsen, D. B. Mastbergen, and B. D. Willson, "PLANAR LASER INDUCED

FLUORESCENCE IMAGING OF GAS INJECTION FROM FUEL VALVES FOR LARGE BORE NATURAL GAS ENGINES," in *Proceedings of the ASME 2001 Internal Combustion Engine Division Fall Technical Conference. Volume 2: Large-Bore Engines, Fuel Effects, Homogeneous Charge Compression Ignition, Engine Performance and Simulation. Argonne, Illinois, USA*, 2001. doi: https://doi.org/10.1115/2001-ICE-409.

[19] G.-H. Kim, A. Kirkpatrick, and C. Mitchell, "COMPUTATIONAL MODELING OF NATURAL GAS INJECTION IN A LARGE BORE ENGINE," *J Eng Gas Turbines Power*, vol. 126, no. 3, pp. 656–664, 2004, doi: 10.1115/1.1762906.

[20] G. Hoffmann, B. Befrui, A. Berndorfer, and W. F. Piock, "Fuel System Pressure Increase for Enhanced Performance of GDi Multi-Hole Injection Systems," *Varble Source SAE Int. J. Engines*, vol. 7, no. 1, pp. 519–527, 2014, doi: 10.2307/26277782.

[21] T. Venugopal and A. Ramesh, "Experimental studies on the effect of injection timing in a SI engine using dual injection of n-butanol and gasoline in the intake port," *Fuel*, vol. 115, pp. 295–305, Jan. 2014, doi: 10.1016/j.fuel.2013.07.013.

[22] X. Duan, Y. Li, Y. Liu, J. Liu, S. Wang, and G. Guo, "Quantitative investigation the influences of the injection timing under single and double injection strategies on performance, combustion and emissions characteristics of a GDI SI engine fueled with gasoline/ethanol blend," *Fuel*, vol. 260, p. 116363, Jan. 2020, doi: 10.1016/j.fuel.2019.116363.

[23] A. C. Alkidas, "Combustion-chamber crevices: the major source of engine-out hydrocarbon emissions under fully warmed conditions," pp. 253–273, 1999.

[24] G. Vieira, T. Banji, R. Lorenzen, and D. B. Olsen, "Methane Abatement from LB NG 2-Stroke Cycle Engines Through In-Cylinder Modifications," 2024. [Online]. Available: http://www.prci.org

[25] S. Shiga *et al.*, "Effect of Fuel Injection Timing Relative to Ignition Timing on the Natural-Gas Direct-Injection Combustion," *J. Eng. Gas Turbines Power-Trans. Asme - J ENG GAS TURB*

POWER-T ASME, vol. 125, Jul. 2003, doi: 10.1115/1.1563243.

[26] S. Sahoo and D. K. Srivastava, "Experimental Study of Effect of Injection Timing on Port Fuel Injection Gasoline, Port Fuel Injection Compressed Natural Gas, and Direct Injection Compressed Natural Gas Engine Performance, Combustion, and Emissions Characteristics," *J. Eng. Gas Turbines Power*, vol. 145, no. 061014, Feb. 2023, doi: 10.1115/1.4056263.

[27] D. Kim, J. Shin, Y. Son, and S. Park, "Characteristics of in-cylinder flow and mixture formation in a high-pressure spray-guided gasoline direct-injection optically accessible engine using PIV measurements and CFD," *Energy Convers. Manag.*, vol. 248, Nov. 2021, doi: 10.1016/j.enconman.2021.114819.

[28] K. Pan and J. Wallace, "Computational studies of fuel injection strategies on natural gas combustion characteristics in direct-injection engines," *Fuel*, vol. 288, p. 119823, Mar. 2021, doi: 10.1016/j.fuel.2020.119823.

[29] M. Li, H. Wu, T. Zhang, B. Shen, Q. Zhang, and Z. Li, "A comprehensive review of pilot ignited high pressure direct injection natural gas engines: Factors affecting combustion, emissions and performance," *Renew. Sustain. Energy Rev.*, vol. 119, Mar. 2020, doi: 10.1016/j.rser.2019.109653.

[30] A. C. Alkidas, "Combustion-chamber crevices: the major source of engine-out hydrocarbon emissions under fully warmed conditions," pp. 253–273, 1999.

[31] N. D. Thompson and J. S. Wallace, "Effect of Engine Operating Variables and Piston and Ring Parameters on Crevice Hydrocarbon Emissions," 1994. [Online]. Available: https://www.jstor.org/stable/44632829

[32] C. Kim, C. Bae, and S. Choi, "Gas Flows Through the Inter-Ring Crevice and Their Influence on UHC Emissions," 1999. [Online]. Available: https://www.jstor.org/stable/44716749

[33] V. M. Salazar and J. B. Ghandhi, "Initial Estimation of the Piston Ring Pack Contribution to Hydrocarbon Emissions from a," 2007. [Online]. Available: https://www.jstor.org/stable/44699356

[34] J. Ladd, B. Neuner, and D. B. Olsen, “Variable Fuel Composition Air Fuel Ratio Control of Lean Burn Engines Prepared for the,” 2016. [Online]. Available: http://www.prci.org

[35] A. E. Quintero Castillo, A. Zdanowicz, B. Windom, and D. B. Olsen, “Characterization of Crankcase Ventilation Gas on Stationary Natural Gas Engines,” presented at the Western States Section of the Combustion Institute Fall 2023 Technical Meeting, 2023.

[36] K. J. Richards, P. K. Senecal, and E. Pomraning, *CONVERGE 3.1 Manual*. Madison, WI: Convergent Science, 2023.

[37] M. Namazian, “Studies of combustion and crevice gas motion in a flow- visualization spark-ignition engine,” 1981.

[38] C. D. Rakopoulos, G. M. Kosmadakis, A. M. Dimaratos, and E. G. Pariotis, “Investigating the effect of crevice flow on internal combustion engines using a new simple crevice model implemented in a CFD code,” *Appl. Energy*, vol. 88, no. 1, pp. 111–126, 2011, doi: 10.1016/j.apenergy.2010.07.012.

[39] S. N. Kurbet and R. Krishna Kumar, “Finite element modelling of piston-ring dynamics and blow-by estimation in a four-cylinder diesel engine,” *Proc. Inst. Mech. Eng. Part J. Automob. Eng.*, vol. 221, no. 11, pp. 1405–1414, 2007, doi: 10.1243/09544070JAUTO177.

[40] B. Willson, G. Hutcherson, S. Hawley, and K. Willett, “Relative Performance of High-Pressure Fuel Gas Delivery,” presented at the GMRC Gas Machinery Conference, Austin, Texas, Oct. 6-8, 1997.

[41] K. J. Richards, P. K. Senecal, and E. Pomraning, *CONVERGE 3.0 Manual*. Madison, WI: Convergent Science, 2022.

[42] M. Namazian and J. B. Heywood, “Flow in the Piston-Cylinder-Ring Crevices of a Spark-Ignition Engine: Effect on Hydrocarbon Emissions, Efficiency and Power,” *SAE Trans.*, vol. 91, pp. 261–288, 1982.

[43] R. S. Barlow, A. N. Karpetis, J. H. Frank, and J.-Y. Chen, “Scalar Profiles and NO Formation in Laminar Opposed-Flow Partially Premixed Methane/Air Flames,” 2001.

[44] G. Smith *et al.*, "Berkeley GRI 3.0 Mechanism", [Online]. Available: http://combustion.berkeley.edu/gri-mech/version30/text30.html

[45] C. G. Kim, C. S. Bae, and S. M. Choi, "Importance of inter-ring crevice volume as a source of unburned hydrocarbon emissions - numerical considerations," *Proc. Inst. Mech. Eng. Part C J. Mech. Eng. Sci.*, 2000.

[46] J. Hiltner, A. Loetz, and S. Fiveland, "Unburned Hydrocarbon Emissions from Lean Burn Natural Gas Engines-Sources and Solutions," presented at the CIMAC Congress, Helsinki, 2016. [Online]. Available: www.tcpdf.org

[47] L. K. Shih and D. N. Assanis, "Effect of Ring Dynamics and Crevice Flows on Unburned Hydrocarbon Emissions," *ASME J. Gas Turbines Power*, 1994, [Online]. Available: http://asmedigitalcollection.asme.org/gasturbinespower/article-pdf/116/4/784/5702139/784_1.pdf

[48] A. C. Alkidas, R. J. Drews, and W. F. Miller, "Effects of Piston Crevice Geometry on the Steady-State Engine-Out Hydrocarbons Emissions of a S.I. Engine," *SAE Trans.*, vol. 104, pp. 2437–2458, 1995.

[49] R. M. Green and L. D. Cloutman, "Planar LIF Observations of Unburned Fuel Escaping the Upper Ring-Land Crevice in an SI Engine," 1997. [Online]. Available: https://www.jstor.org/stable/44730741

[50] A. Kharazmi, "Three Dimensional Analysis of the Gas Flow in Piston Ring Pack," 2017.

[51] K. Beurlot, G. Vieira, T. Ritchie, J. Nowlin, D. Olsen, and T. Jacobs, "Evaluation of New Ignition Concepts on Large Bore NG Engines for Methane Emissions," 2022. [Online]. Available: http://www.prci.org

[52] Q. Tang *et al.*, "Effects of fuel trapping in piston crevice on unburned hydrocarbon emissions in early-injection compression ignition engines," *Combust. Flame*, vol. 231, Sep. 2021, doi: 10.1016/j.combustflame.2021.111496.

[53] H. Huang, K. Xing, T. Lin, X. Guo, and Y. Wang, “Evaluating potential of increasing flow intensity and reducing crevice volume to improve thermal efficiency and hydrocarbon emission in spark-ignition natural gas engines,” *Fuel*, vol. 373, Oct. 2024, doi: 10.1016/j.fuel.2024.132286.

[54] T. I. Banji, G. Arney, M. Patterson, and D. B. Olsen, “Reduction of Methane Emissions from Natural Gas Integral Compressor Engines through Fuel Injection Control,” *Sustain. Switz.*, vol. 16, no. 14, Jul. 2024, doi: 10.3390/su16145943.

[55] D. B. Olsen and B. D. Willson, “THE IMPACT OF CYLINDER PRESSURE ON FUEL JET PENETRATION AND MIXING,” presented at the Proceedings of the ASME 2002 Internal Combustion Engine Division Fall Technical Conference. Design, Application, Performance and Emissions of Modern Internal Combustion Engine Systems and Components. New Orleans, Louisiana, USA, 2002, pp. 233–240. doi: 10.1115/ICEF2002-502.

[56] T. I. Banji, G. Arney, and D. B. Olsen, “Fuel Injection Optimization for Large-Bore Two-Stroke Natural-Gas Engines,” *Energies*, vol. 18, no. 3, Feb. 2025, doi: 10.3390/en18030624.

[57] J. H. Ferziger, M. Perić, and R. L. Street, *Computational Methods for Fluid Dynamics*. 2002.

[58] C. E. Mitchell and D. B. Olsen, “Formaldehyde Formation in Large Bore Natural Gas Engines Part 1: Formation Mechanisms Introduction and Problem Identification,” 2000.

Appendix A. Supplemental Content: Improved In-Cylinder Mixing

A.1. Baseline Combustion Cycle Heat Release Rate

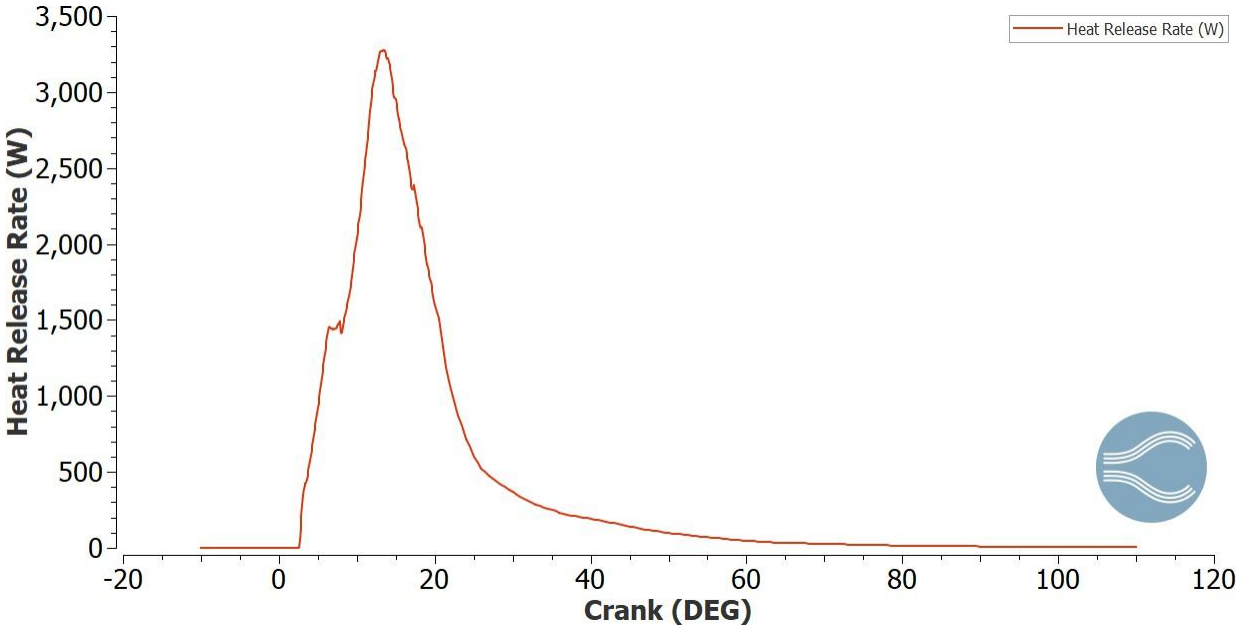

Figure A-1 **Baseline Combustion Cycle Heat Release Rate**

A.2. Injected Fuel Slip

A.2.1 Cases with significant fuel slip

Example calculation, nominal point (experimental data)

$$\%THC\ slip\ by\ mass = \frac{Exhaust\ THC\ emissions}{Engine\ fuel\ consumption} \times 100\%$$

$$= \frac{7.83\ g/bhp \cdot hr}{170\ lb/hr \times 2205\ g/lb} \times 100\%$$

$$= \frac{3445.7\ g/hr}{77100\ g/hr} \times 100\%$$

$$= 4.47\%$$

A.2.2 Percentage slip from CFD cases

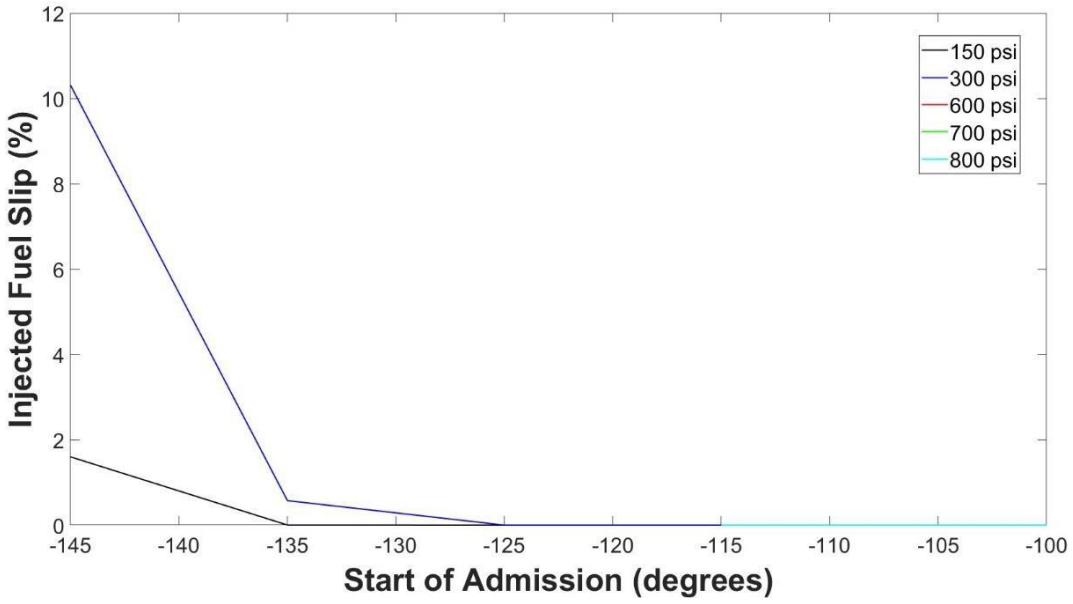

Figure A-2 Percentages of Injected Fuel Slip

A.3. Calculation of flow areas for low-pressure, high-momentum cases

A.3.1 Seat-flow area

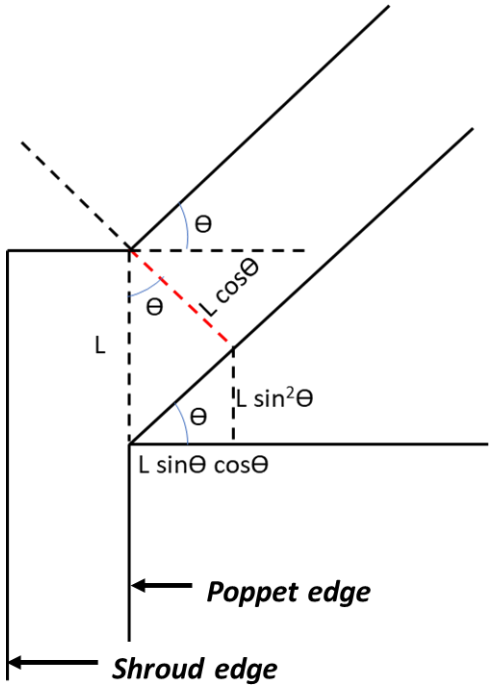

Figure A-3 Seat Flow Area (red dotted line shows cross-section point)

$$Seat\ flow\ area\ (\text{fulcrum surface area}) = \pi \times (R + r) \times length\ of\ slant\ edge$$

$$Seat\ flow\ area = \pi \times \left(\frac{d+(d-l\cdot sin\theta\cdot cos\theta)}{2}\right) \times l \cdot cos\theta$$

Where d is the poppet diameter, l is the lift, and r and R represent the bounding radii of the seat- flow (curtain) area.

*A.3.2 **Shroud-poppet annulus***

$$Shroud - poppet\ annulus = \pi\left(\frac{D^2 - d^2}{4}\right)$$

Where D is the shroud diameter, and d is the poppet diameter.

*A.3.3 **Port annulus***

$$Port\ annulus = \pi\left(\frac{D_p^2 - d_p^2}{4}\right)$$

Where Dp is the outer diameter of the injection port, and dp is the inner diameter of the injection port.

A.4. Mixing in high-pressure fuel injection CFD cases

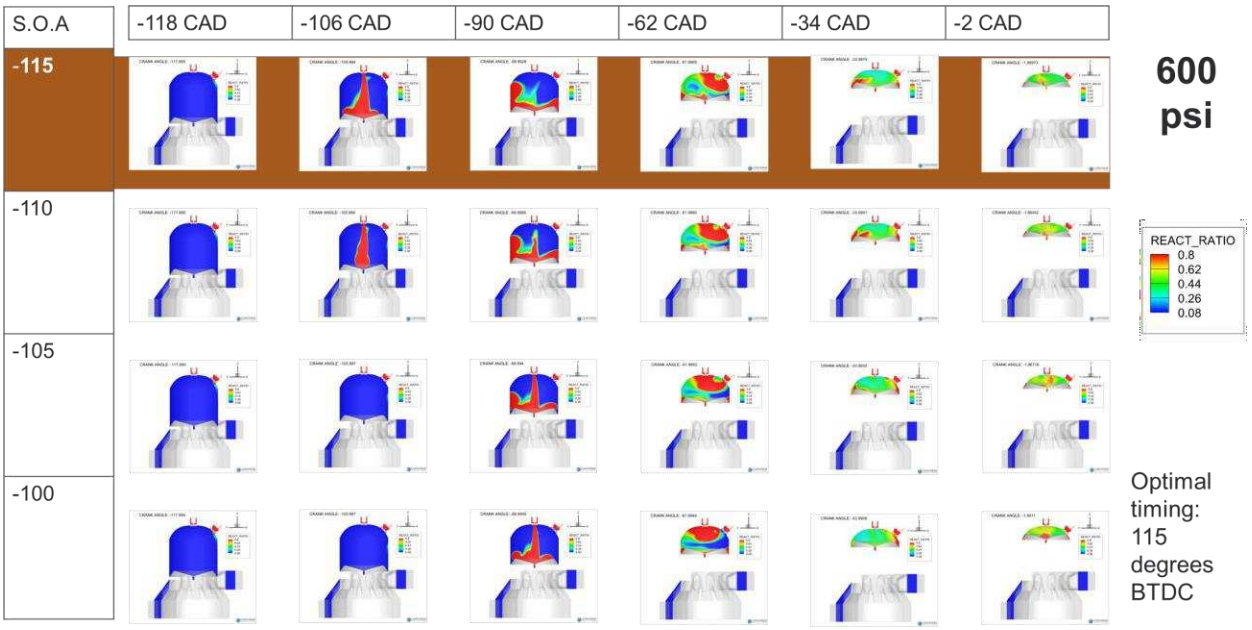

Figure A-4 Mixing in 600 psi Fuel Injection during Optimal Injection Timing Investigation.

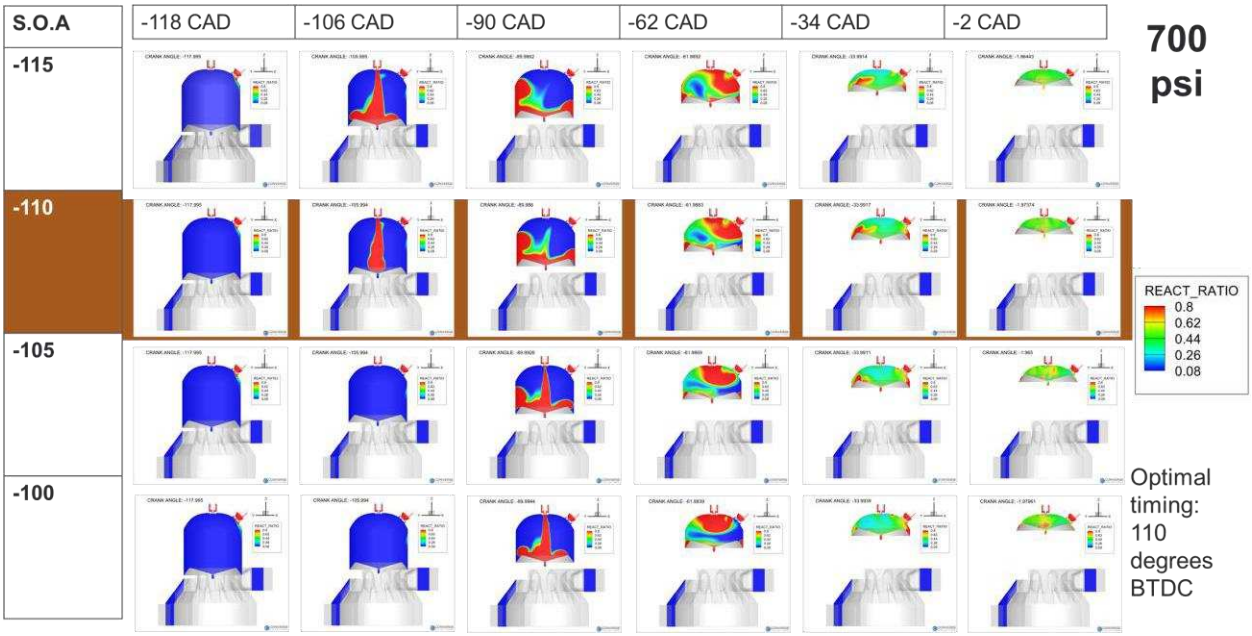

Figure A-5 Mixing in 700 psi Fuel Injection during Optimal Injection Timing Investigation.

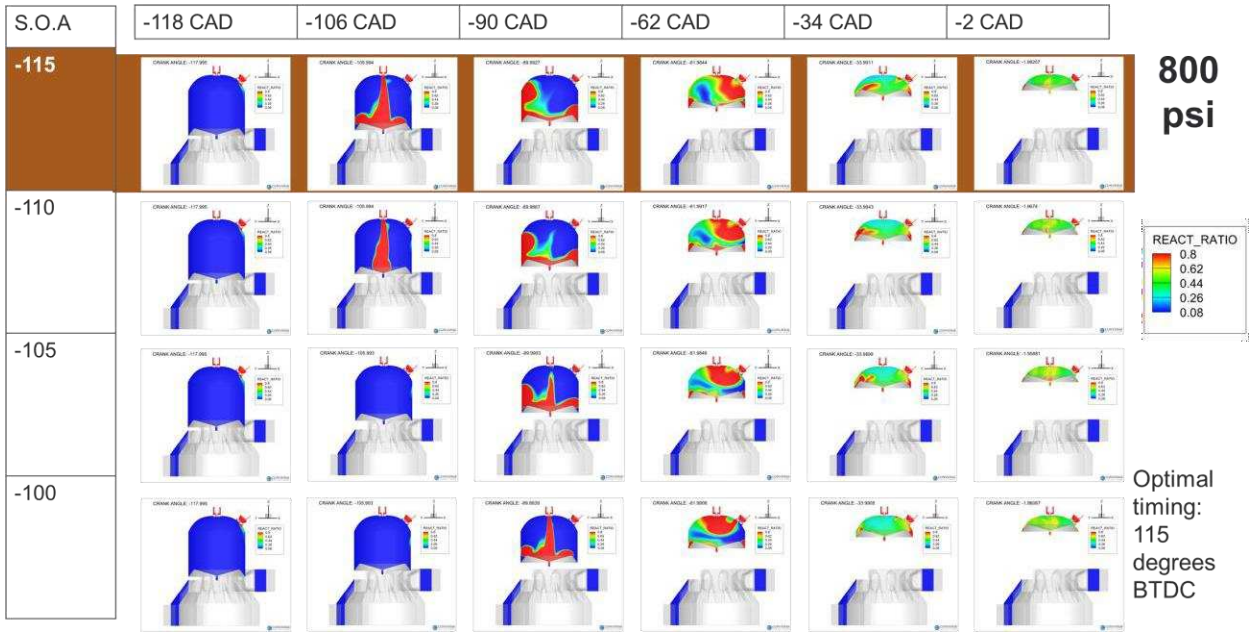

Figure A-6 Mixing in 800 psi Fuel Injection during Optimal Injection Timing Investigation.

Appendix B. Supplemental Content: Late-Cycle High-Pressure Fuel Injection Investigation

B.1. Methane Blowby Through Ring Pack Crevice Volume

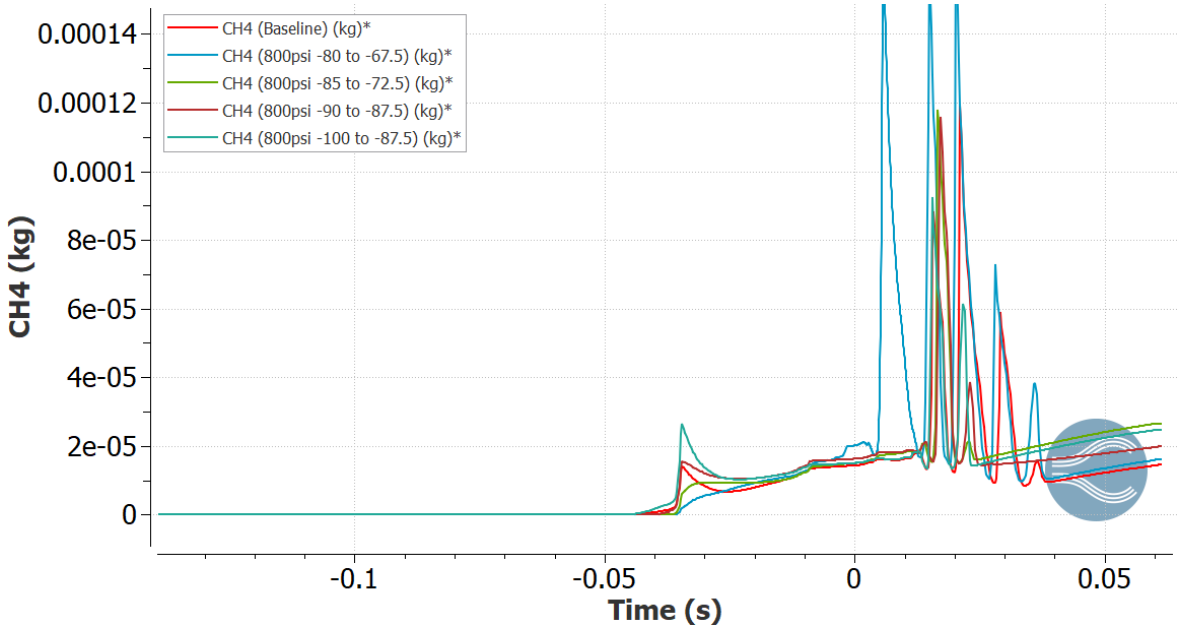

Figure B-1 Methane Blowby through Ring Pack at 800 psi and Various Injection Timings

B.2. Total Blowby Through Ring Pack Crevice Volume

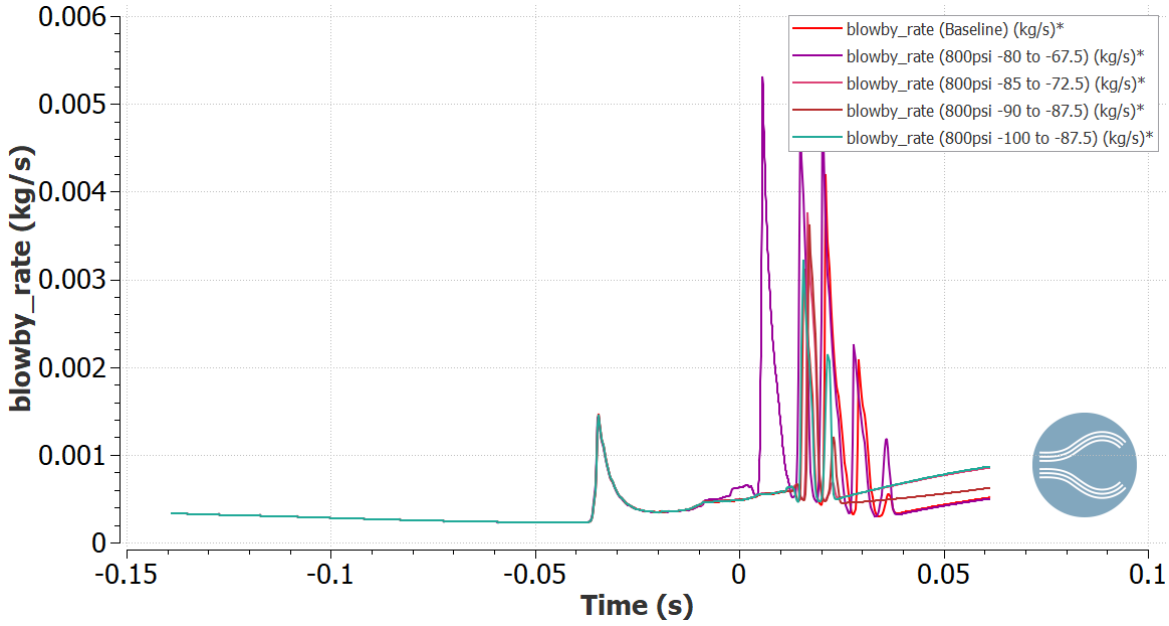

Figure B-2 Total Blowby through Ring Pack at 800 psi and Various Injection Timings

B.3. Methane Trapped in Ring Pack Crevice Volume

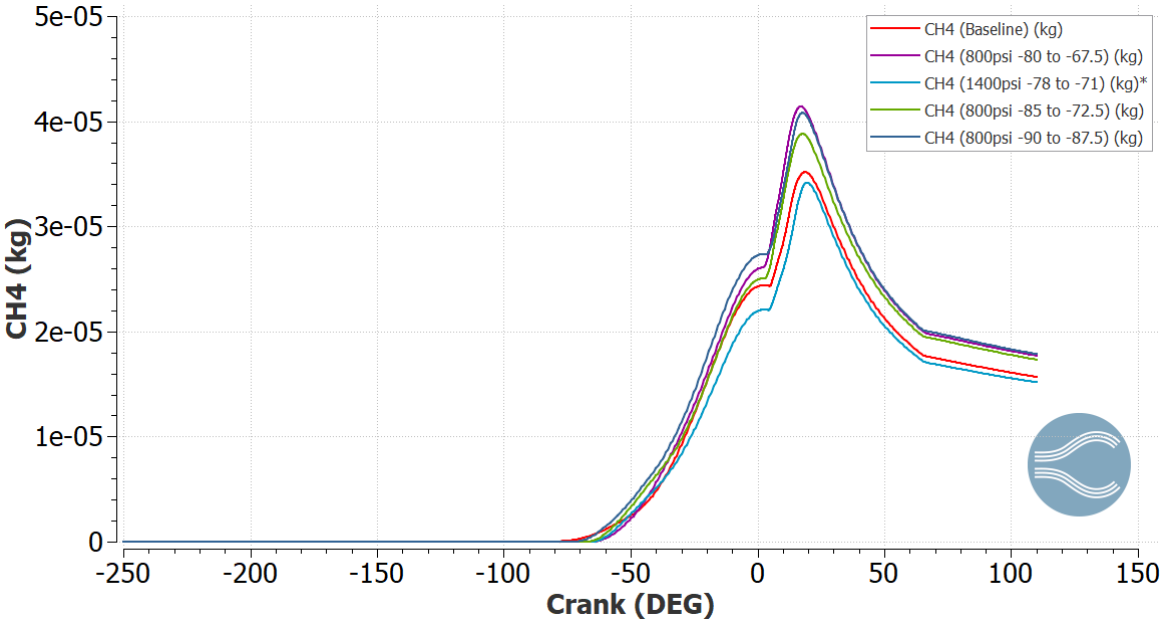

Figure B-3 Methane Trapped in Ring Pack Crevice Volume at 800psi and Various Injection Timings

B.4. Level of Mixing in Main Cylinder at Different Injection Timings

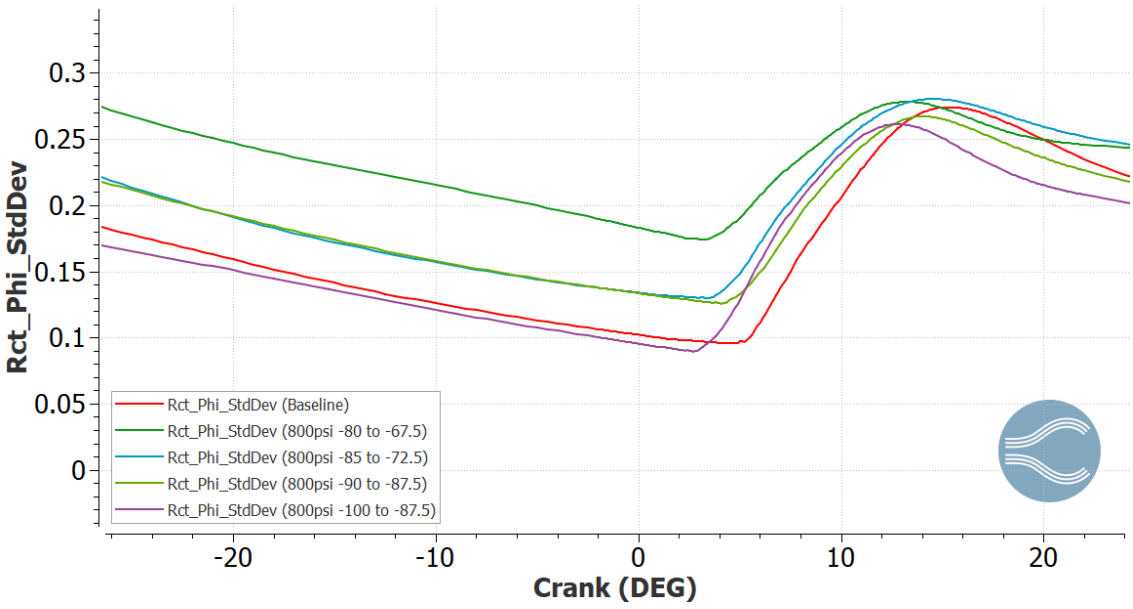

Figure B-4 In-Cylinder Mixing at 800 psi and Various Injection Timings

B.5. Total Injector Gas Flow from Fuel Injector to Main Cylinder

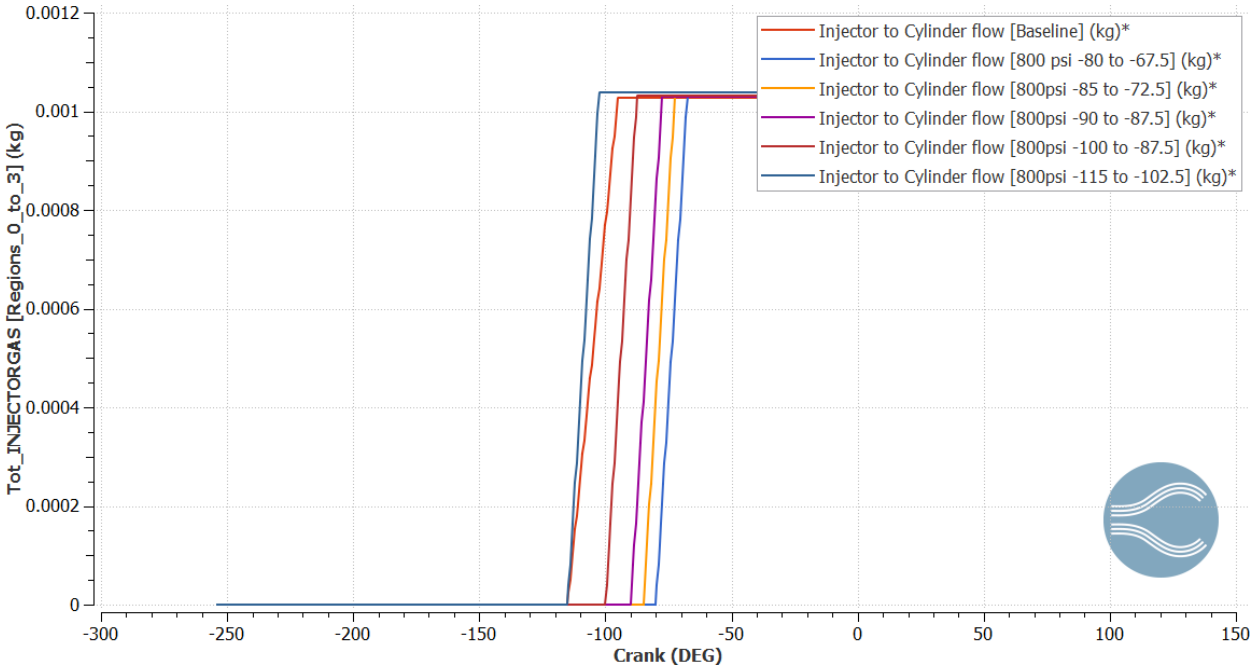

Figure B-5 Mass of Fuel Delivered at 800 psi and Various Injection Timings

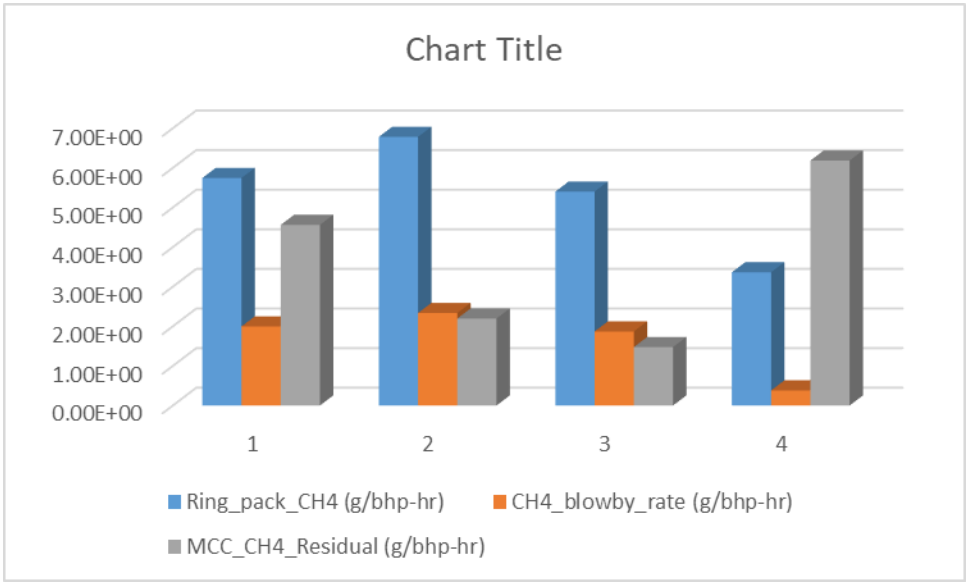

Figure B-6 Estimated methane trapped in the ring pack (blue), methane blowby rate (orange), and methane residual in the MCC (gray) across four simulation cases. Cases 1–3 correspond to top-land-in-MCC geometries with 8 mm, 6 mm, and 4

mm grid resolutions, respectively. Case 4 represents the baseline top-land-in-ring-pack geometry. While the ring pack sub-model was applied in all cases, only the baseline case includes the correct physical top-land height and crevice dimensions. In the top-land-in-MCC cases, the top-land height was set to 1 mm to enforce the MCC assumption, which likely results in overestimation of ring pack CH_4 and blowby due to unintended crevice volume artifacts. These results are presented here for completeness but are not included in the main analysis due to their limited physical accuracy.

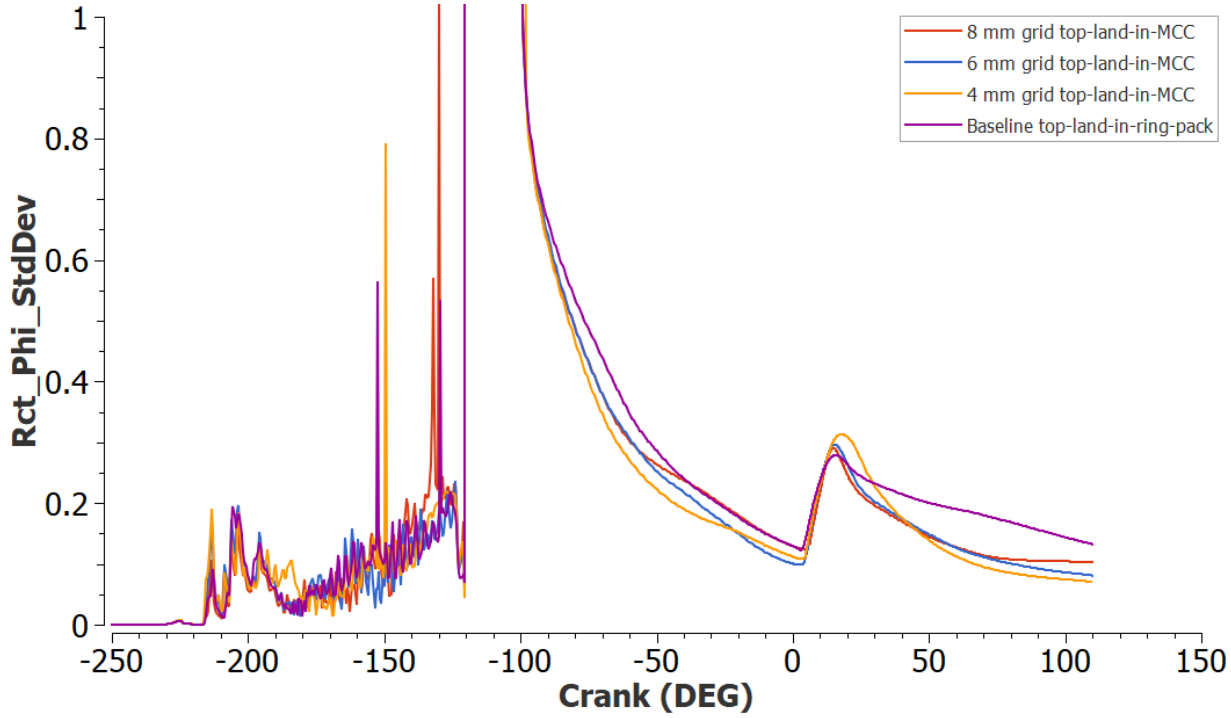

Figure B-7 MCC Mixing Levels for the Top-Land-in-MCC and Top-Land-in-Ring-Pack Cases

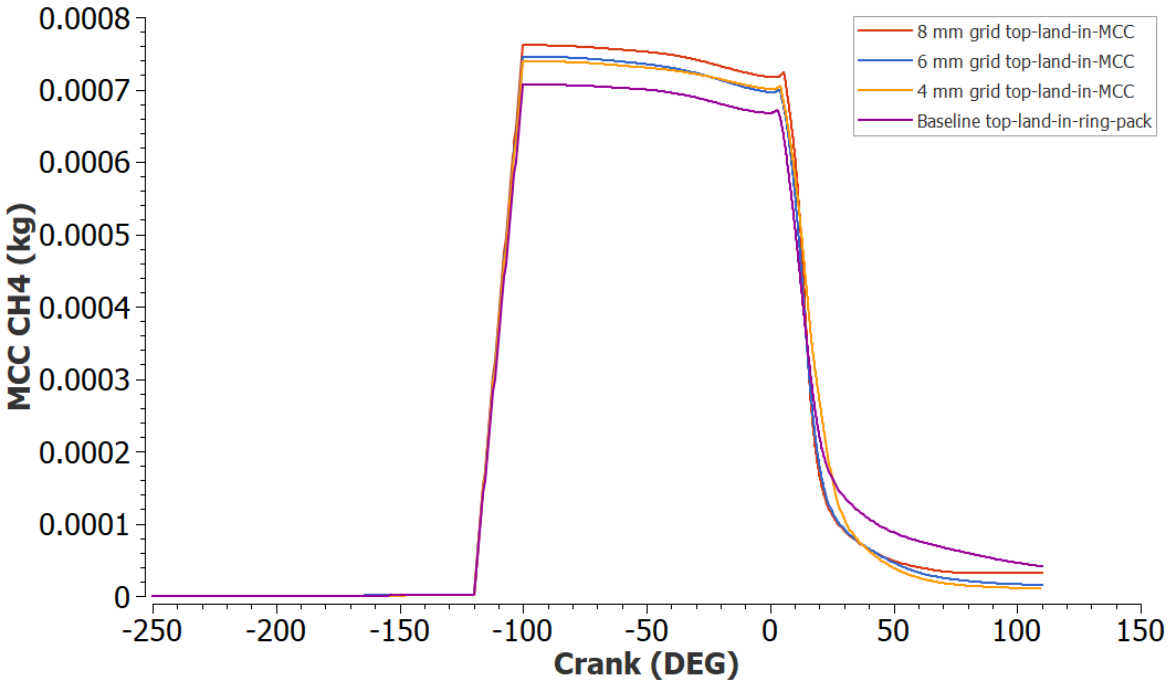

Figure B-8 Methane in the MCC for the Top-Land-in-MCC and Top-Land-in-Ring-Pack Cases

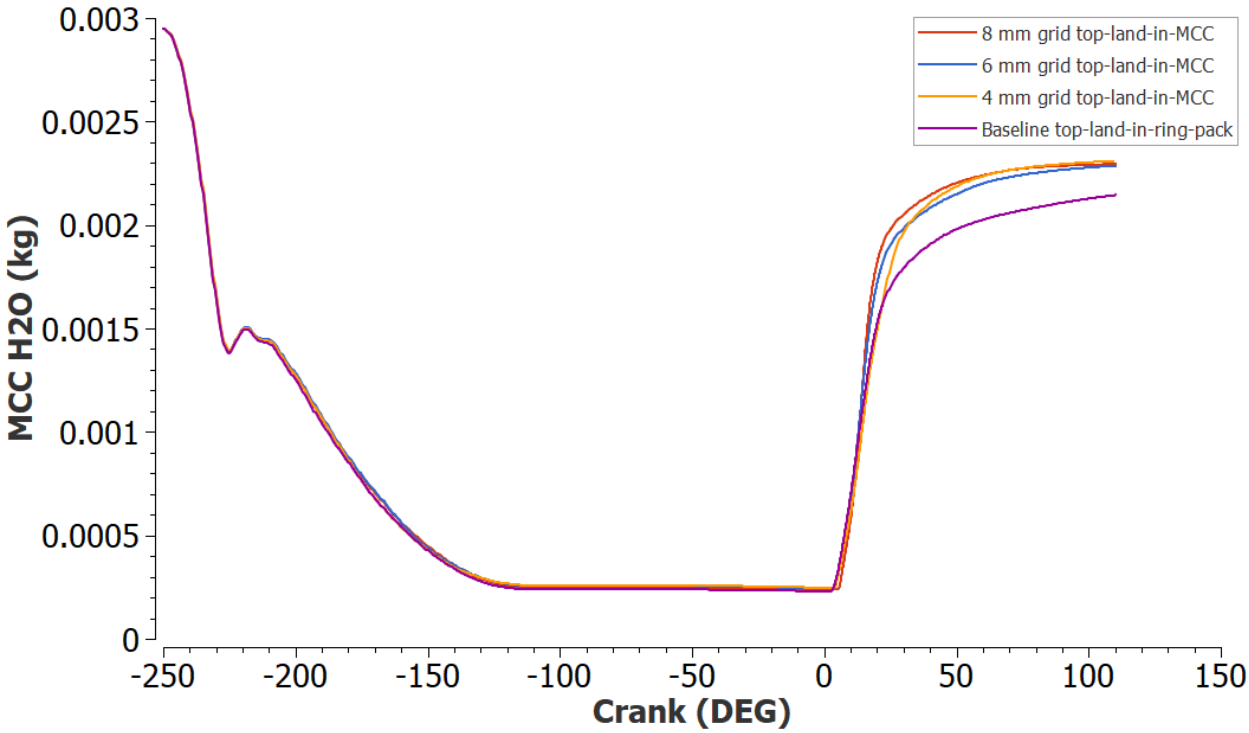

Figure B-9 H2O in the MCC for the Top-Land-in-MCC and Top-Land-in-Ring-Pack Cases

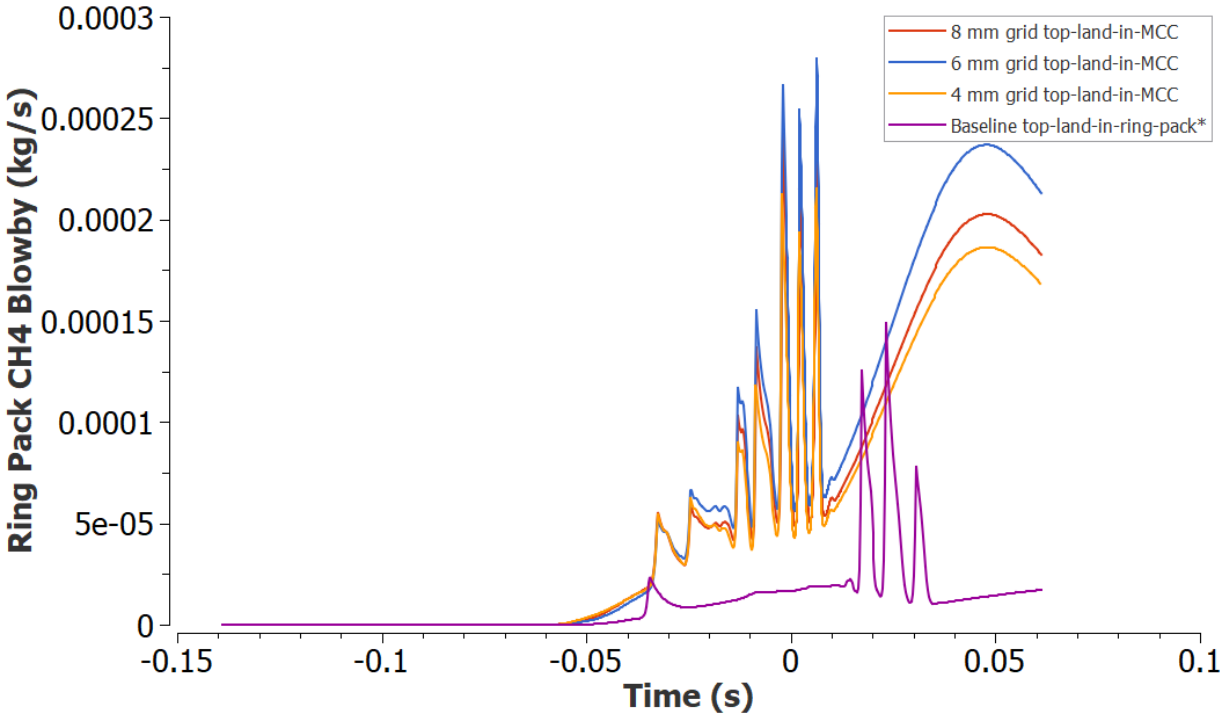

Figure B-10 Ring Pack Methane Blowby for the Top-Land-in-MCC and Top-Land-in-Ring-Pack Cases

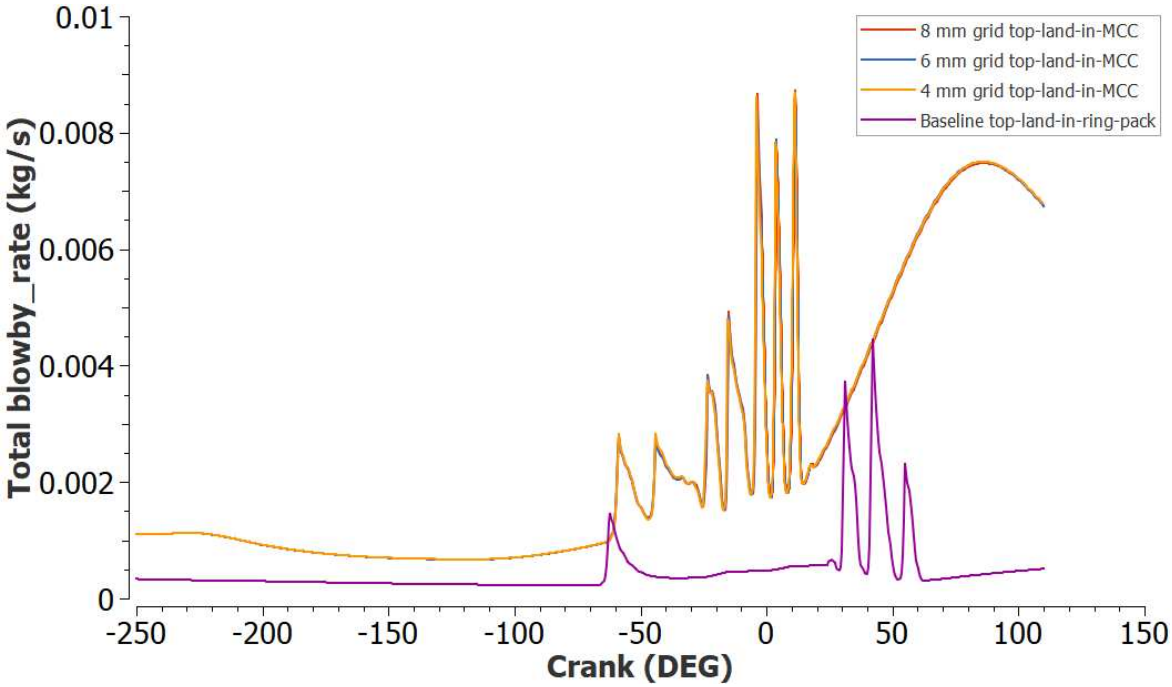

Figure B-11 Total Blowby through the Ring Pack for the Top-Land-in-MCC and Top-Land-in-Ring-Pack Cases

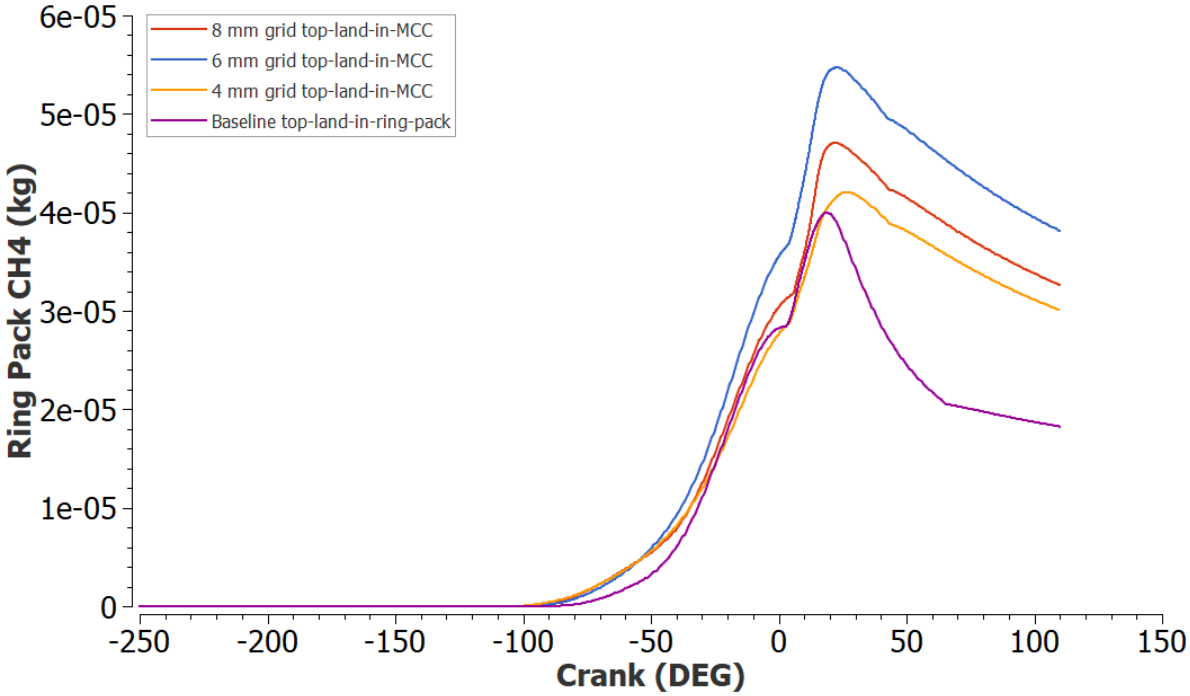

Figure B-12 Trapped Ring Pack Methane for the Top-Land-in-MCC and Top-Land-in-Ring-Pack Cases

LIST OF ABBREVIATIONS

aTDC	After top dead center
AFR	Air-fuel ratio
Bhp-hr	Brake horsepower hour
Btu	British thermal unit
BSFC	Brake specific fuel consumption
BSUHC	Brake specific unburned hydrocarbons
CH_4	Methane
CH_2O	Formaldehyde
CO	Carbon monoxide
CO_2	Carbon dioxide
CO_2e	Carbon dioxide effective
COV	Coefficient of variance
Deg	Degree
GHG	Greenhouse gas

HPFI	High-pressure fuel injection
IMEP	Indicated mean effective pressure
K	Kelvin
LB	Lean-burn
LoPP	Location of peak pressure
MCC	Main combustion chamber
MFB	Mass fraction burned
MGAV	Mechanical gas-actuated valves
NG	Natural gas
NO_x	Oxides of nitrogen
PCC	Pre-combustion chamber
SI	Spark ignited
THC	Total hydrocarbons
UHC	Unburned hydrocarbons